SPATIAL LIGHT MODULATOR TECHNOLOGY

MATERIALS, DEVICES, AND APPLICATIONS

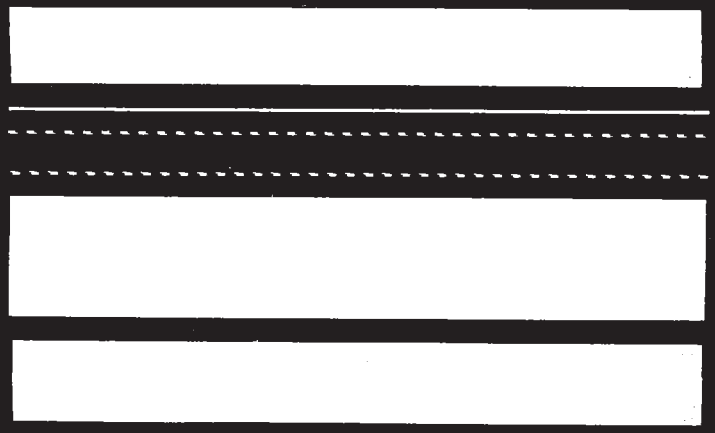

EDITED BY
UZI EFRON

SPATIAL LIGHT MODULATOR TECHNOLOGY

SPATIAL LIGHT MODULATOR TECHNOLOGY

MATERIALS, DEVICES, AND APPLICATIONS

EDITED BY

UZI EFRON

Hughes Research Laboratories
Malibu, California

Marcel Dekker, Inc.

New York • Basel • Hong Kong

Library of Congress Cataloging-in-Publication Data

Spatial light modulator technology : materials, devices, and applications / edited by Uzi Efron.
p. cm. — (Optical engineering; 47)
Includes bibliographical references and index.
ISBN 0-8247-9108-8
1. Light modulators. 2. Light modulators—Materials. 3. Optical data processing—Equipment and supplies. I. Efron, Uzi. II. Series: Optical engineering (Marcel Dekker, Inc.); v. 47.
TA1750.S7 1994
621.36—dc20

94-27860
CIP

The publisher offers discounts on this book when ordered in bulk quantities. For more information, write to Special Sales/Professional Marketing at the address below.

This book is printed on acid-free paper.

Marcel Dekker, Inc.
270 Madison Avenue, New York, New York 10016

Current printing (last digit):
10 9 8 7 6 5 4 3 2 1

PRINTED IN THE UNITED STATES OF AMERICA

6
Ferroelectric Liquid Crystal Spatial Light Modulators

Garret Moddel
University of Colorado at Boulder
Boulder, Colorado

1 INTRODUCTION

Ferroelectric liquid crystal (FLC) technology has only recently yielded practical light modulation devices. It provides a high-performance alternative to the well-established nematic liquid crystals in both optically and electrically addressed spatial light modulators (SLMs). The desirable properties of FLCs include bistability, fast response, and wide viewing angle.

The purpose of this chapter is to provide an overview of the rapidly advancing field of FLC SLM technology. The structure and materials characteristics of FLCs which are most important to spatial light modulation are described in simple terms. The modeling and processing required to design and fabricate an FLC device are outlined. This is followed by a description of the three main types of FLC SLMs that are currently under development. The first type of SLM is optically addressed, providing direct replication of an image for optical processing and projection displays. These devices exhibit the highest optical resolution of the three types, limited only by the physical properties of the materials. The second is a matrix-addressed SLM, consisting of an array of electrically addressed pixels. Although this technology is important for optical processing applications, the largest market is in flat-panel displays. The third type is the VLSI-backplane SLM, in which a liquid crystal cell is formed directly on an integrated circuit which drives it. In addition to affording high speed this approach yields a "smart" SLM which can perform logic operations.

2 FERROELECTRIC LIQUID CRYSTAL STRUCTURES

The physics of FLCs has been discussed in Chapter 2. Here the basic structural, electrical, and optical properties which are most relevant to SLMs are reviewed.

2.1 Background

From the perspective of optical modulation, liquid crystals may be viewed as lying between electrons in solids and mechanical shutters. Liquid crystals have mechanical and symmetry properties which are between those of an isotropic liquid and a crystalline solid. They are like a liquid in that their molecules have at least some of the degrees of freedom of a liquid, allowing them to respond sensitively to an applied force. They are like a solid in having long range orientational order, with the result that the molecules, which are locally anisotropic, are arranged to yield macroscopic anisotropy. This yields strong electro-optic effects, which may be used to produce excellent optical modulation. They are much more sensitive to applied field than solids, in which electro-optic properties depend upon electronic and nuclear motion, and exhibit much greater spatial resolution than mechanical shutters.

To form a device the liquid crystal is usually sandwiched between two plates. Conducting electrodes on the inner surface of the plates provide the electrical signal which drives the liquid crystal. So that light may enter and exit the device at least one of the plates is transparent, and is typically coated with a transparent conducting oxide (TCO). At least one of the two surfaces which bound the liquid crystal is treated to provide a preferred orientation to the liquid crystal molecules. These alignment layers are important in determining the liquid crystal properties and are the subject of Section 3.

The most commonly used liquid crystal has been the nematic liquid crystal described in Chapter 1, whose molecules exhibit orientational order but no positional order [de Gennes 1974]. When an electric field is applied, the dielectrically anisotropic molecules become polarized, creating dipoles which then respond to the field with a torque which is proportional to the square of the field. When the field is switched off, the molecules relax back to their initial orientations in response to elastic forces. This relaxation usually limits the cycling time of nematics. Because the sign of the polarization is a function of the sign of the field, the direction of the torque is independent of the sign of the field, depending only upon its rms value. Nematic liquid crystals are sensitive to the rms average value of the voltage and are thus switched to an on-state by ac fields in which the period is smaller than the response time of the liquid crystal. This is illustrated by the thin line in Fig. 1.

In contrast, FLCs have an electrical polarization even in the absence of an externally applied electric field. Therefore the molecules respond directly to an applied electric

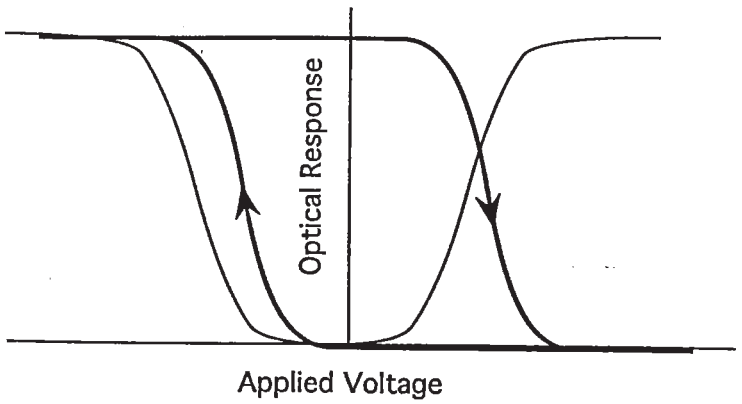

Figure 1 Transfer characteristics: nematic (thin line) versus ferroelectric (thick line) liquid crystals.

field and the torque varies linearly with its magnitude. A field of one polarity drives the FLC into what may be defined as an on-state, and the FLC is switched off with a field of the opposite polarity. One of desirable features of FLCs is the fast switching which results from the spontaneous polarization and from the ability to drive the FLC to its off-state. FLCs exhibit a hysteresis, as do all ferroelectrics, illustrated by the thick line in Fig. 1 [Reynaerts and De Vos 1991b]. If the hysteresis is sufficiently broad and the slope of the transition from one state to the other is sufficiently steep, the FLC remains in its prior state when the applied field is switched off (to zero). This bistability is another of the desirable features of some FLCs.

In 1975 Meyer showed that the chiral smectic C liquid crystal phase ought to be ferroelectric and, along with chemists from Orsay, demonstrated this [Meyer et al. 1975]. Smectic liquic crystals exhibit positional order in that the molecules form parallel layers. These layers are usually perpendicular to the bounding planes, i.e., the layer normal is parallel to the planes. In the smectic C phase the average orientation of the long axis of the molecules, which defines the molecular director, is tilted with respect to the layer normal. A smectic C phase is shown in Fig. 2. In each rod-shaped molecule an electrical dipole is perpendicular to the long axis. A *chiral* smectic C phase (denoted as smectic C*) consists of molecules which are chiral, i.e., which do not have mirror symmetry. What Meyer realized was that within each of these microscopic layers the molecular directors, and hence the dipole moments of neighboring molecules, would be in alignment with each other, with the result that each layer would be ferroelectric. Thus smectic C* liquid crystals are FLCs. In a smectic C* phase a helical structure tends to form in which molecular tilt angle (and hence the director) advances slightly from one layer to the next. Because the net polarization of each layer is different, over the distance of a helical pitch the net polarization is zero. Thus the ferroelectricity is not macroscopic.

2.2 Surface Stabilized Ferroelectric Crystals

In 1980 Clark and Lagerwall demonstrated that macroscopic polarization could be obtained in smectic C* liquid crystals by suppressing the helix [Clark and Lagerwall 1980]. This is accomplished by constraining the material to fill a region between two plates which are separated by a distance of less than a few times the helical pitch, typically 1 to 5 μm. These are known as surface-stabilized ferroelectric liquid crystals (SSFLCs). This discovery opened the way to practical application of FLCs.

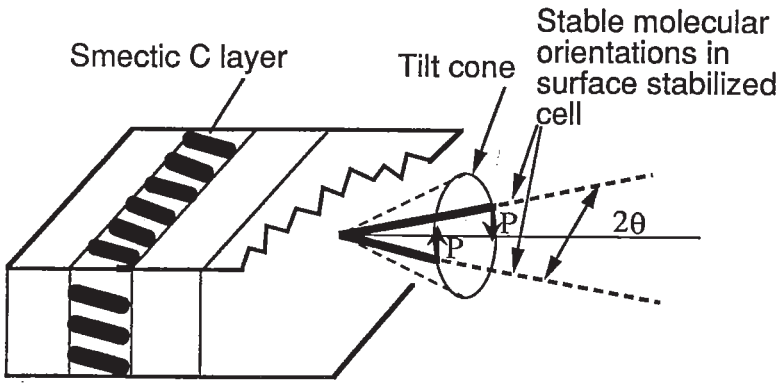

Figure 2 Smectic C phase liquid crystal.

Structure and Switching

In an ideal SSFLC the molecules form parallel layers which extend from one boundary plane to the other. This structure is referred to as the bookshelf geometry because the layers are next to each other like books in a bookshelf, with the shelves forming the boundary planes. The molecules are constrained to move about a tilt cone, shown in Fig. 2. For a tilt angle θ with respect to the layer normal the molecules have two stable orientations, separated by 2θ, which lie in the plane normal to the layers (and hence parallel to the boundary planes). The spontaneous polarization (P) of FLC mixtures ranges from the order of one to hundreds of nC/cm^2. To switch the molecules from one state to the other requires a charge of $2P$. Additional charge is required to produce a voltage across the plates which bound the FLC, as with any capacitor. Thus the total charge required to switch an FLC is $2P + CV$, where V is the change in the applied voltage and C is the geometric capacitance of the cell. For a 2-μm-thick cell filled with an FLC having a relative permittivity of 3.5, $C = 1.5$ nF/cm^2. With the application of a 15-V step to a cell containing FLC with $P = 30$ nC/cm^2 the spontaneous polarization charge is 60 nC/cm^2 and the geometric charge is 23 nC/cm^2. As a voltage is applied to the cell, current flows nearly instantaneously to the cell, charging the geometric capacitance and decaying with an RC decay time. After a delay the molecules rotate, causing a displacement current to flow. The combination of the two currents is shown in Fig. 3. For the values given above, 72% of the current may be attributed to the spontaneous polarization. In addition to the capacitive and displacement components, current also flows due to ionic transport (as discussed in Section 3.5), usually on a longer time scale. Often this ionic component of the current may be ignored in comparison to the other components.

Ideally the layers of SSFLCs are perpendicular to the boundary planes. In practice SSFLCs are often tilted, forming a chevron structure in which the bend where the two oppositely tilted sections meet is parallel to the boundary planes [Clark and Reiker 1988], as shown in Fig. 4. The reason for the tilting is that the layers become thinner as the cell is cooled during formation of the smectic C* phase from the higher temperature smectic A* phase (described in Section 2.4). This chevron structure complicates the

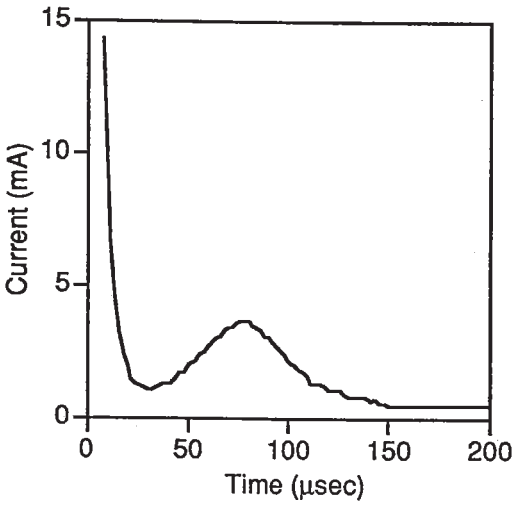

Figure 3 Switching current in response to a step voltage for a surface-stabilized ferroelectric liquid crystal cell. (Courtesy R. A. Rice)

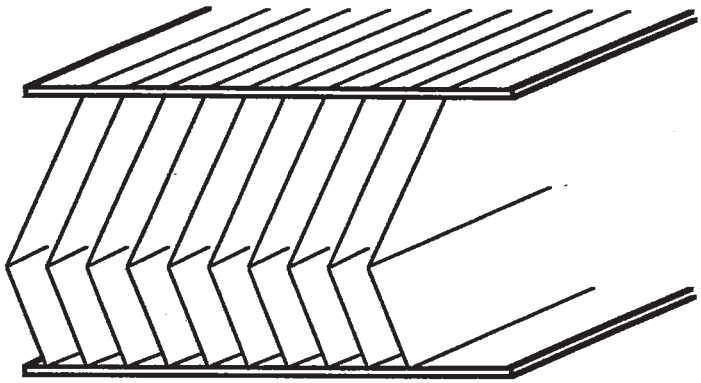

Figure 4 Chevron structure in a surface-stabilized ferroelectric liquid crystal cell.

dynamic and optical properties of the materials because the molecular director is no longer parallel to the boundary layers. The situation is more complicated than shown in Fig. 4 in that the molecular director is splayed in one half of the chevron, such that it rotates continuously with position [Elston and Sambles 1990, Maclennan et al. 1990]. An important consequence of chevron formation in SSFLCs is the zigzag wall defect formed at the interface between two areas in which the sense of the chevron bend is opposite [Handschy and Clark 1984, Ouchi et al. 1988a]. This and other defects reduce the quality of the image in SSFLC SLMs, and their elimination has been the subject of extensive research. In the following discussion these effects are ignored.

Upon the application of an electric field of magnitude E the molecular response time for switching from one state to the other is

$$\tau = \frac{\eta}{PE} \tag{1}$$

where η is the viscosity. For η = 150 mPa-s (equivalent to nJ-s/cm^3 and cP), P = 50 nC/cm^2, and $E = 10^5$ V/cm, τ = 30 μs. Usually as chiral dopant is added to a FLC mixture to increase P, there is a concomitant increase in η with the result that $1/\tau$ does not increase as quickly as P. With increasing P there is also a decrease in the helical pitch of the material and a loss of surface stabilization if the pitch becomes significantly smaller than the cell thickness.

The switching proceeds by the nucleation and growth of domains of the new state of the SSFLC within a region of the old state [Clark and Lagerwall 1980, Orihara and Ishibashi 1984]. These domains are separated by domain walls having a width which is on the order of the thickness of the cell, typically 1 to 2 μm. The movement of these domain walls allows the SSFLC to switch from one state to another without having to go through a high-energy intermediate state, thus greatly enhancing the switching speed of SSFLCs.

As seen from Fig. 1, in the absence of an applied field the molecules ideally remain in either of the bistable states indefinitely. Practically, the period over which molecules remain in a state is a function of the fabrication conditions for the cells, some of which are described in Section 3.3.

Optical Properties

Birefringence. SSFLCs rely on birefringence to modulate light. The refractive index along the optic axis parallel to the molecular director (the extraordinary axis) is signif-

icantly different from the index along an optic axis which is perpendicular to the director (the ordinary axis). This difference, the birefringence (Δn), is quite substantial for FLC molecules, typically ~0.14. Incident light which is linearly polarized decomposes into two components along these two axes such that the phase of one component is retarded with respect to that of the other. In a half-wave plate the thickness (d) is such that

$$\Delta nd = (2m + 1)\frac{\lambda}{2} \tag{2}$$

where λ is the wavelength of the light and m is a positive integer. For incident light which passes through a polarizer to become linearly polarized with an axis that is 45° with respect to one of the optic axes of the half-wave plate, the light is split into equal amplitude components along the extraordinary and ordinary axes of the half-wave plate. The component of the wave passing through the half-wave plate polarized along the extraordinary axis is delayed with respect to the component polarized along the ordinary axis by $(2m + 1)180°$. The emerging components recombine to form light that is linearly polarized with a plane of polarization that has been rotated by 90°. This polarization change may be converted into amplitude modulation by passing the beam through a second polarizer (the analyzer) whose axis is oriented 90° with respect to that of the first one.

In switching an SSFLC from one state to the other the optic axis is rotated by twice the tilt angle θ. For an incident beam that is aligned with one of the SSFLC axes in its off-state, the transmitted light is extinguished upon switching the SSFLC to its other state if 2θ equals 45°. Fortunately FLC mixtures can be synthesized for which θ is approximately 22.5°. Thus SSFLCs can act as a switchable half-wave plates.

Optical Transmission. Given any d and θ for which the SSFLC is not necessarily a half-wave plate, the optical transmission may be extinguished by aligning the axis of the polarizer to the tilt direction of the SSFLC in one state and orienting the axis of the analyzer perpendicular to that of the polarizer. The transmission coefficient is ideally zero but in practice is a function of the spatial uniformity of the SSFLC cell and the quality of the polarizers. Upon applying a field to switch the SSFLC to its other state the transmittance at normal incidence becomes

$$T = \sin^2 2\Omega \sin^2 \frac{\pi d\Delta n}{\lambda} \tag{3}$$

where Ω (equal to 2θ for SSFLCs) is the angle between the entrance polarizer and an optic axis of the liquid crystal. The $\sin^2 2\Omega$ term is a function only of the tilt angle of the FLC mixture. If it is not the ideal 22.5° the transmission in the on-state is diminished, i.e., the insertion loss is increased. As the $\sin^2(\pi d\Delta n/\lambda)$ term is an oscillatory function of the cell thickness (d) it would appear acceptable to have a cell in which d is greater than the minimum half-wave plate thickness dictated by the $m = 0$ case in Eq. 2. Because this thickness is typically 2 μm for a transmission-mode cell, one might want to make a thicker cell to make the fabrication easier. This is usually not desirable, however. As can be seen from Eq. 3, the transmission is an oscillatory function of wavelength and oscillates more quickly for thicker cells. Thus the performance is closest to achromatic for the thinnest cell meeting the half-wave plate condition. Nonoptimal values for d $\Delta n/\lambda$ result in increased insertion loss.

Optical Response Time. The optical response time is not simply the molecular response time defined in Eq. 1 because the optical transmission is not a linear function of the molecular orientation. We define two components of the optical response time:

the delay time, which is the time between the application of the field and when T has reached 10% of its maximum, and the rise time, which is the time between the 10% and 90% of maximum transmission states. The delay time is a substantial fraction of the optical response time because the initial orientation of the polarization is approximately antiparallel to the applied field, providing only a small initial torque. The theoretically determined optical delay, rise, and response times are approximately 3.6τ, 1.8τ, and 5.4τ, respectively, where τ is defined in Eq. 1 [Xue et al. 1987]. Although the experimental delay and response time values may vary significantly from these values due to molecular solitary wave motion and flow, they still provide an indication of the relationship between the molecular and optical response times.

Gray Levels. Because of the existence of two stable orientations, the terminal response of SSFLCs is in principle binary. A continuously variable response or gray levels may be obtained, however, by spatial averaging over areas in which the SSFLC is switched on and areas in which it is off, or by temporal averaging over periods during which the SSFLC is switched on and off. Both spatial and temporal averaging may be accomplished by the control of extrinsic driving parameters, or by taking advantage of the intrinsic properties of the SSFLC. The basic concepts of gray levels are introduced here, and are discussed in more detail in Section 4.3 for optically addressed SLMs, and in Section 5.4 for matrix addressed SLMs.

The spatial averaging may be accomplished intrinsically by allowing domains which cover only a fraction of the area of interest to be switched. In intrinsic approaches the SSFLC is operated near its threshold. A micrograph of partially switched SSFLC is shown in Fig. 5. Such multidomain switching was demonstrated by applying voltage for a critical time so that only some domains switch [Lagerwall et al. 1985], but this approach greatly constrains the electrical drive which can be used. As described in Section 5.4,

Figure 5 Micrograph of partially switched surface-stabilized ferroelectric liquid crystal, showing the multidomain structure. (From B. Landreth and G. Moddel, *Proc. SPIE*, *1296*, 64–72 (1990))

this approach has been applied successfully in matrix addressed SLMs. A different approach to multidomain switching is to control the charge which is delivered to the SSFLC [Hartmann 1989a, Killinger 1991 et al.]. Because a charge of $2P$ is required to fully switch an area, an amount less than that will suffice to switch only a fraction of the area.

In contrast to intrinsic approaches, extrinsic approaches to obtaining gray levels involve operating the SSFLC in well defined states far from its threshold. An extrinsic approach to spatial averaging is to separate the area over which the averaging is to take place into several regions, each of which is addressed independently. Then each region which is addressed may be switched fully on, with the gray level resulting from the fraction of the area which is switched [Lagerwall et al. 1989]. Extrinsic approaches limit the spatial resolution to that of the resolution to which the regions can be patterned.

Switching the device on and off frequently, or temporal dithering, can provide multiple gray levels extrinsically [Clark et al. 1985]. An intrinsic approach to temporal averaging is based upon the fact that the switching time is a function of the applied field [Landreth and Moddel 1990], as described by Eq. 1. The lower the voltage used to switch the device on and off, the larger the time is during which the SSFLC is in an intermediate state. This might appear to result from a decreasing area fraction of switched liquid crystal domains, but has been shown to be due to a spatially uniform rotation of the optic axis [Landreth and Moddel 1992]. Thus spatially uniform switching occurs on the fly while domain switching dominates at longer times, after the charge to switch the SSFLC has been supplied and distributes itself into domains.

Simulation of Switching

In designing devices which incorporate SSFLCs it is important to be able to simulate the optical and electrical characteristics. The optical and electrical response of an SSFLC to an arbitrary electrical drive waveform is a function of the FLC mixture spontaneous polarization, viscosities, elastic constants, tilt angle, and birefringence, and cell thickness, type of alignment, surface anchoring [Uchida et al. 1989], chevron characteristics, defect structure and temperature. Although much of the fundamental dynamics of the switching is understood [Xue et al. 1987, Clark and Lagerwall 1991], the experimental characteristics of SSFLC cells have not been modeled accurately. It is therefore necessary to develop a phenomenological simulation, based on experimental characteristics.

A circuit model, shown in Fig. 6, has been developed which simulates both the optical and electrical characteristics [Rice and Moddel 1992b]. The response of the circuit is simulated using the SPICE (Simulation Program with Integrated Circuit Emphasis) computer program. In the input impedance circuit the input voltage (V_{flc}) produces a current which is divided among the polarization current (I_{pol}), leakage through the FLC resistance (R_{flc}), and charging of the geometric capacitance (C_{flc}). The integrator circuit and clamp produce the correct general time dependence of the response to the input, but do not give the correct detailed response. For example, the response to a step function input is a linear ramp which is clamped at 1 V, but it does not produce the sigmoidal response a real FLC cell would. The correct response is formed using the smoothing circuit, whose parameters depend upon characteristic delay, rise and fall time ratios for the particular type of FLC cell. The optical output is represented by V_{out}. Finally, the polarization current is found from the derivative circuit. This polarization current is the one which is used in the input impedance circuit. The circuit values are determined from four parameters derived from the experimental step response of the SSFLC cell. Once

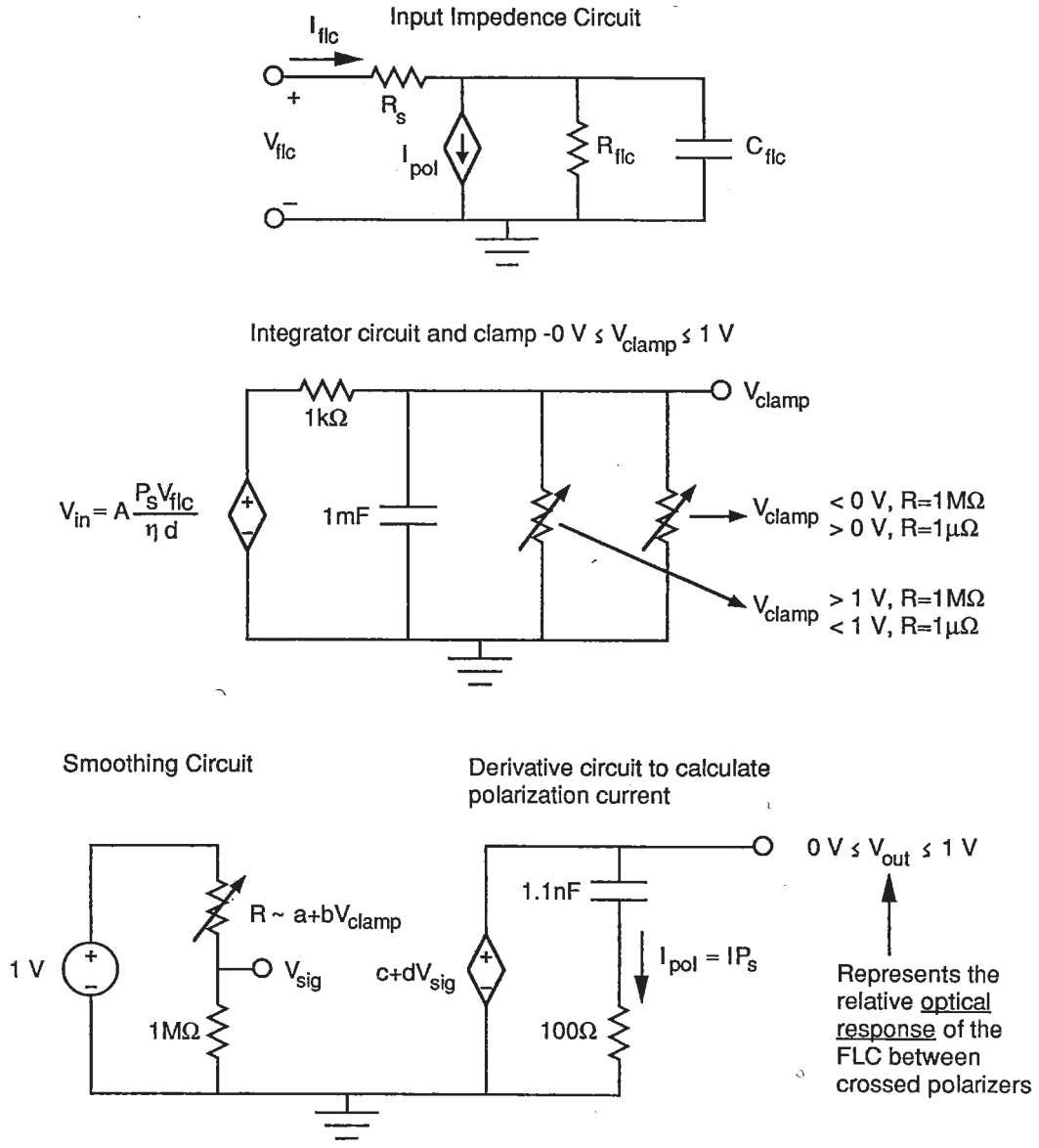

Figure 6 Circuit model which simulates the optical and electrical characteristics of an SSFLC cell in response to an arbitrary driving voltage. (From R. A. Rice and G. Moddel, Soc. Information Display Int. Symp., *Digest of Technical Papers*, Vol. 23, SID, 1992, pp. 224–227.)

they are set, the simulation provides the optical and electrical response to an arbitrary input voltage waveform.

A comparison of a measured and simulated optical response for an SSFLC cell to a ramp input drive voltage is shown in Fig. 7. Both the optical and electrical measured and simulated response to a step change in voltage are shown in Fig. 8.

2.3 Distorted Helix Ferroelectric Crystals

In contrast to the condition for forming a SSFLC described in Section 2.2, distorted helix ferroelectric liquid crystals (DHFLCs) are formed in the smectic C* phase when the thickness of the cell is greater than the helical pitch. DHFLCs have been studied

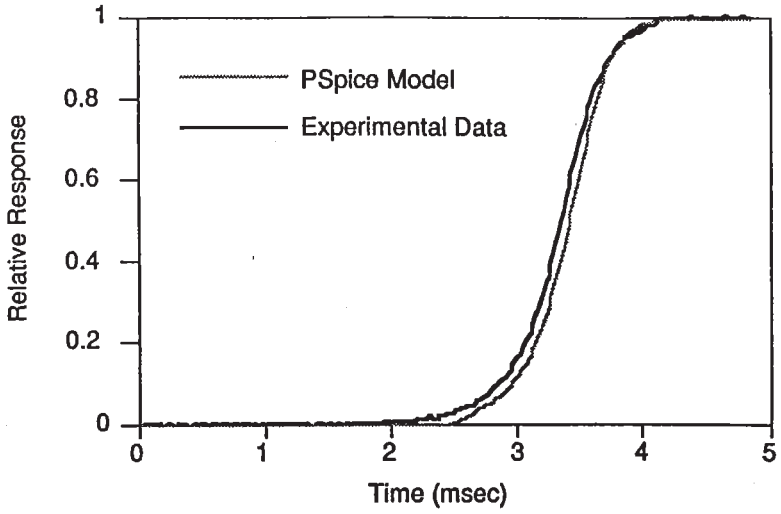

Figure 7 Comparison of a measured and simulated optical response to a ramp input drive voltage. (Courtesy R. A. Rice)

for a number of years [Meyer 1977, Ostrovskii and Chigrinov 1980, Beresnev et al. 1988a] but have become attractive for SLM applications more recently because of the availability of short-pitch, high-polarization mixtures [Fünfschilling and Schadt 1989, Yoshino et al. 1986]. In DHFLC cells the electro-optic effect is linear so that gray scales may easily be obtained. They can also be used to display multiple colors using a white-light source [Abdulhalim and Moddel 1991a], and operate at lower voltages than SSFLCs.

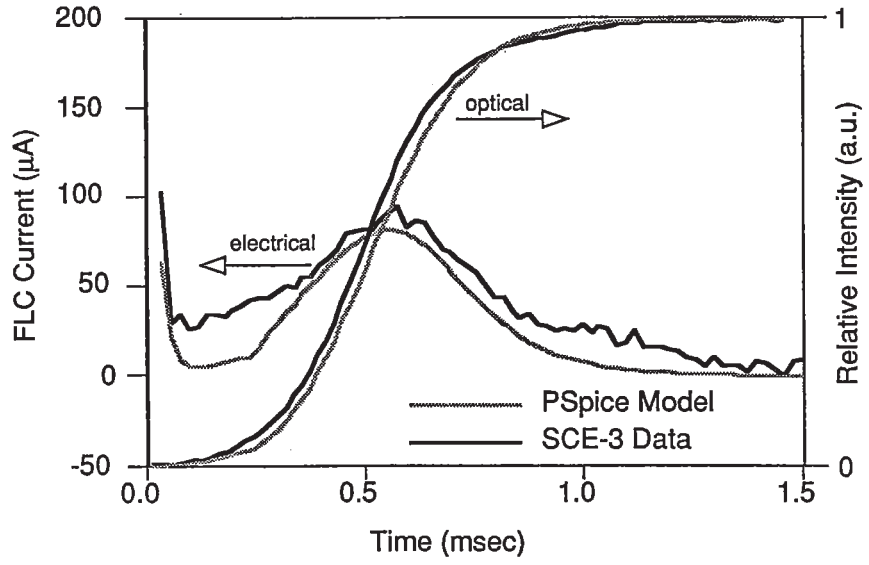

Figure 8 Comparison of measured and simulated optical and electrical response of an FLC cell to a step-change in voltage. (From R. A. Rice and G. Moddel, Soc. Information Display Int. Symp., *Digest of Technical Papers*, Vol. 23, SID, pp. 224–227)

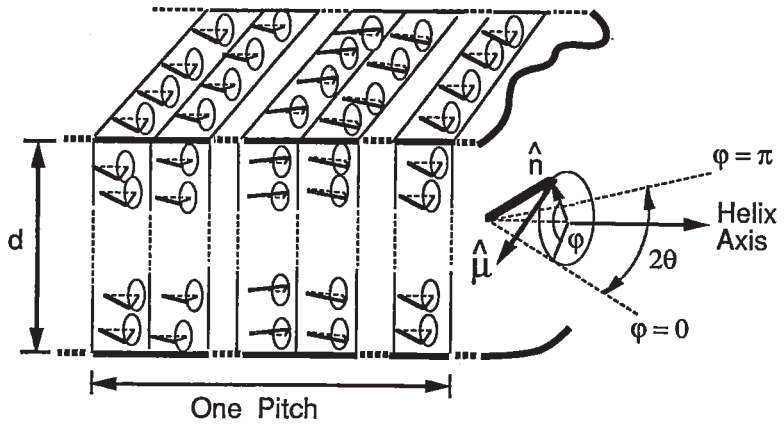

Figure 9 Structure of the distorted helix ferroelectric liquid crystal, showing one period of the helix. (From I. Abdulhalim and G. Moddel, *Mol. Cryst. Liq. Cryst.*, *200*, 79–101 (1991))

Structure and Switching

In a DHFLC cell a bookshelf geometry is formed, as in an SSFLC cell, but the natural helix is not suppressed by the surfaces. This requires FLC mixtures having a very short pitch (e.g., 0.35 μm), cell thicknesses much greater than the helical pitch, and weak anchoring at the surfaces [Fünfschilling and Schadt 1989]. The helix is manifested in the advance of the molecular director from layer to layer, as shown in Fig. 9. The molecular director varies sinusoidally as a function of position, as shown in Fig. 10a.

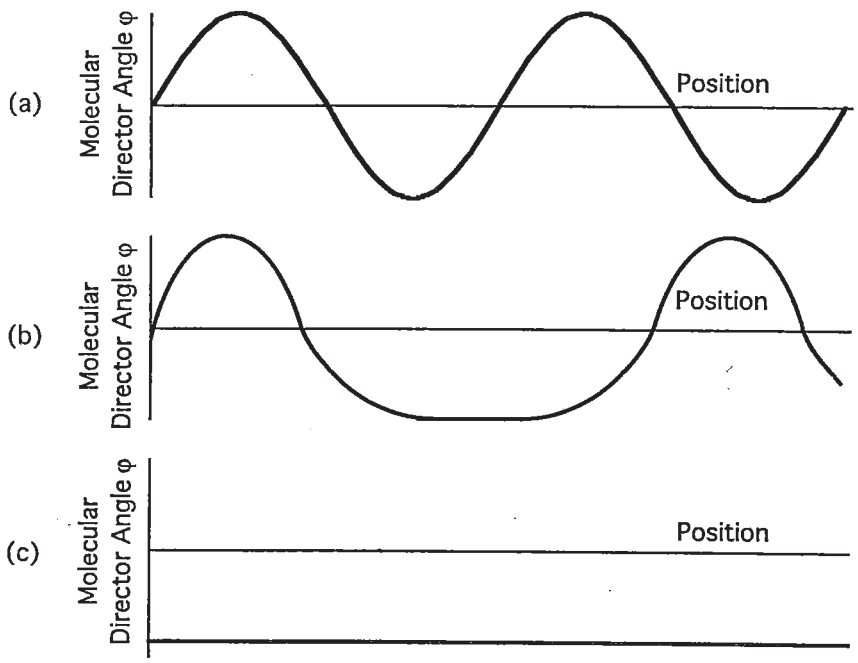

Figure 10 Variation of the molecular director in a distorted helix ferroelectric liquid crystal as function of position parallel to the boundary planes, for (a) no applied electric field; (b) a moderate applied field; and (c) an applied field which is greater than the critical field for unwinding.

As an electrical field is applied, the helix distorts such that regions in which the polarization is favorably oriented with the field grow [Meyer 1977, Ostrovski and Chigrinov 1980], as shown in Fig. 10b. Along with the distortion the helical pitch grows. As the applied field is increased the distortion grows until, at the critical field, the helix is unwound. This uniform structure is depicted in Fig. 10c. In this state the structure of the DHFLC is similar to that of an ideal SSFLC in one of its two stable orientations [Beresnev et al. 1988c]. A field of the opposite polarity causes a growth of regions having the opposite orientation of the polarization.

As with SSFLCs, DHFLCs exhibit the sort of hysteresis curve shown in Fig. 1. One generally drives DHFLCs with fields below the critical field to avoid the unwound state for several reasons: Switching from an unwound state is substantially slower than from an intermediate state [Fünfschilling and Schadt 1989], and switching from one unwound state to the other proceeds without attaining an intermediate helicoidal state [Bawa et al. 1987]. Thus the linear response available from the intermediate states is missed, and gray levels are not obtained. Because in DHFLCs the spontaneous polarization is not initially aligned with the applied field when switching between one intermediate state and another, the initial torque is generally larger than that in SSFLCs and hence the response time is shorter. (Compare to the case described in Section 2.2 under "Optical Response Time.")

There are three different regions in the switching time as a function of electric field [Abdulhalim and Moddel 1991a]. In the low-field region, where the helix is hardly distorted, the net polarization is approximately zero and the switching exhibits relaxation-type behavior. The switching time is a function only of the elastic relaxation time and is independent of field. For intermediate fields a net polarization appears, and couples to the field in the same way as an SSFLC. The switching time in this region varies inversely with the field, as in Eq. 1. At high fields walls form between the areas in which the polarization is favorably oriented with respect to the field and shrink with a solitary wave behavior. In this case the response time $\tau \propto 1/\sqrt{E}$.

Optical Properties

Because the pitch of a DHFLC is on the order of a wavelength of light it diffracts light. This diffraction can be used to determine if the structure is DHFLC as opposed to SSFLC, and to monitor the elongation and disappearance of the helix with applied field [Fünfschilling and Schadt 1989].

The main approach to modulating light using DHFLCs relies on birefringence. Although microscopic birefringence varies as a periodic function of position the layer spacing is on the order of only 20 Å so that an average birefringence may be defined [Ostrovskii and Chigrinov 1980, Abdulhalim and Moddel 1991a]. Thus Eqs. 2 and 3 apply.

One important difference between DHFLCs and SSFLCs regards gray levels. Whereas SSFLCs produce gray levels only through spatial or temporal averaging, terminal states in DHFLCs can yield gray levels, i.e., stable states may be obtained for which the optical transmission varies approximately linearly with applied field [Beresnev et al. 1988a, Fünfschilling and Schadt 1989].

The second important difference between DHFLCs and SSFLCs is evident from Fig. 11. In it the optical transmission is shown as a function of the average optical axis orientation (Ω) during the switching transient. For an SSFLC the function appears as the diagonal line in the figure, corresponding to a simple rotation of Ω in Eq. 3. The data for a DHFLC clearly deviates from this line, resulting from a change in birefringence

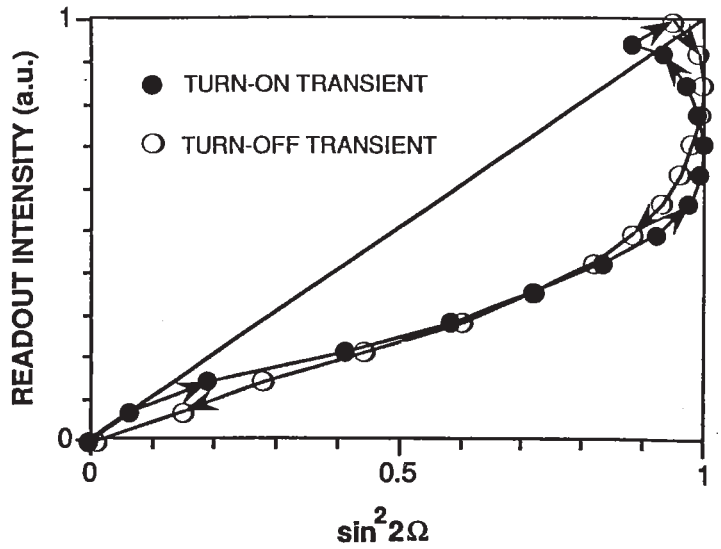

Figure 11 Optical transmission as a function of the average optical axis orientation (Ω) during the switching transient for a distorted helix ferroelectric liquid crystal. The diagonal line represents the dependence expected from Eq. (3) for a constant birefringence (Δn), and observed for a surface-stabilized ferroelectric liquid crystal. (From B. Landreth, C.-C. Mao, and G. Moddel, *Jpn. J. Appl. Phys.*, *30*, 1400–1404 (1991))

(Δn) during switching. As is evident from Eq. 3, this change in Δn changes the wavelength for maximum transmission. This effect may used to be produce color changes in the light from a white light source transmitted through a DHFLC cell [Abdulhalim and Moddel 1991a].

2.4 Electroclinic Liquid Crystals

Electroclinic liquid crystals (ELCs) are not ferroelectric but they are such close cousins to FLCs—both are chiral smectic liquid crystals—that they are included in this chapter. Their desirable characteristics are that they exhibit a very fast and linear response to an electric field, but the response usually varies strongly with temperature and is not bistable. ELCs are smectic A* liquid crystals, usually formed by heating smectic C* above a phase transition temperature T_c which removes the spontaneous molecular tilt [Garoff and Meyer 1977 and 1979]. The term electroclinic arises because the application of an electric field induces a tilt. These are also called soft-model ferroelectric-effect liquid crystals [Andersson et al. 1988] because as the liquid crystal is cooled through T_c one of the elastic constants vanishes, softening the restoring force which keeps the molecules perpendicular to the smectic layers.

Structure and Switching

ELC molecules form parallel layers which are perpendicular to the boundary plates, as with SSFLCs, but there is no spontaneous tilt, as shown in Fig. 12. Under an applied field the molecules tilt in the plane of the substrate rather than around a tilt cone. The direction the induced molecular tilt is a function of the polarity of the applied field. The induced tilt decreases with temperature and is at least a factor of 2 smaller than that in SSFLCs.

The response is very fast, typically 100 times as fast as the response of the corresponding SSFLC [Andersson et al. 1988]. Over a limited temperature range [Abdulhalim

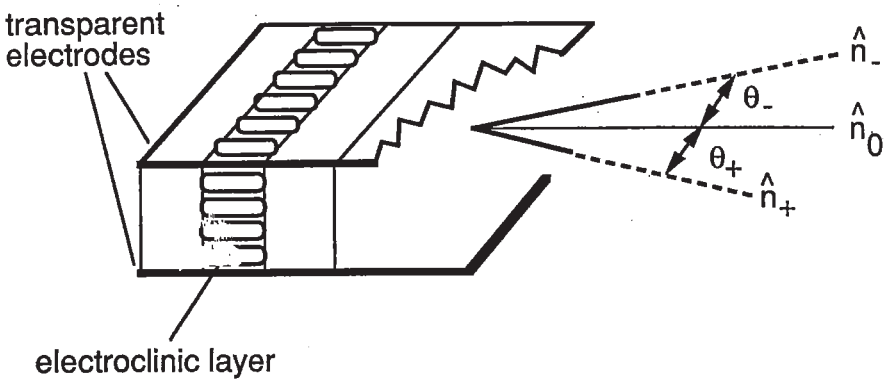

Figure 12 Structure of the electroclinic liquid crystal. (Courtesy I. Abdulhalim)

and Moddel 1991a] the molecular response time τ varies strongly with temperature, described by

$$\tau = \frac{\eta}{\alpha(T - T_c)} \tag{4}$$

where η is the viscosity, α is a constant for the material, and T is the temperature. In a mixture for which $\eta/\alpha = 30$ μs-K, $T_c = 28$°C, and $T = 50$°C, $\tau = 1.4$ μs. The response time is independent of the applied field.

Optical Properties

As with SSFLCs, ELCs rely on birefringence to modulate light and Eqs. 2 and 3 apply. Because the tilt angle θ is at least a factor of 2 smaller than that of SSFLCs formed from the same substance, most available mixtures cannot provide the tilt angle of 22.5° to rotate the optic axis 45° which is required to obtain a 90° phase shift in the transmitted light through a half-wave plate. However, using a multiple-cell technique with a 11.25° tilt, large modulation has been achieved [Andersson et al. 1991], and materials with tilt angles approaching 22.5° have been developed [Williams et al. 1991]. Unlike DHFLCs the birefringence does not vary significantly with applied field.

Because the tilt is a linear function of the applied electric field, gray levels may be obtained directly. The transmittance varies nearly linearly with applied field near T_c [Abdulhalim and Moddel 1991b].

The theoretically determined optical delay, rise, and response times are approximately 0.38τ, 2.58τ, and 2.96τ, respectively, where τ is defined in Eq. 4 [Abdulhalim and Moddel 1991b].

2.5 Other Ferroelectric Liquid Crystals

There are several other types of FLCs, including short-pitch bistable FLCs and twisted smectic FLCs.

Short-pitch bistable FLCs [Fünfschilling and Schadt 1991] have chevrons for which the chevron axis is perpendicular to the boundary planes, as shown in Fig. 13, as opposed to the parallel chevron structure of SSFLCs shown in Fig. 4. They are formed by applying a low-frequency ac field as the cells, filled with short-pitch high spontaneous polarization (P) FLC, are cooled. In this way, surface stabilization is not required to suppress the helix. In SSFLCs one is generally restricted to incorporating FLCs in which P is not so large that the concomitant reduction in the helical pitch causes a loss of surface stabi-

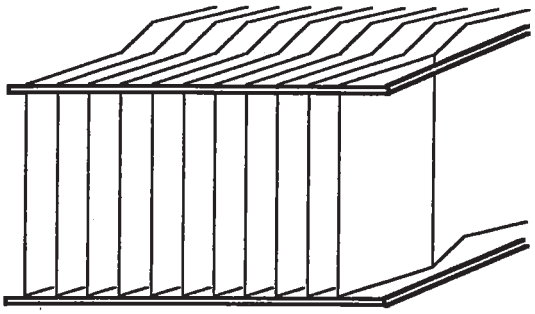

Figure 13 Chevron structure in the short-pitch bistable ferroelectric liquid crystal. (Adapted from J. Fünfschilling and M. Schadt, *Jpn. J. Appl. Phys.*, *30*, 741–746 (1991).)

lization. In short-pitch bistable FLCs, in which this restriction does not apply, one may incorporate large P mixtures. The electro-optic response is fast and bistable, but the contrast ratio is limited to approximately 35:1 because of the characteristic chevron structure.

In twisted smectic FLCs [Patel 1992] the FLC molecules are constrained by alignment layers (discussed in Section 3.2) to be rotated by 90° between one of the boundary planes and the other, as shown in Fig. 14(a). These liquid crystals produce optical modulation by the adiabatic following of the twist by a particular polarization of incident light [Yariv and Yeh 1984], as is the case with twisted nematic liquid crystals, rather than by birefringence. The device is placed between crossed polarizers. Upon passing through the entrance polarizer the incident beam becomes linearly polarized. The polarization follows the twist and comes into alignment with the second polarizer (the analyzer) which is crossed with respect to the entrance polarizer, and passes through it. When an electric field is applied the electric polarization of the molecules aligns with the applied field, and the structure loses its twist, as shown in Fig. 14(b). This eliminates the rotary effect so that the incident beam maintains its initial polarization as it passes through the liquid crystal and is blocked by the analyzer. It is possible to obtain continuously variable transmission by applying a smaller electric field which only partially unwinds the twisted structure. Whereas the FLC devices which rely upon modulation by birefringence perform optimally only over a limited range of wavelengths, the adiabatic following of twisted smectic structure is more nearly achromatic.

A variation of the SSFLC is the antiferroelectric liquid crystal [Ouchi et al. 1991]. In it the molecules in neighboring layers change with applied field from opposing to uniform orientations. In an applied ac field all the molecules switch between the two uniform orientations, which produce equal optical transmission for an appropriately aligned polarizer, and relax to the antiferroelectric orientation when the field goes to zero. Thus antiferroelectric liquid crystals may be operated much like nematic liquid crystals, with an ac field having no dc component. Because of this they are less susceptible to ion-induced degradation than are SSFLCs, discussed in Section 3.5, and are of growing interest for practical applications.

3 SURFACE ALIGNMENT

Surface alignment technology is developing from an art into a science as the nature of the surface interactions and the structures they create become better understood. Layers at the cell boundary surfaces are required to orient the surface layers of the liquid crystal

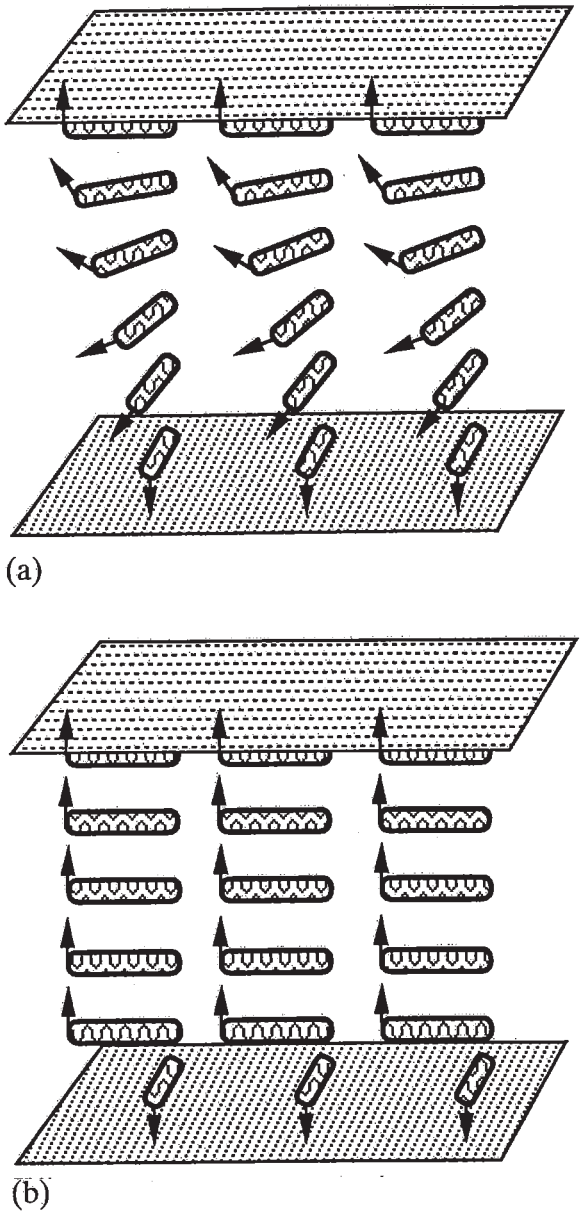

Figure 14 Structure of the twisted smectic ferroelectric liquid crystal in (a) its twisted state, and (b) its parallel state under an applied field. The arrows indicate the direction of the spontaneous electric polarization.

molecules, which in turn, serve to align the bulk of the liquid crystal. The surface alignment is crucial in determining many of the properties of the liquid crystal, such as bistability, response time, defects, and degradation.

An abstruse nomenclature is used to describe the general molecular orientation [Lagerwall 1988]. When the long axis of the molecules is aligned perpendicular to the boundary plane it is called "homeotropic" alignment. With "homogeneous" alignment the long axis lies parallel to the boundary plane oriented in a particular direction. Usually for FLCs the desired alignment is close to homogeneous, with the long axis tilted away from the substrate at a small "pretilt" angle.

3.1 Cell Fabrication

FLC cells are fabricated with glass forming at least one of the pair of boundary layers. For SLMs in which optical uniformity is critical, optical flats are used for the glass. The glass is usually coated with a transparent conducting oxide (TCO) such as indium tin oxide (ITO). An alignment layer, described in the following section, is formed over the surfaces. A spacer, consisting of polystyrene microspheres, glass rods, or deposited and patterned insulating layers, is applied to separate the two alignment-layer-coated surfaces to form a cavity for the FLC. The desired thickness is determined by Eq. 2, and is typically a few microns.

The two alignment-layer-coated surfaces are then set in opposition, separated by the spacers, and held in a fixture. A small amount of liquid crystal mixture is placed on an open edge of the cavity, and the device is set on a temperature-controlled stage, often in a vacuum chamber which reduces air bubble formation. After evacuating the chamber the stage is heated to a temperature at which the liquid is in its isotropic phase [Clerc 1988], typically 70–120°C. The liquid crystal fills the cavity by capillary action. The cell is cooled slowly to room temperature. During the cooling the liquid crystal undergoes phase changes, typically isotropic → nematic* → smectic A* → smectic C*, but other sequences are possible [Hatano et al. 1986].

3.2 Alignment Methods

The first method used to align SSFLCs was gently shearing the boundary plates while the liquid crystal is in the smectic A* phase and then cooling to the smectic C* phase [Clark and Lagerwall 1980]. Another method is the application of a magnetic field during slow cooling of the cell, but this works only for thick, non-surface-stabilized cells [Kondo et al. 1983]. A third approach is to maintain a lateral thermal gradient from the edge of a spacer to produce alignment, but this technique works best only for cells greater than 2 μm thick [Ishikawa et al. 1984]. None of these techniques yielded high quality, large-area, thin SSFLC cells.

Rubbed polymer layers had been used to align nematic liquid crystals for years, but were thought to be inappropriate for SSFLCs because they would overly constrain the molecules, not allowing the molecular director to rotate freely on the surface. Bistability can, in fact, be obtained in SSFLC cells with a rubber polymer alignment layer [Patel et al. 1984, Patel 1985, Mochizuki et al. 1991a, Panarin et al. 1992]. Because of strong surface-molecule interactions, however, the molecules in the bulk switch more quickly than those at the surface. To produce the alignment layer a solution of a polymer, such as polyvinyl alcohol or nylon, is spun onto the surface at a few thousand rpm. The layer is dried and then rubbed with a cloth repeatedly in a single direction. For SSFLC, DHFLC and ELC devices the cell is assembled with the alignment layers facing and parallel to each other. For twisted smectic FLC devices the alignment layers are rotated 90° with respect to each other. Rubber polymer alignment has gained acceptance as a simple method to obtain acceptable SSFLC cells having the chevron structure of Fig. 4, and remains the method of choice for mass production of SSFLC cells [Mochizuki et al. 1991a].

An alignment technique which has produced among the most uniform and bistable SSFLC cells is oblique evaporation [Ouchi et al. 1988b, Armitage 1991, Doroski et al. 1994]. Usually a dielectric, such as silicon monoxide, is evaporated onto the surface at an oblique angle, forming a layer on the order of 200 Å thick. Because of coalescence

of the evaporated adatoms on the surface and subsequent shadowing, microscopic "stalagmites" grow anisotropically in the direction of the vapor source. The angle of evaporation affects the pretilt of the layers. As shown in Fig. 15, if the layers are oriented antiparallel to each other a uniform SSFLC structure results, while a parallel alignment results in a chevron structure [Ouchi et al. 1988b]. A two-step oblique evaporation process, the first at a low 60° angle and the second orthogonal to the first and at a high 85° angle, provides the combined benefits of the high contrast obtained from a moderate angle and the good bistability of a high deposition angle [Bawa et al. 1990].

Another approach to controlling the pretilt angle is to use a polyimide alignment layer [Myrvold 1988b, Kuniyasu et al. 1988, Yamamoto et al. 1989]. Polyimide layers are spin-coated and rubbed, as were the polymers described earlier. The direction of rubbing determines the direction of the pretilt, so that parallel and antiparallel alignments can be produced, as with the obliquely evaporated layers. Creation of zigzag wall defects can be suppressed by using an alignment layer with a pretilt which favors one sense of the chevron bend and promotes bistability [Orihara et al. 1989, Kanbe et al. 1991].

A material that appears promising is short-chained silanes [Doroski et al. 1994]. Good homogeneous (parallel) alignment is formed by spinning on a monolayer of the material, baking it, and rubbing it. The advantages of silane monolayers over that standard polymers is that it is very thin, improving bistability and reducing ion-induced performance gradation, as discussed in the following sections.

The way that an alignment layer orients the liquid crystal is not as obvious as it might seem. When grooves are formed, they are much larger than the liquid crystal molecules (which are about 15 Å long) and therefore cannot influence the orientation of the molecules directly in contact with them. Instead the alignment occurs via long-range forces which influence molecules which are not in immediate contact with the alignment layer, and cause the long axis of the molecules to align with the valleys of the grooves. In other cases an epitaxial alignment is in effect [Myrvold 1988a], in which the crystal structure of the alignment layer induces a matching alignment of the liquid crystal molecules. In such cases it is possible for the long axis of the liquid crystal to align normal to the rubbing direction.

Once an SSFLC cell has been assembled, filled, and cooled to the smectic C* phase some zigzag defects may appear. It is possible to remove these with the application of a low-frequency ac electric field [Umeda et al. 1988]. A small voltage, approximately 2 V for polyvinyl-alcohol alignment layers [Hartmann and Luyckx-Smolders 1990], applied at a frequency between 0.1 and 200 Hz, transforms the chevron structure which contains zigzag defects into a quasi-bookshelf geometry which is defect free. This pro-

Figure 15 Cross section of a surface-stabilized ferroelectric liquid crystals, showing the effect of parallel (left) and antiparallel (right) obliquely evaporated alignment layers on the liquid crystal layer structure.

cedure also works for cells incorporating rubbed nylon alignment layers [Bawa et al. 1989].

3.3 Bistability

Bistability has been mentioned several times in this chapter as an important, though sometimes elusive, property of good SSFLC cells. In this section bistability is more clearly defined, and methods for obtaining it are outlined.

One method to determine the bistability is from the hysteresis curve, as shown in Fig. 1. A very low frequency bipolar triangular-wave voltage is applied to the cell and the optical response (e.g., optical transmission through crossed polarizers) is monitored. Another, perhaps more direct, method is shown in Fig. 16. A positive voltage pulse is applied to the cell, followed by a longer period during which the cell is short circuited. Then a negative pulse is applied, followed by another zero-voltage period. As the cell responds to the pulses the optical response (e.g., optical transmission through crossed polarizers) is monitored. During the pulse the transmission attains its saturated value (T_{sat}). During the following zero-voltage period the optical transmission decays to one of two final levels, depending upon its starting level, which have a difference ΔT_{final}. The ratio $\Delta T_{final}/T_{sat}$ is a measure of the quality of the bistability, and is equal to unity for perfect bistability. Other more involved techniques for measuring the bistability have been developed to determine its immunity to modulation by disturbing pulses [Hartmann and Luyckx-Smolders 1990].

To form a bistable SSFLC cell, ideally the surface alignment should constrain the molecules to be parallel to the boundary planes, but allow the molecular director to rotate freely on this plane [Clark and Lagerwall 1980]. If this were not the case, the

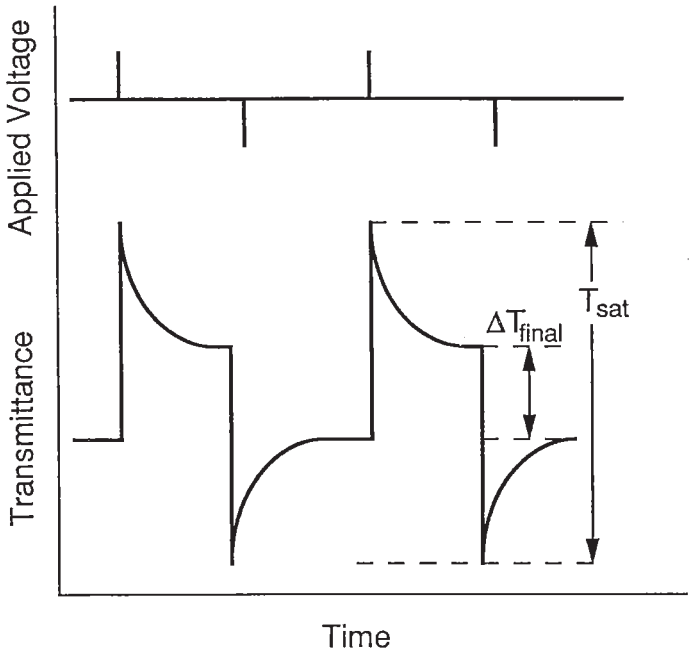

Figure 16 Test to determine the quality of bistability. The upper curve is the applied voltage, and the lower curve is the optical response as measured by the optical transmission through crossed polarizers.

molecules would have a preferred orientation, producing asymmetric bistability which is described in Section 3.4. Applying an electric field would rotate the molecules in the bulk, but once the field was removed the pinned surface molecules would reorient those in the bulk and the bistability would be lost. Often the fabrication of an SSFLC cell which exhibits true bistability is a key goal in developing an alignment method.

Insulating alignment layers degrade the bistability [Yang et al. 1989]. The cause for this is shown schematically in Figs. 17(a) and (b). When a voltage is applied to the cell, a field is dropped across the SSFLC and the alignment layers, causing the SSFLC molecular dipoles to become oriented such that their polarity is opposite to that of the applied field. This may be visualized as a net charge which is created at the interface between the alignment layers and the liquid crystal which is opposite in polarity to that of the adjacent electrode, as shown in Fig. 17(a). When the voltage across the cell is switched to zero by shorting the two electrodes together, initially the interface charge remains, as shown in Fig. 17(b). It produces a field across the SSFLC which is opposite in polarity to that originally produced by the applied voltage. This depolarization field tends to switch the SSFLC away from its saturated orientation (defined in Fig. 16). The larger the spontaneous polarization (P) of the SSFLC, the greater the density of interface

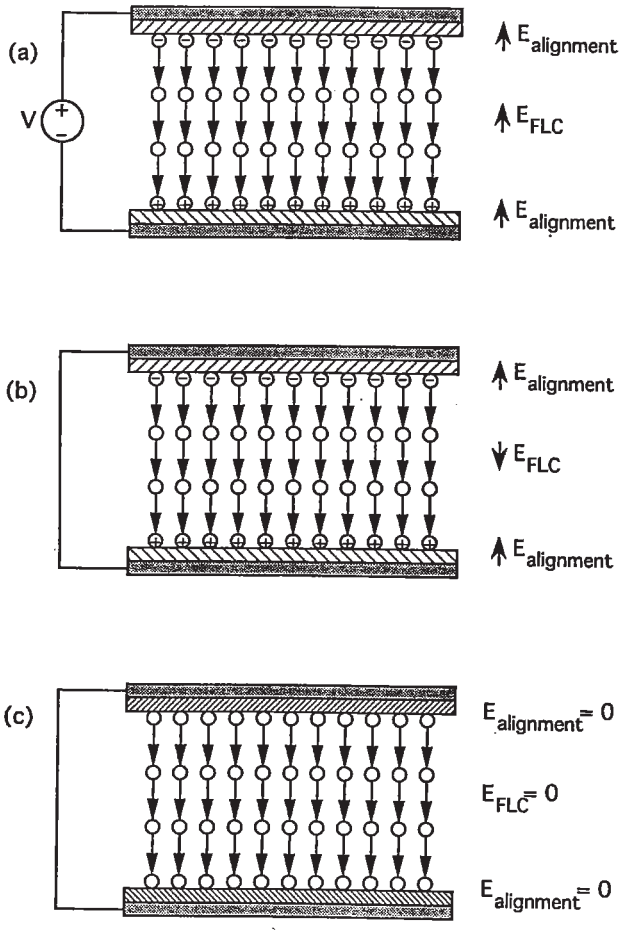

Figure 17 Effect of the conductivity of the alignment layer on the bistability of SSFLC cells, as explained in the text. (a) Insulating alignment layer with an applied field. (b) Insulating alignment layer after applied field is switched to zero, which produces a depolarization field across the SSFLC. (c) Conductive alignment layer after applied field is switched to zero.

charge is, resulting in a larger depolarization effect. To obtain bistability in cells with an insulating alignment layer, P is limited to approximately 20 nC/cm^2 [Dijon et al. 1988a], which severely limits the switching speed of the SSFLC defined by Eq. 1. The drift of impurity ions in the SSFLC cell affects this degradation of the bistability, as discussed in Section 3.5.

A solution to this problem is to use conductive alignment layers [Chieu and Yang 1990]. If the alignment layer is sufficiently conductive, after switching the applied voltage to zero, charge flows to balance the interface charge, which eliminates the depolarization field. This is shown in Fig. 17(c). The quality of the bistability, defined as T_{final}/T_{sat}, is a function of the conductivity of the alignment layer and the spontaneous polarization of the FLC, as shown in Fig. 18. One method to form more conductive alignment layers is to dope them with a charge-transfer complex (CTC) [Nakaya et al. 1989]. Another approach is to use an obliquely evaporated metal alignment layer, which also acts as a polarizer, but the film is fragile [Armitage 1990]. Very thin alignment layers of insulating material, such as silane monolayers and 75-Å-thick evaporated SiO_x, also yield bistable SSFLCs [Doroski et al. 1994] because they are thin enough for carriers to cross them or because their capacitance is so large that the voltage drop across them is negligible.

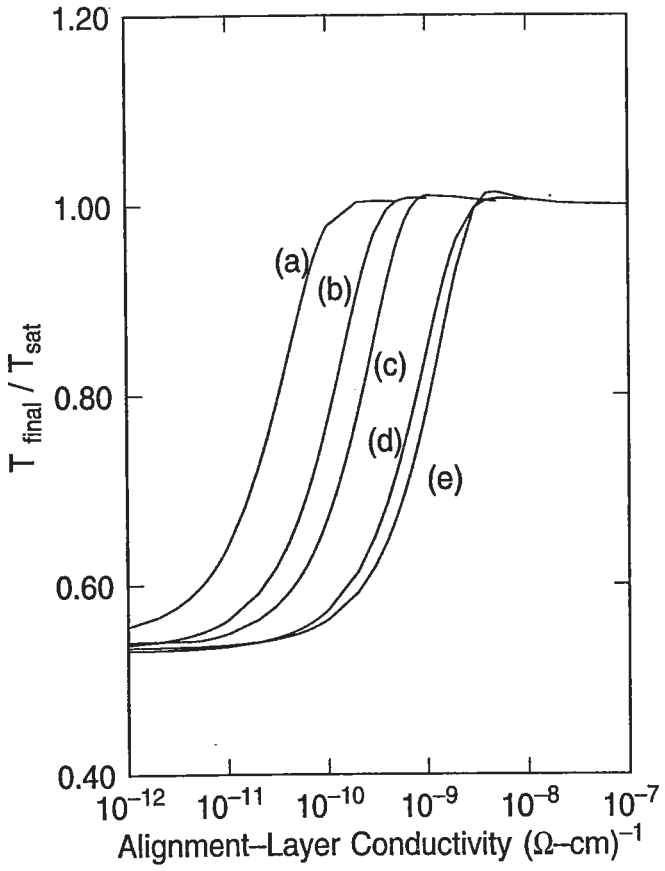

Figure 18 The quality of the bistability defined as T_{final}/T_{sat}, as a function of the conductivity of the alignment layer for different FLC spontaneous polarization values (P). For curves (a), (b), (c), (d), and (e) P is equal to 20, 40, 60, 100, and 140 nC/cm^2, respectively. (From T. C. Chieu and K. H. Yang, *Appl. Phys. Lett.*, *56*, 1326–1328 (1990))

A completely different approach to obtaining bistability is to apply a high-frequency ac field to the FLC during its operation, which tends to keep it in its current state. This was originally thought to be due to negative dielectric anisotropy [Le Pesant et al. 1985, Nagata et al. 1988] but more recently has been attributed to biaxiality in the dielectric tensor [Elston et al. 1990, Jones et al. 1991]. This ac stabilization voltage can be applied in series with the lower frequency switching voltage.

The chevron structure shown in Fig. 4, which is common in SSFLC cells, limits the bistability. In such a tilted structure the polarization is not perpendicular to the surfaces. The application of a sufficiently large electric field drives the SSFLC to a full-contrast optical state, but when the field is removed it relaxes into a less optically favorable state [Crossland et al. 1990, Underwood et al. 1991]. The result is that T_{final} is smaller than T_{sat} and the bistability is diminished. Thus the best bistability is obtained in cells having a true bookshelf structure in which the layers are not tilted. A permanent bookshelf structure can be induced by the application of a low-frequency ac electric field in a preoperation curing step, described in the preceding section.

3.4 Asymmetric Bistability

An asymmetric bistable SSFLC is one which switches to one of its two saturated states when no electric field is applied. It exhibits a hysteresis curve which is displaced from zero volts, as shown in Fig. 19, as opposed to that of Fig. 1 which is symmetric in voltage. Asymmetric bistability is useful when a normally-off-state is desired, or when a bipolar voltage is not available to switch off the SSFLC, as is the case for the self-powered optically addressed spatial light modulator described in Section 4.2 under "Self-Powered OASLM."

Most FLCs pass through a smectic A* phase which is untilted (see Section 2.4). The layer structure is established in this phase with the molecular director aligning itself parallel to the rubbing direction of the alignment layer, which causes all the layers to become oriented normal to the rubbing direction. This layer orientation is maintained upon cooling into the smectic C* phase in which the molecular director becomes tilted.

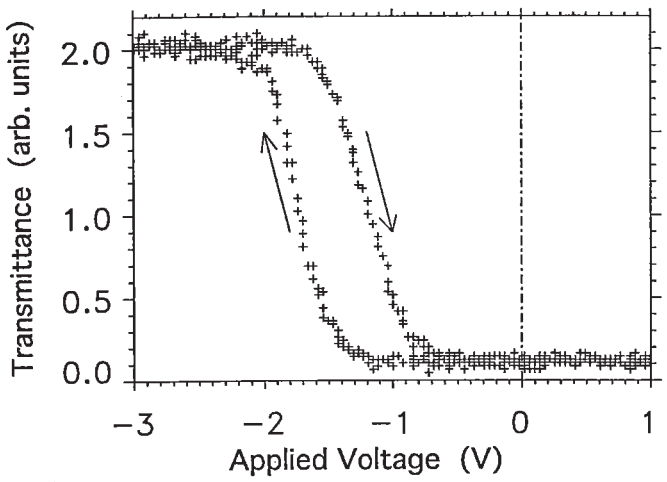

Figure 19 Transfer characteristic of a surface-stabilized ferroelectric liquid crystal cell which exhibits asymmetric bistability. (From Z. Zou, N. A. Clark, and G. Moddel, Int. Conf. Liquid Crystals, Pisa, Italy, 1992)

The two saturated molecular orientations lie on either side of the rubbing direction, as shown in Fig. 20(a). This approach can yield bistable cells, described above.

Asymmetric bistability can be achieved by using an FLC mixture which passes directly from a nematic to a smectic C* phase as it cools from the isotropic phase, without passing through a smectic A* phase [Patel and Goodby 1986, Hatano et al. 1986, Zou et al. 1992]. The molecules align their long axis with the rubbing direction, as was the case for mixtures in the smectic A* phase, but in this case the molecules have two energetically equivalent ways to form smectic layers, as shown in Fig. 20(b). They differ in that on the left side of Fig. 20(b), the polarization points into the paper, represented by ⊗, while on the right side the polarization points out of the paper, represented by ⊙. The result is a cell filled with a mixture of domains, each having one of the two orientations of Fig. 20(b). One of the two orientations can be formed exclusively by applying a dc electric field during the transition from the nematic to the smectic C* phase. The field orients the polarization uniformly so that there is only one way to form the smectic layers, as shown in Fig. 20(c).

After the cooling, an applied field of the opposite polarity rotates the molecules above their tilt cones to the orientation shown in Fig. 20(d). In the absence of an applied field the molecules return to the orientation of Fig. 20(c) in which they are aligned parallel to the rubbing direction. The nonequivalence of the two orientations results in asymmetric bistability, as shown in Fig. 19.

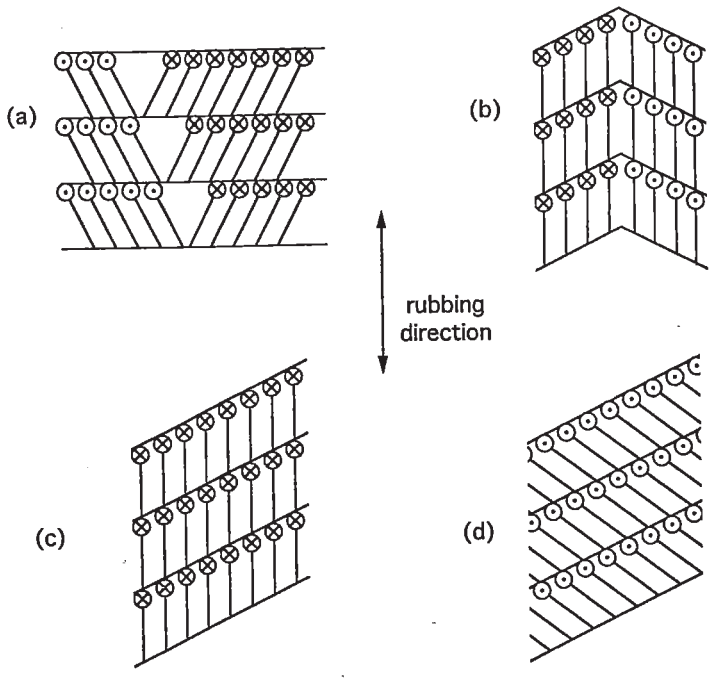

Figure 20 (a) Liquid crystal which has cooled through a smectic A* phase to the smectic C* phase. The two saturated molecular orientations lie on either side of the rubbing direction. (b) Liquid crystal which has cooled directly from the nematic phase to the smectic C* phase. It exhibits two energetically equivalent ways to form smectic layers. On the left side the polarization points into the paper (⊗), and on the right side the polarization points out of the paper (⊙). (c) Liquid crystal which has cooled directly from the nematic phase to the smectic C* phase under an applied dc field. (d) Liquid crystal shown in Fig. 20(c) under a field of the opposite polarity applied after cooling.

3.5 Ionic Impurities

As with nematic liquid crystals, if there is a finite dc component to the field which is applied across a FLC cell it sweeps ions to the alignment layer interfaces and may degrade the device performance [Lagerwall et al. 1985, Mada and Suzuki 1987, Dijon et al. 1988a]. There are always ionic impurities in liquid crystals, and usually in concentrations which are electrically significant. As shown in Fig. 1, nematic liquid crystals may be driven with a pure ac field. FLCs, on the other hand, require a voltage of one polarity to switch them to one state and the other polarity to switch them to the other state. Ingenious schemes (described in Section 5) have been developed to balance the applied voltages so that the average applied dc voltage is zero. There is always, however, a time scale over which the net dc voltage is nonzero, and unfortunately significant ion motion often occurs during these periods. The effect of ionic impurities is important and has been one of the greatest impediments to commercialization of FLC devices. As measured by transient currents, there are ionic species having at least two mobilities, their generation appears to be field dependent, and they accumulate at surfaces within the cell [Chieu and Yang 1989].

One consequence of ionic drift may be thought of as being beneficial. When an SSFLC is in one stable state with an applied field of zero, the depolarization field, described in Section 3.3, sweeps ions to the alignment layer interfaces, causing the depolarization field to be screened [Dijon et al. 1988a, Escher et al. 1991]. In this way the ions reduce the instability caused by the depolarization field. In such a situation the time needed to establish one of the bistable states is not the FLC switching time (Eq. 1) but instead an ionic transit time on the order of milliseconds [Dijon et al. 1988a].

The deleterious effects are much greater [Yang et al. 1989]. With the application of a field of one polarity the ions drift in a direction to cancel the field, accumulating at the interfaces in tens of milliseconds [Vaxiviére et al. 1989, Maximus et al. 1991, Zou et al. 1991]. When the applied field is switched to zero these ions, which remain at the interfaces for a time which is long compared to the switching time of the SSFLC, add to the depolarization and can destroy bistability [Inaba et al. 1988]. Sufficiently conductive alignment layers can drain this additional depolarization charge and thus maintain bistability [Chieu and Yang 1990]. However, the ions sloshing around in the cell still at least partially screen an applied field, which can reduce the switching time and contrast ratio.

Some SSFLC shutter devices seem to remain operable even after application of a monopolar field for months. In other devices, such as the optically addressed spatial light modulators described in the following section, it is very difficult to balance the voltage across the FLC because of additional circuit elements which distort or rectify the applied voltage, even if it is balanced [Perlmutter et al. 1992]. Nevertheless, it is clearly desirable to balance the applied voltage to avoid the effects of long-term ionic accumulation. To both balance the time-averaged voltage and at the same time arbitrarily determine the ratio of on-to-off times the SSFLC must be bistable [Crossland et al. 1990].

4 OPTICALLY ADDRESSED SLMs

Optically addressed SLMs (OASLMs) can process information at a higher rate than electrically addressed SLMs because electrically addressed devices are limited ultimately by the rate at which the addressing information may be read from memory and by the

density of pixels which can be fabricated by lithography. In an OASLM the addressing information arrives in parallel, in the form of a write-light image, and in many OASLMs the density of pixels is limited only by the physical properties of the materials.

The write image is absorbed in a photosensor layer, which creates a spatially varying electric field that modifies the state of the modulating layer, encoding a replica of the write-light image. In the OASLMs discussed here the modulating layer is an FLC, which modulates a read light. In a reflection-mode OASLM the read light is incident on the side with the FLC. This beam is transmitted and reflected back through the FLC, emerging from the OASLM on the side from which it entered. In a transmission-mode OASLM, the read light emerges from the OASLM on the side opposite that from which it entered, passing through the modulating layer only once. It may be incident onto either side. To avoid having it write over the image on the OASLM, the read light must differ from the write light in wavelength, intensity or timing.

OASLMs which incorporate SSFLC or DHFLC light modulating layers and hydrogenated amorphous silicon (a-Si:H) photosensors exhibit response times on the order of 100 μs, spatial resolution on the order of 70 lp/mm at 50% MTF, write-light sensitivity on the order of 100 $\mu W/cm^2$, and a contrast ratio on the order of 20:1. Similar OASLMs incorporating ELCs have a response times which are an order of magnitude smaller.

4.1 Background

The practical liquid crystal OASLM was pioneered in 1972 by Hughes Research, and called a liquid crystal light valve [Beard et al. 1973]. (Because "light valve" is used for OASLMs, single-pixel optically addressed shutters, and electrically addressed SLMs, ambiguity is reduced by calling such devices OASLMs.) It incorporated a CdS photosensor and a twisted nematic liquid crystal. The most recently developed Hughes OASLMs incorporate an a-Si:H photoconductor [Sterling et al. 1990].

The feasibility of optically addressing SSFLCs was demonstrated by Armitage et al. using a bismuth silicon oxide (BSO) crystal as the photosensor [Armitage et al. 1987], and BSO and other crystalline semiconductors by Chigrinov et al. [Chigrinov et al. 1988]. The Colorado group proposed [Moddel et al. 1987] and demonstrated [Moddel et al. 1988] that a hydrogenated amorphous silicon (a-Si:H) photodiode could provide greatly improved performance. Takahashi et al. demonstrated a single-element optically addressed shutter based on the a-Si:H/SSFLC combination [Takahashi et al. 1987]. Williams et al. demonstrated a high-performance device using a single-layer a-Si:H photosensor [Williams et al. 1988], and the Colorado group showed high performance in a device utilizing an a-Si:H *p-i-n* photodiode [Li et al. 1989, Moddel et al. 1989]. A number of companies have developed improved SSFLC/a-Si:H OASLMs including Seiko Electronics [Yamamoto 1990, Yamamoto et al. 1991], NTT [Fukushima et al. 1990, Kurokawa and Fukushima 1992], STC Technology [Chittick et al. 1990], Mitsubishi [Horikawa et al. 1991], Matsushita [Akiyama et al. 1991], Greyhawk Systems [Bone et al. 1991], NEC [Gomes et al. 1991], and Displaytech. These devices have been characterized by several independent laboratories [Roe and Schehrer 1993, Hudson et al. 1991]. Special function devices, such as a variable-threshold three-terminal OASLM [Rice et al. 1989, 1992a], an OASLM incorporating thin film transistors [Tsujikawa et al., 1990], a self-powered OASLM [Mao et al. 1991b], and a GaAs/SSFLC OASLM that performs AND operations upon two sequential input signals [Hashimoto et al. 1992], have been developed. Other OASLMs, which incorporate a silicon integrated circuit active backplane, are described in Section 6.4.

Distorted helix ferroelectric liquid crystal (DHFLC) OASLMs were demonstrated by Beresnev et al. using a ZnCdS photosensor [Beresnev et al. 1988b], and by the Colorado group using an a-Si:H *p-i-n* photodiode [Landreth et al. 1991]. STC Technology incorporated electroclinic liquid crystals (ELCs) into an OASLM having a BSO photosensor [Collings et al. 1988], and the Colorado group coupled an ELC modulating layer to an a-Si:H *p-i-n* photodiode to obtain a very high speed OASLM [Abdulhalim et al. 1989].

4.2 Photosensor Structure and Operating Modes

Hydrogenated amorphous silicon was first used as an OASLM photosensor with a nematic liquid crystal [Samuelson et al. 1979], and has become the most commonly used photosensor in liquid crystal OASLMs [Moddel 1991a]. It combines the desirable characteristics of high photosensitivity, large area coverage, excellent spatial resolution, appropriate wavelength response, low-temperature deposition, low cost [Moddel et al. 1987], and higher speed [Barbier and Moddel 1992, Moddel and Barbier 1991b] than any currently available photosensor. It is usually deposited by plasma-enhanced chemical vapor deposition from silane and other gases. An a-Si:H/FLC OASLM is shown in Fig. 21.

The cross section of an a-Si:H/FLC OASLM is shown in Fig. 22. Optical flats are often used as the substrates to achieve the desired phase flatness and liquid crystal uniformity. To avoid multiple reflections in the flats which would reduce the spatial resolution they may be coated with an antireflection coating. Electrical power is supplied to the two TCO layers. In the reflection-mode device shown a reflector reflects the read light. The reflector is usually a dielectric stack, but may be a patterned metal mirror [Xue et al. 1992, Wu et al. 1994]. To provide high optical gain the read light is much more intense than the write light. A light blocking layer between the reflector and the photosensor provides additional isolation to the photosensor from the read beam, which might otherwise write. The first light blocking layers were CdTe [Beard et al. 1973].

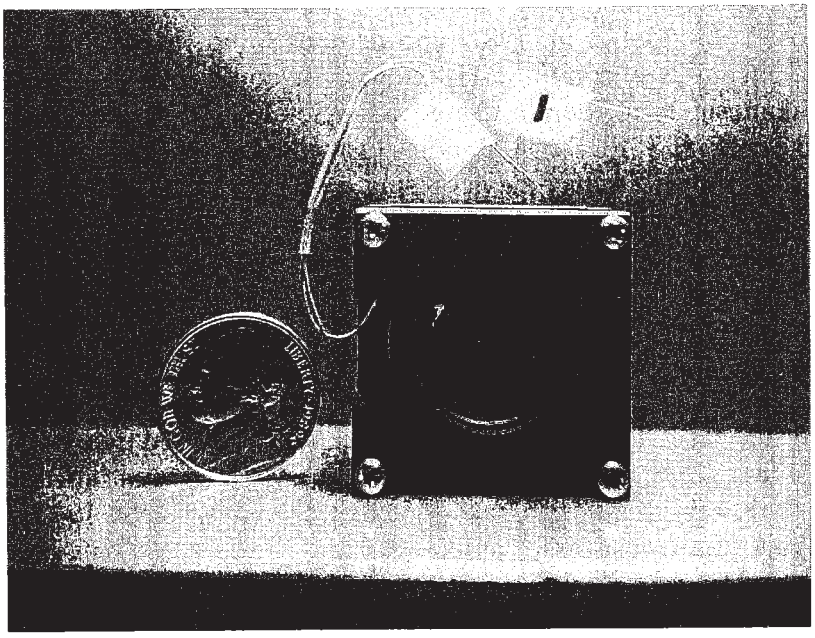

Figure 21 An a-Si:H/FLC OASLM prototype.

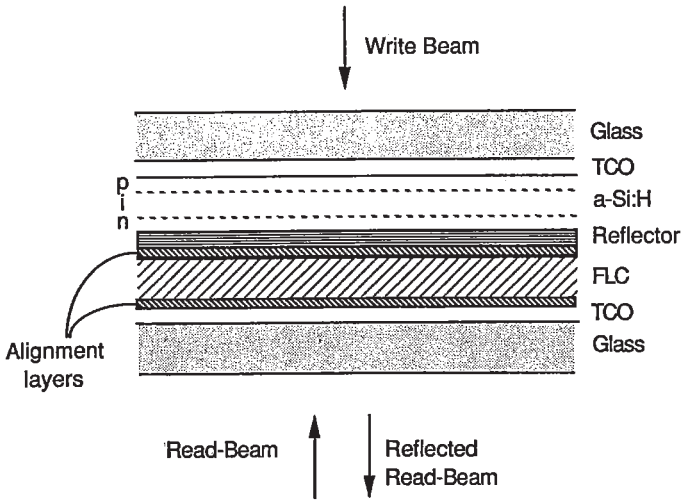

Figure 22 Cross section of an a-Si:H/FLC OASLM.

Reflection-mode test devices can be made without a reflector or light blocking layer as long as the read-light intensity is sufficiently low that it does not write. Reflection occurs due to the step in the index of refraction at the photosensor/liquid crystal interface. In a reflection-mode OASLM the FLC thickness is usually half that dictated by Eq. 2 because the read light passes through it twice.

Photodiode

The symmetric voltage response of nematic liquid crystals, shown in Fig. 1, matches the symmetric voltage response of a photoconductor. An ac voltage is applied across the combination, such that when the photoconductor is illuminated the voltage drops across the liquid crystal, switching it on. In the absence of a write light the voltage drops across the photoconductor and the liquid crystal relaxes to its off-state. Because FLCs respond to the polarity of the applied field, an asymmetry must be introduced into the driving scheme to switch them off without having to expose the photosensor to an erase light. Therefore a photodiode, with its asymmetric current-voltage characteristic, seems to be the natural mate for an FLC [Moddel et al. 1987].

Photodiodes may be formed from *p-i-n* structures, Schottky barriers, and MIS (metal-insulator-semiconductor) structures. In a *p-i-n* diode the doped *p*-layer blocks electrons from entering the intrinsic region through it from the adjacent TCO electrode. It is formed by doping a thin layer (~200 Å) of a-Si:H or a-SiC:H with boron during deposition. In a Schottky diode the barrier is formed by a metal or TCO [Drevillon et al. 1989] instead of a *p*-layer in contact with the intrinsic a-Si:H, but the reliability and barrier height of many Schottky barriers is inferior to those of *p*-doped layers. For a photodiode under reverse bias, when a photon is absorbed to produce an electron-hole pair in the intrinsic layer, the hole and electron are separated and drift to the *p*- and *n*-type contacts, respectively. The blocking contacts stop the carriers from being injected from the opposite contacts, so that once the carriers have been collected the response is complete. Because the electron is usually the more mobile carrier, the blocking by the *p*-layer is expected to be more important than blocking of holes by the *n*-layer. Therefore a *p-i* rather than a *p-i-n* diode often suffices. The photocurrent varies linearly with the light intensity over a wide range of intensities because one electron-hole pair is collected for each absorbed photon.

An equivalent circuit for a photodiode OASLM is shown in Fig. 23. Here the FLC is modeled simply as a resistance in parallel with a capacitor, rather than the more complicated and more accurate model of Fig. 6. The circuit is basically a diode (the photosensor) in series with a capacitor (the FLC). A reset-mode electrical driving scheme and ideal response are shown in Fig. 24. A square-wave voltage is applied to the TCO electrode that forms a contact to the a-Si:H, and the TCO layer that contacts the liquid crystal is grounded. With the application of a positive applied voltage, V_+, the photodiode is forward biased so that all the voltage drops across the FLC. This resets the FLC to a state which may be defined as off. The absence or presence of a write light does not affect the state of the liquid crystal significantly while a positive voltage is applied. With a negative applied voltage, V_-, the photodiode is reverse biased, blocking the current, so that ideally the voltage across the liquid crystal is unchanged. When a write light illuminates the photodiode, a photocurrent charges the FLC to a negative voltage, switching it on. This voltage is maintained across the liquid crystal until the drive voltage goes positive again, resetting the liquid crystal once more. Thus the reset (erase) operation occurs during the positive voltage period, and the write and read operations occur during the negative voltage period. The frame rate is the frequency of the electrical drive waveform.

In reality the photodiode OASLM cannot be modeled simply as a photodiode in series with a capacitor. We consider first the effect of the geometric capacitance associated with the photodiode, which can result in electrical switching of the FLC in the absence of a write light (dark switching). When the applied voltage is switched from V_+ to V_-, the change in the peak-to-peak voltage (V_{pp}) is divided between the photodiode

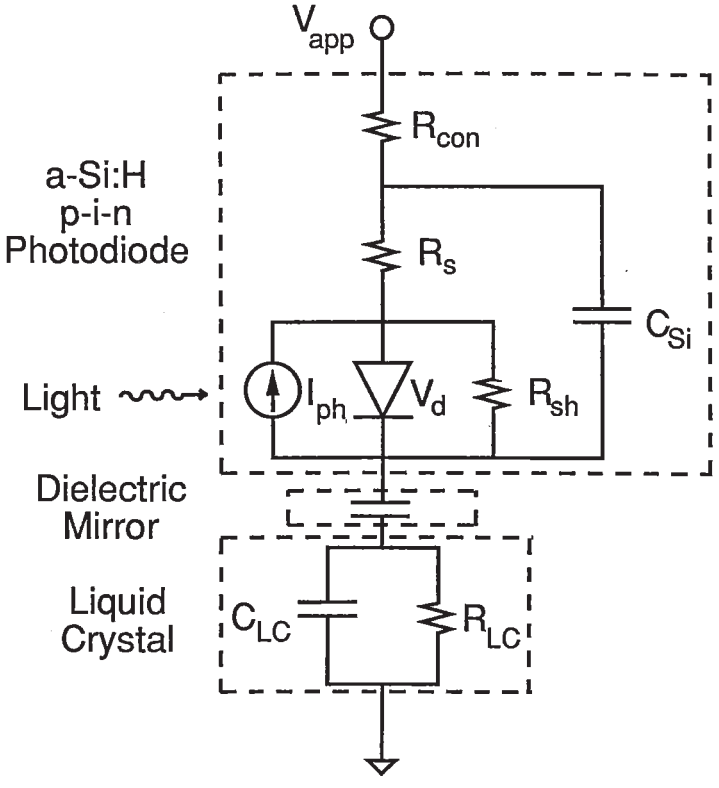

Figure 23 Equivalent circuit for a section of a photodiode OASLM.

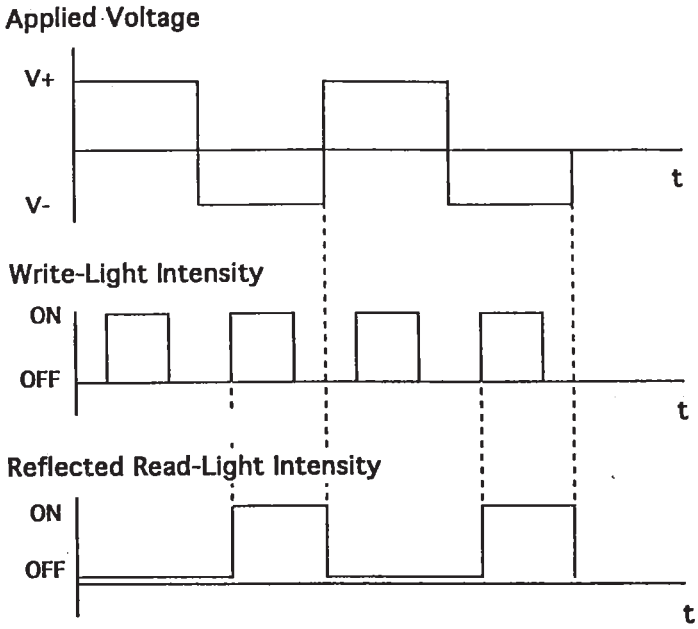

Figure 24 Ideal photodiode OASLM response in the reset mode. (Note that for the photodiode OASLM a negative voltage is defined as switching the device into the on state, consistent with polarity of the diode in Fig. 23.) (Adapted from W. Li, R. A. Rice, G. Moddel, L. A. Pagano-Stauffer, and M. A. Handschy, *IEEE Trans. Electron Dev.*, *36*, 2959–2964 (1989).)

and the FLC because of the capacitances associated with each of these elements. The instantaneous change in the voltage across the liquid crystal is [Moddel 1991a]

$$\Delta V_{LC} = -\frac{C_{GSi}}{C_{GLC} + C_{GSi}} V_{pp} \tag{5}$$

where C_{GSi} and C_{GLC} are the geometric capacitances associated with the a-Si:H photodiode and the FLC, respectively. If ΔV_{LC} is too large dark, switching occurs. Since C_{GSi} is inversely proportional to the photodiode thickness, to keep the magnitude of ΔV_{LC} small the photodiode must be sufficiently thick. In addition the applied square-wave voltage may be biased positive [Li et al. 1989]. Too large of a positive bias, however, severely unbalances the average voltage across the FLC and increases degradation due to ionic impurities.

The effect of photodiode thickness is shown in Fig. 25. A thin photodiode has a large capacitance, so that most of applied voltage is dropped across the liquid crystal during the write (negative applied voltage) period, even in the absence of write light. This large negative voltage across the liquid crystal results in unacceptable dark switching. A thick photodiode, on the other hand, has a small capacitance, so that most of the applied voltage is dropped across it rather than the liquid crystal during the write period. The beneficial consequence is that there is no dark switching, but this comes at a cost. As can be seen for the period during which the write light is on, a substantial fraction of the photocurrent is required just to drive the voltage across the liquid crystal down to zero volts. Thus the sensitivity of the device suffers. An optimal thickness for the photodiode corresponds to the case when G_{GSi} is approximately equal to C_{GLC} [Barbier and Moddel 1992].

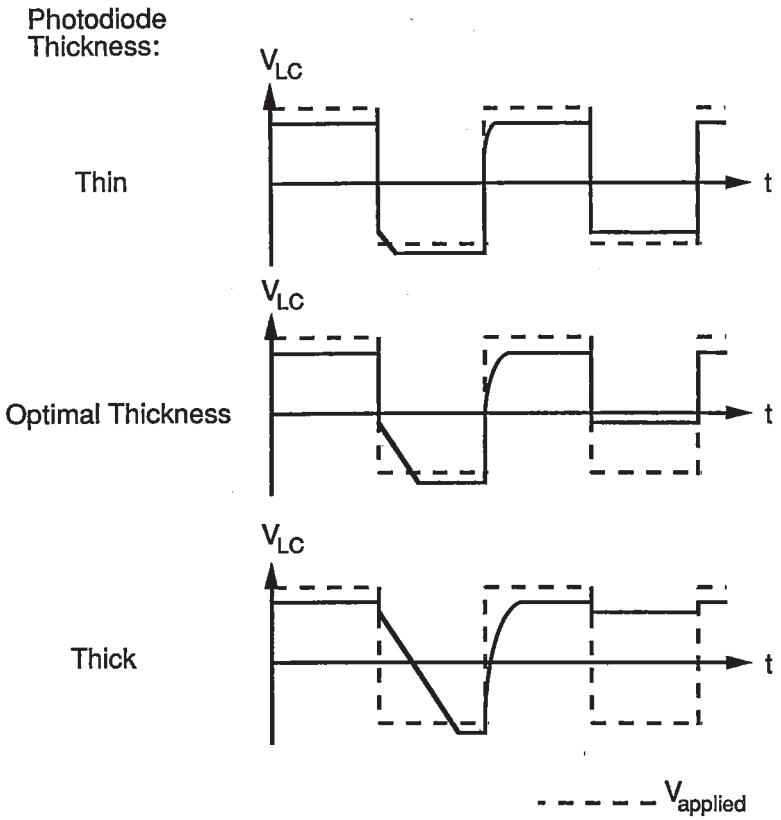

Figure 25 The effect of photodiode thickness on the voltage dropped across the liquid crystal (V_{LC}), showing the applied voltage (dashed line) and the voltage dropped across the liquid crystal (solid line). The write light is on only during the first write (negative applied voltage) period.

Another factor which affects the performance of the OASLM is the series resistance (R_s), which limits the erase time. Under forward bias the current varies superlinearly with voltage due to double injection from the *n* and *p* layers in the photodiode. This produces a voltage-dependent R_s, and limits the frame rate of the OASLM to approximately 100 kHz at room temperature [Barbier and Moddel 1992, Moddel and Barbier 1991b]. As mentioned earlier, a *p-i* diode rather than a *p-i-n* diode often suffices, but without an *n* layer the electron injection may be reduced. In such a case there is only limited double injection and R_s is increased, increasing the erase time, particularly in thick (>2.5 μm) photodiodes.

There is a residual charge which remains in the photodiode after the termination of illumination and subsequently leaks out under reverse bias. Because the shunt resistances associated with the FLC and the photodiode drain this charge, it does not present a significant problem, and the OASLM may be operated down to frame rates of 0 Hz [Barbier and Moddel 1992, Moddel and Barbier 1991b].

In the reset mode, described above, the liquid crystal can respond fully to the voltage level during each part of the drive period, and the device is reset fully to its off-state during the forward-bias part of each period. By driving the OASLM at a higher frequency, an integrating mode is obtained in which the readout response extends over several driving periods [Gabor et al. 1993]. The rise and fall of the output in response to a pulse of write light occur over several driving periods, during which the liquid crystal responds to the time-averaged field. The integrating-mode operation can be understood

by considering the time-averaged voltage across the FLC, shown as the dashed lines in Fig. 26. When the write light illuminates the photodiode the time-averaged voltage is negative, switching the FLC on. In the absence of a write light the time-averaged voltage becomes positive, switching the FLC off. As shown in Section 4.3, a continuous gray-level response is obtained, but at the cost of sensitivity and response time when compared to the reset mode. The reset mode is in effect for frame rates of approximately 1 kHz and lower, and the integrating mode for approximately 10 kHz. At much higher frequencies the reactive part of the impedances of the capacitances associated with the photodiode and the FLC become sufficiently small that the effect of the write light is negligible, and the OASLMs can no longer be optically addressed.

Because of its highly nonlinear current-voltage characteristic the photodiode presents an unbalanced voltage to the combination of the FLC and the reflector. Even if the applied voltage were biased to provide a balanced voltage with no write light, the presence of a write light would shift the time-averaged voltage and unbalance it. A perfectly insulating dielectric stack reflector (or alignment layer) absorbs the dc component of the voltage and does provide a balanced voltage to the FLC, but when the write light is switched on or off a transition period occurs during which the voltage across the dielectric varies. During this period, which is an RC decay time where R is a function of the FLC and photosensor resistances, the sensitivity and threshold of the OASLM vary. The RC product must be sufficiently small for this transition to occur quickly compared to the drive period.

Photoconductor

By introducing an asymmetry in the driving scheme, a photoconductor can be mated with an FLC to form an OASLM [Moddel et al. 1987]. To form a photoconductor the contacts to the a-Si:H must be ohmic, such that the potential drop across the contact regions is small compared to that across the bulk. In a sandwich structure this usually requires that layers of heavily phosphorus-doped n-type ($n+$) a-Si:H lie between the bulk of the a-Si:H and the electrodes, providing ohmic contacts for electrons, which usually dominate the photoconductivity. One indication for ohmic contacts, and hence the formation of a photoconductor as opposed to a photodiode, is a linear and symmetric

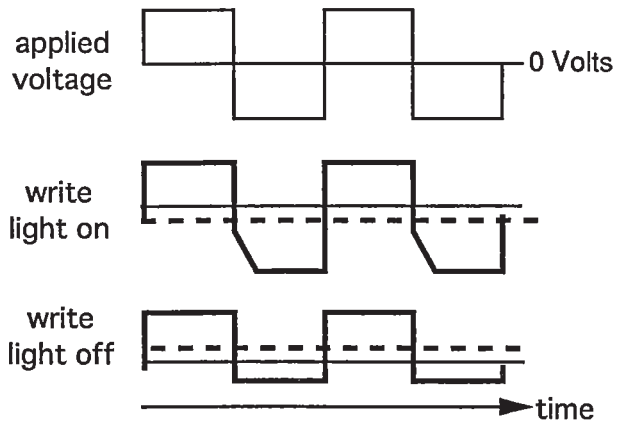

Figure 26 Integrating mode operation. The instantaneous (thick solid line) and time-averaged (dashed line) voltage which is dropped across the liquid crystal is plotted as a function of time for the case in which the write light on and the case in which it is off. (Adapted from A. M. Gabor, B. Landreth, and G. Moddel, *Appl. Opt.*, *32*, 3064–3067 (1993).)

current-voltage characteristic. When intrinsic a-Si:H is deposited directly on a transparent conducting oxide, at least partially blocking Schottky barrier contacts often result [Drevillon et al. 1989], as described in the previous section on photodiodes. It is very difficult to obtain a truly ohmic contact to intrinsic a-Si:H. Many of the intrinsic a-Si:H photosensors for OASLMs are described as photoconductors, but perhaps could better be described as "photoconductive diodes," as their characteristics are between those of a photodiode and a photoconductor [Barbier et al. 1994]. Their current-voltage characteristics are more nearly symmetric than those of a photodiode, and the magnitudes of their dark current are lower than those of a photoconductor. This is significant because without a truly symmetric current-voltage characteristic it is impossible to perfectly balance the time-averaged voltage across the FLC, and ionic charge buildup can result.

In a photoconductor, when a photon is absorbed and produces an electron-hole pair in an applied field, the electron drifts to a contact. As it exits the semiconductor another electron is injected from the opposite contact to preserve space-charge neutrality. This occurs many times until the electron and hole recombine. Thus one absorbed photon may cause the passage of many charges. The ratio of the number of charges collected by the contact to the number of photogenerated electron-hole pairs is the photoconductive gain. This gain equals the recombination time divided by the transit time, the time it take the carrier to drift from one contact to the other, and can be ~1000 in an a-Si:H sandwich structure. Because the recombination time and hence the gain often decreases with increasing light intensity, the photocurrent may not vary linearly with the intensity.

An equivalent circuit for a photoconductor OASLM is shown in Fig. 27. As in Fig. 23 the FLC is modeled simply as a resistance in parallel with a capacitor, rather than the more complicated and more accurate model of Fig. 6. The photoconductor is simply a variable resistance in parallel with a geometric capacitance.

A straightforward operating mode for a bistable SSFLC/photoconductor OASLM is shown in Fig. 28. The photoconductor must be illuminated during the reset (erase)

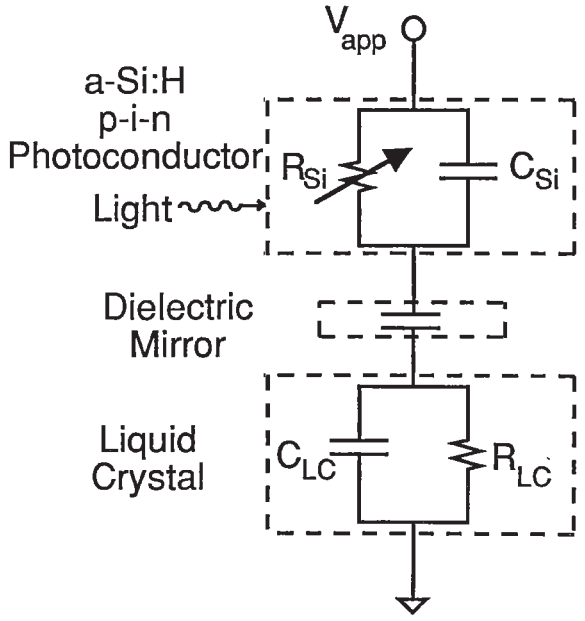

Figure 27 Equivalent circuit for a section of a photoconductor OASLM.

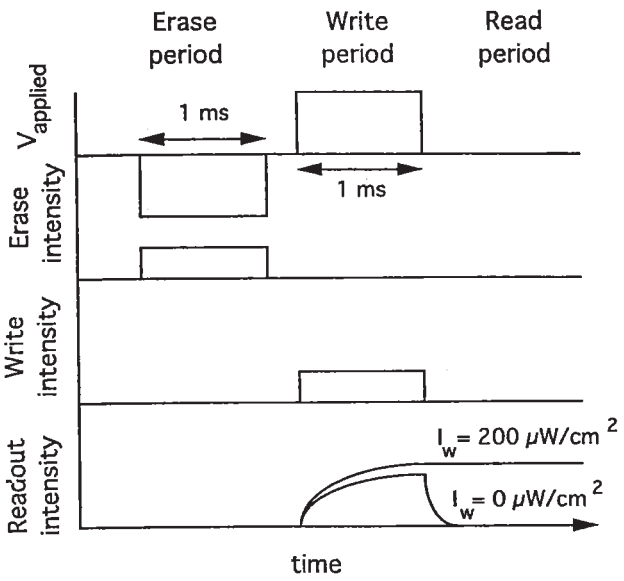

Figure 28 Basic operating mode for a bistable SSFLC OASLM in which the photosensor has symmetric current/voltage characteristics. (Adapted from S. Fukushima, T. Kurokawa, S. Matsuo, and H. Kozawaguchi, *Opt. Lett.*, *15*, 285–287 (1990).)

period when a negative voltage is applied to the OASLM. The intensity of illumination during the write period, when a positive voltage is applied, determines whether the liquid crystal attains its stable on-state. If the illumination is insufficient, the device switches off during the read period, during which zero volts is applied. A negative image may be obtained by reversing the polarities described above during the reset and write periods [Fukushima et al. 1990, Kurokawa and Fukushima 1992]. An ac stabilization voltage may be applied in series with the lower frequency drive voltage to enhance bistability [Yamamoto et al. 1991].

A disadvantage of the simple driving mode described above is that it does not balance the voltage across the liquid crystal (unless the reset light is on only during reset periods that follow write periods during which the write light was on), and also that it requires the photosensor to be illuminated during reset period. A driving scheme which avoids these problems is shown in Fig. 29. After the larger positive and negative voltage pulse pair have been applied, the SSFLC is reset, switching off because the later pulse is negative. It is reset even in the absence of write-light illumination because the magnitude of the voltage is sufficiently large that the capacitively coupled field switches the SSFLC. This is not the case for the smaller negative and positive voltage pair. It leaves the SSFLC in an on-state only if the write light is on, allowing sufficient current to flow to the SSFLC to switch it on. With this driving scheme the voltage is balanced as long as the photoconductor has a truly symmetric current-voltage characteristic.

There are several problems with a-Si:H photoconductor OASLMs with truly ohmic contacts. If the write light does not illuminate the entire thickness of the photoconductor there is a resistive layer in series with the photoconducting layer which blocks the current. Therefore the write light must be of a wavelength which is uniformly, and therefore weakly, absorbed in the photoconductor, approximately 750 nm for a-Si:H [Sterling et al. 1990]. Alternatively, the photoconductor may be sufficiently thin, generally less than 0.5 μm for visible light, for the write light to illuminate it uniformly [Chevrier et al.

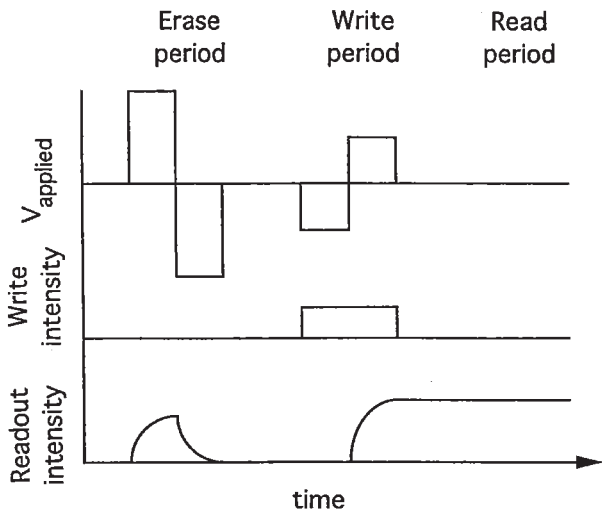

Figure 29 Operating mode that provides a time-averaged voltage of zero to the SSFLC for a bistable SSFLC OASLM in which the photosensor has symmetric current/voltage characteristics.

1991], but this would cause capacitively coupled voltage problems [see Eq. 5]. Another problem involves the dark current, which must be sufficiently low that it not switch the device within a frame time. This would require the a-Si:H film to be much thicker than 30 μm for video frame times [Chevrier et al. 1991], which is unreasonably thick. Even if very resistive a-Si:H were used to make the photoconductor thinner, injected charge would dwarf any photoconductive effect. Therefore incorporating genuine photoconductors into FLC OASLMs is not feasible [Barbier et al. 1994].

Back-to-Back Photodiodes

An approach to combining the low leakage current of the photodiode and the symmetry of the photoconductor is to use a back-to-back photodiode structure [Chevrier et al. 1991, Cambon et al. 1991]. An a-Si:H photosensor is deposited in a *n-i-p-i-n* configuration and incorporated with an SSFLC into an OASLM. When a voltage of one polarity is applied, one photodiode is reverse biased and the other is forward biased. Reversing the polarity reverses the bias sense on each photodiode. In both cases the current is limited by the reverse-biased diode, and thus by the write light which illuminates it. The operating mode for the back-to-back photodiode OASLM is similar to that of the photoconductor OASLM.

The first diode must be sufficiently thin that the write light is only partially absorbed in it and penetrates to the second diode. This requirement affects the performance in that the large capacitance associated with the thin diode results in a large voltage which is capacitively coupled to the SSFLC. This limits the operating range of the device.

Back-to-back photodiodes can also be used to provide a color-sensitive subtracting OASLM [Barbier and Moddel 1993]. In such a device a *p-i-n-i-p* configuration is deposited with the first *p-i-n* diode being much thinner than the second *n-i-p* diode. When a negative voltage is applied to the OASLM, short-wavelength (e.g., green) light is absorbed dominantly in the first, reverse-biased *p-i-n* photodiode and produces a photocurrent that tends to switch on, or excite, the SSFLC. When a positive voltage is applied to the device, long-wavelength (e.g., red) light is absorbed dominantly in the second, reverse-biased *n-i-p* photodiode, and produces a photocurrent that tends to

switch off, or inhibit, the SSFLC. Because the excitation and inhibition lights are absorbed dominantly at different depths corresponding to different photodiodes in the device, they may illuminate the device continuously, such that the difference in their intensities determines how much inhibition or excitation occurs. A different approach to image subtraction is to use a single-layer photosensor and synchronize the excitation and inhibition lights to periods of opposite polarity in the electrical drive [Robinson 1992].

Three-Terminal OASLM

In a three-terminal OASLM a third terminal, in addition to the two TCO electrodes, provides dynamic control of the optical threshold and continuous operation [Rice et al. 1989]. The third terminal is connected to the continuous metal layer, shown in Fig. 30. To operate the device, a negative dc voltage is supplied to the TCO layer adjacent to the photodiode, a positive dc voltage to the continuous metal, and the other TCO layer is grounded. When a write light illuminates the a-Si:H photodiode above a pixel the metal disk is pulled to a negative voltage, switching the pixel on. When the write light is switched off the charge on the metal disk leaks through the a-Si:H across the annulus to the continuous layer until the spot is pulled to a positive voltage, switching the pixel off. This provides for continuous operation as opposed to that for the alternating drive modes described in previous sections. Another feature of this device is the ability to vary the threshold by varying the positive voltage applied to the continuous layer [Rice et al. 1992a], useful in image processing applications.

There are advantages and disadvantages to an OASLM which is patterned. The patterned metal pixels [Xue et al. 1992], in this case disks and in other cases squares [Wu et al. 1994], can provide well-defined areas which cannot wander across the device, which is important in applications in which the data is in the form of discrete elements. A disadvantage is that the spatial resolution is limited by the metal pattern. In addition, the read light is diffracted from the pixel array. For applications involving the Fourier transform of the reflected read light, the image appearing in the Fourier plane includes a pattern corresponding to the Fourier transform of the metal array in addition to that of the write-light image.

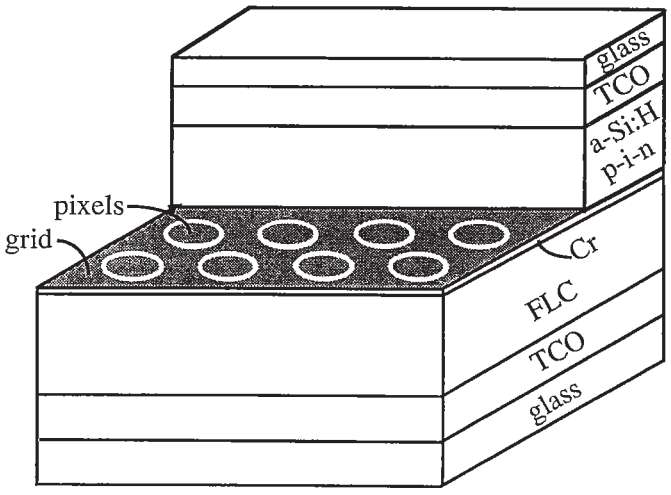

Figure 30 Three-terminal OASLM. (From R. A. Rice, G. Moddel, I. Abdulhalim, and C. M. Walker, *J. Non-Cryst. Solids*, *115*, 96–98 (1989).)

Self-Powered OASLM

Generally the photodiode in an OASLM is under reverse bias during the write operation, but if instead the device is short-circuited the photodiode operates in a photovoltaic mode, converting the write light into electric power. To obtain a sufficiently high voltage to fully switch an FLC a photovoltaic stack is used, as shown in Fig. 31 [Mao et al. 1991b]. The photodiodes are progressively thicker so that each produces the same photocurrent when the stack is illuminated through the thinnest layer, and the series combination produces 3 V. The shunt resistances in the photodiode and the FLC are important in allowing the device to switch off quickly, with charge draining through one or both of the resistances. Because the output voltage of the photovoltaic stack is monopolar, a bistable SSFLC would not switch off. Therefore the asymmetric bistable SSFLC described in Section 3.4, in which the hysteresis curve is shifted in voltage, is required [Zou et al. 1992]. Alternatively, a dc offset can be supplied to the OASLM to aid in switching the device off [Mao et al. 1991b].

4.3 Optical Response

Sensitivity and Response Time

The optical response of an OASLM may be measured with the apparatus shown in Fig. 32. A pulse/delay generator provides signals to synchronize a pulse generator, an acousto-optic modulator, and an oscilloscope. The pulse generator provides the periodic electrical drive to the OASLM. The acousto-optic modulator controls the write light from an argon ion laser. The only reason that a laser is used to produce the write light is that it provides a beam which may be modulated conveniently with an acousto-optic modulator. A lamp and color filter, or another laser, provides a read light which passes through the polarizer,

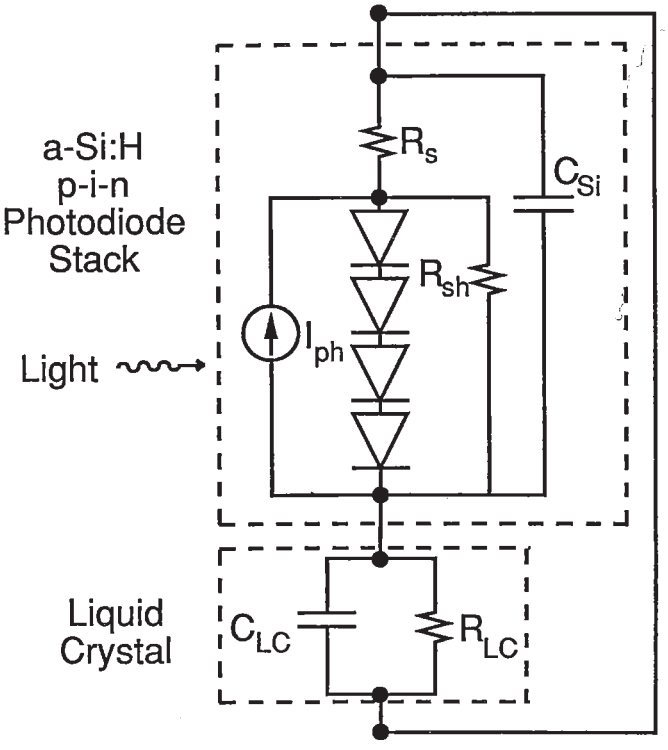

Figure 31 Equivalent circuit for a section of a self-powered OASLM.

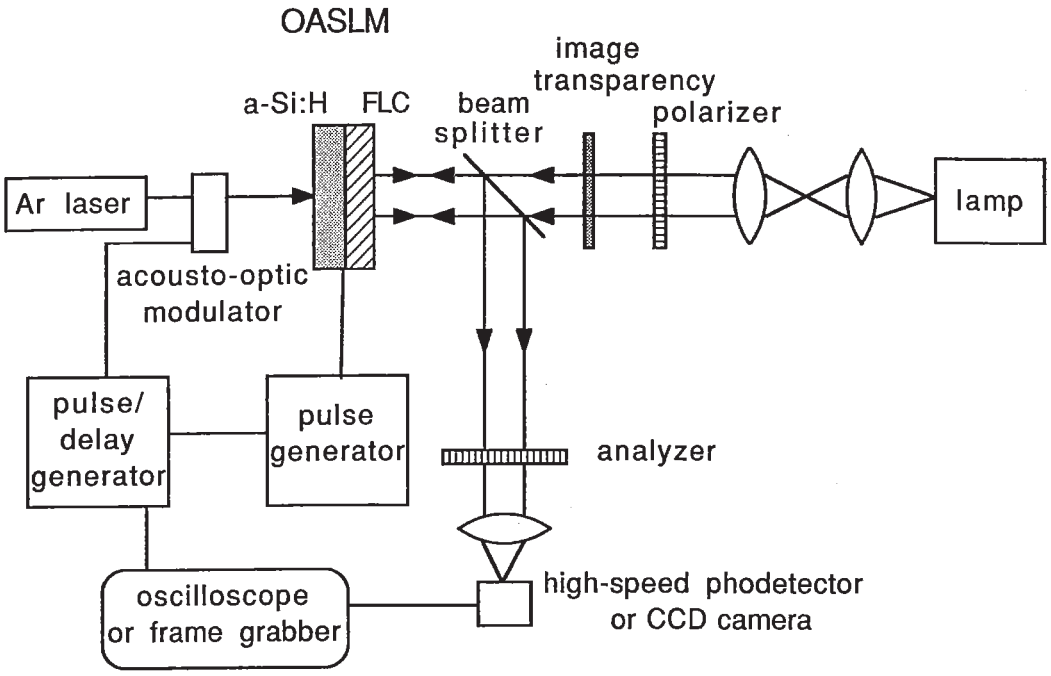

Figure 32 Measurement apparatus for the OASLM response.

reflects through the liquid crystal, passes through the analyzer which is crossed with respect to the polarizer, and is detected with a photodetector. If a polarizing beamsplitter is used in place of the polarizer, nonpolarizing beamsplitter, and analyzer, then more of the reflected beam is collected, but the separately rotatable polarizer and analyzer give added flexibility to cancel the effects of liquid crystal nonidealities.

From Eq. 1 it can be seen that the response time is a function of the spontaneous polarization and viscosity of the FLC and of the applied field. In an OASLM the applied field increases as charge passes through the photosensor and accumulates at the interface between the photosensor and the reflector, or if there is no reflector, at the FLC alignment layer. The minimum write-light energy required to completely switch an SSFLC OASLM is

$$E_{\min} = \frac{2Ph\nu}{\eta_{\text{col}} e} \tag{6}$$

where P is the spontaneous polarization, $h\nu$ is the write-light photon energy, and η_{col} is the collection efficiency or gain of the photosensor. For $P = 30$ nC/cm^2, $\eta_{\text{col}} = 1$, and $h\nu = 2$ eV, the minimum write-light energy is 120 nJ/cm^2.

As the write-light intensity is increased the switching time decreases until it saturates at an intensity that is sufficiently great to charge the interface to the applied voltage before the FLC switches. The minimum write-light energy required to switch the FLC as fast as possible is approximately twice the minimum write-light energy [Moddel 1991a]. The shortest response times for a given device depend upon the properties of the FLC and the alignment layers, and are typically from tens to hundreds of microseconds.

A write-light intensity of approximately 100 μW/cm^2 is required to switch a typical SSFLC OASLM operating at a frame rate of 1 kHz, and the saturation intensity is a few mW/cm^2. The intensities required vary greatly with the integration time (i.e., the frame rate), and with the FLC and photosensor properties. For a photodiode SSFLC

OASLM the response time is shorter in the reset mode than in the integrating mode, as can be seen from Fig. 33.

The response times for DHFLC OASLMs are similar to those of SSFLC OASLMs. For ELCs the response time is a strong function of temperature. Fig. 34 shows the response of an ELC OASLM as a function of temperature for a liquid crystal which undergoes a SSFLC to ELC phase transition at 28°C.

Transfer Characteristics

The contrast ratio is the ratio of the read-light output intensity for the device in the on-state (I_{on}) to that in the off-state (I_{off}):

$$CR \equiv \frac{I_{on}}{I_{off}} \tag{7}$$

As measured over the entire device when it is switched, the CR is a function of the optical quality of the liquid crystal, and its uniformity over the measured area. For example, an SSFLC for which the CR is above 1000 over an area of 1 mm^2 may yield a CR of 100 when averaged over a 1-cm^2 area. This is due to variations in I_{off} at different locations on the device.

The intensity modulation [Hecht 1987], useful in measuring the fractional change in the output of a device, is

$$M \equiv \frac{I_{on} - I_{off}}{I_{on} + I_{off}} = \frac{CR - 1}{CR + 1} \tag{8}$$

The intensity transfer characteristics relate the read-light output intensity to the write-light input intensity. Binary transfer characteristics are usually desired for thresh-

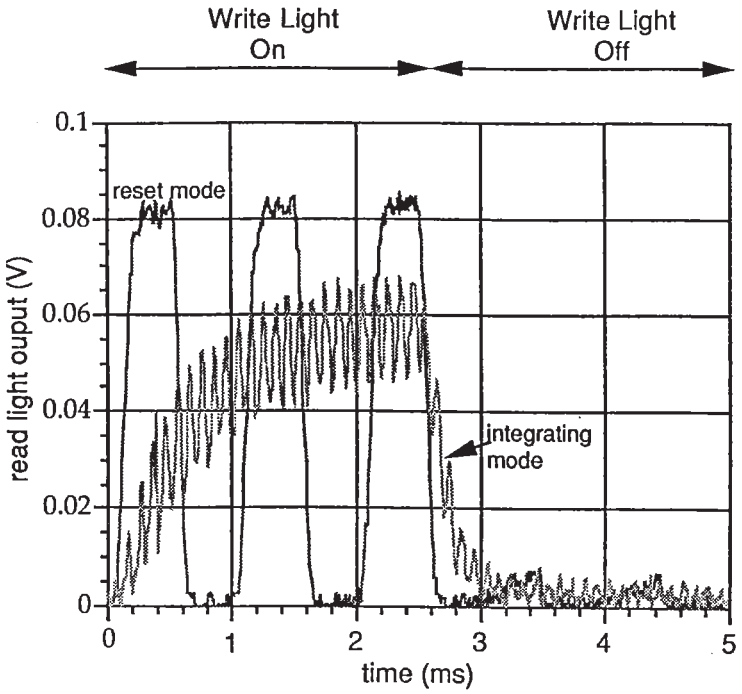

Figure 33 The response of a photodiode SSFLC OASLM in the reset (1-kHz electrical drive frequency) and integrating (10-kHz) modes. The write light is on from $0 < t < 2.5$ ms. (Adapted from A. M. Gabor, B. Landreth, and G. Moddel, *Appl. Opt.*, *32*, 3064–3067 (1993).)

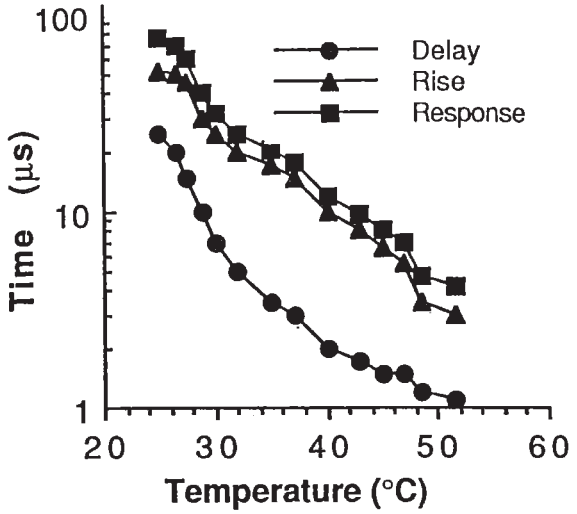

Figure 34 The delay, rise, and response times as a function of temperature for and electroclinic liquid crystal OASLM. (From I. Abdulhalim, G. Moddel, and K. M. Johnson, *Appl. Phys. Lett.*, *55*, 1603–1605 (1989).)

olding, while analog or gray-level transfer characteristics are often desired when thresholding is not required.

As a natural consequence of their bistability SSFLCs are fundamentally binary in that domains switch from one stable state to the other, but gray levels may be obtained by several approaches, as described in Section 2.2 under "Gray Levels." In OASLMs gray levels have been obtained by charge control, with the optical output spatially averaged over many domains [Killinger et al. 1991, 1992, Gomes et al. 1991]. Another approach, using temporal averaging, is based upon the fact that the switching time is a function of the applied field which, in turn, depends upon the write-light intensity [Landreth and Moddel 1990, 1992], as can be seen in Fig. 35. The temporal average correlates

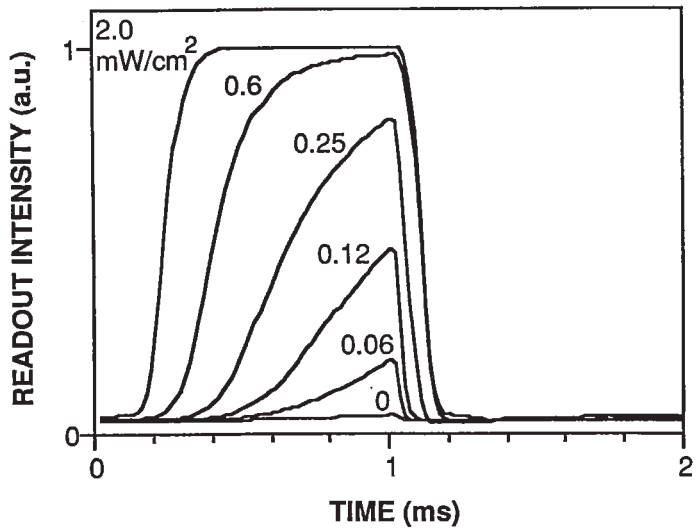

Figure 35 Readout intensity for several write-light intensities as a function of time for a photodiode SSFLC OASLM. The write period (negative bias) occurs between 0 and 1 ms, and the reset period (positive bias) occurs between 1 and 2 ms. (From B. Landreth and G. Moddel, *Appl. Opt.*, *31*, 3937–3944 (1992).)

to the response of the eye or a CCD video camera, which is an integration over many OASLM drive cycles. In Fig. 36 the time-integrated intensity transfer characteristic is shown, exhibiting a gray-level response in which the sensitivity is a function of the electrical driving frequency. A combination of the two approaches can be used to provide a range of gray levels at video rates [Bone et al. 1991].

For DHFLCs and ELCs not only the average response but also the terminal response is analog. The terminal response is the steady-state read-light output intensity under a constant reverse bias after the application of a limited-duration write light. This terminal response is shown as a function of write-light energy in Fig. 37. The liquid crystal of Fig. 37 undergoes a SSFLC-to-ELC phase transition at 28°C [Abdulhalim et al. 1989]. The curve for the SSFLC at 25°C exhibits a sigmoidal shape, characteristic of a binary response. The intermediate modulation values are due to the spatial averaging of binary domains, limited in their switching by charge control. For the higher-temperature curves there is a range over which the read-light modulation is proportional to the write-light energy, providing gray levels.

4.4 Spatial Resolution

Measurement of the Spatial Resolution

One method to measure the resolution is to write a resolution-target image, composed of dark and light lines having different separations, onto the OASLM and to observe the image formed from the reflected read light. This may be done with the apparatus of Fig. 32 by placing a resolution target in the path of the write beam and focusing it onto the OASLM photosensor. The photodetector is replaced by a CCD video camera. The finest lines which can be discerned on the CCD camera image correspond roughly to the spatial resolution of the OASLM. An example of such an image, photographed from a video display, is shown in Fig. 38.

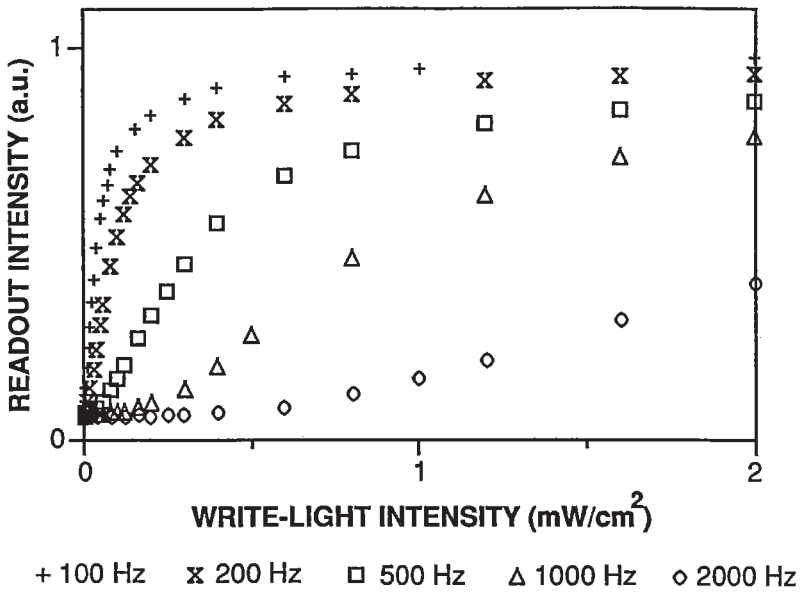

Figure 36 Photodiode SSFLC OASLM time-integrated intensity transfer characteristic vs. write-light intensity for several electrical drive frequencies. The data were obtained from numerical integration of transient responses including those shown in Fig. 34. (From B. Landreth and G. Moddel, *Appl. Opt.*, *31*, 3937–3944 (1992).)

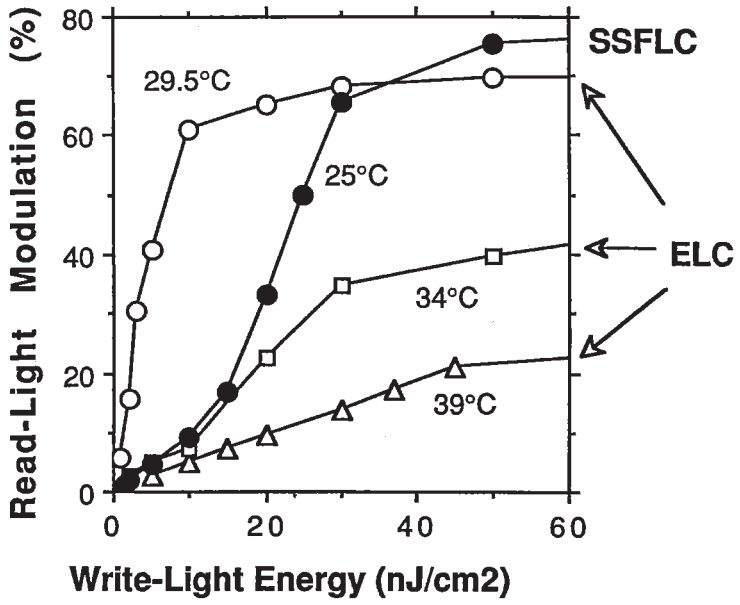

Figure 37 Terminal read-light modulation as a function of write-light energy for different temperatures, for a liquid crystal which undergoes a SSFLC-to-ELC phase transition at 28°C. (Adapted from I. Abdulhalim, G. Moddel, and K. M. Johnson, *Appl. Phys. Lett.*, *55*, 1603–1605 (1989).)

This method is useful for determining the resolution and image quality for display applications, but it has several drawbacks. It does not provide a quantitative measure of how the image quality rolls off with increasing spatial frequency. Another drawback is related to how the eye discerns an image. The eye integrates over the entire length of the bar which grossly overestimates the resolution from bar-shaped test patterns [Rose and Weimer 1989].

A more quantitative method to determine resolution is to measure the diffraction efficiency. A fringe pattern from a Michelson interferometer is written on an OASLM. A read beam is diffracted from the liquid crystal, and the intensity of the first diffracted order is measured as a function of writing spatial frequency. The diffraction efficiency may be converted to a modulation transfer efficiency.

MTF for a Nonlinear SLM

The modulation transfer function (MTF) is a measure of the capability of a device to replicate spatial frequency components from its input to its output. Although the MTF is most applicable to devices with linear intensity transfer characteristics, it is commonly reported as a measure of the spatial resolution of OASLMs.

The MTF is essentially the modulation, defined in Eq. 8, as a function of the spatial frequency (f_x). Often the relative MTF, which is normalized to unity at $f_x = 0$, is plotted as a function of f_x [Roach 1974], where

$$\mathrm{MTF}_{\mathrm{rel}}(f_x) = \frac{1}{M(f_x \to 0)} \frac{I_{\mathrm{on}}(f_x) - I_{\mathrm{off}}(f_x)}{I_{\mathrm{on}}(f_x) + I_{\mathrm{off}}(f_x)} \tag{9}$$

I_{on} and I_{off} are measured at positions of maximum and minimum intensity, respectively. Although a curve of $\mathrm{MTF}_{\mathrm{rel}}$ provides less information than one of the absolute MTF, it is sometimes difficult to determine the absolute magnitude.

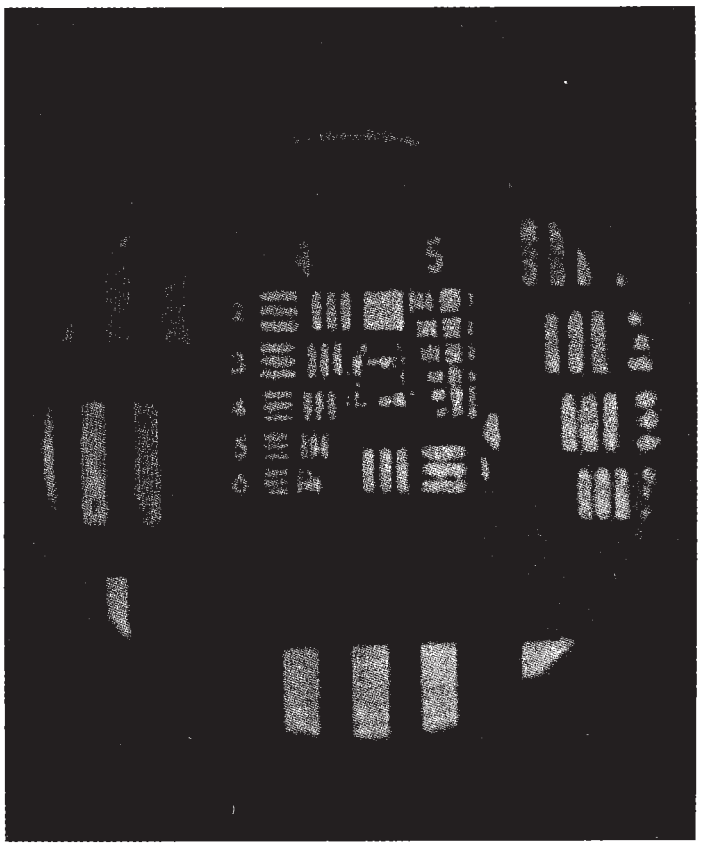

Figure 38 Photograph of a U.S. Air Force resolution target reproduced by an a-Si:H photodiode/SSFLC OASLM, exhibiting a resolution of 40 lp/mm. (From G. Moddel, K. M. Johnson, W. Li, R. A. Rice, L. A. Pagano-Stauffer, and M. A. Handschy, *Appl. Phys. Lett.*, *55*, 537–539 (1989).)

Unfortunately the MTF curve may include some ambiguity because it is well defined only for linear systems. If the OALSM transfer characteristic is nonlinear, which is usually the case of SSFLC OASLMs (see Fig. 36), the readout fringes are distorted replicas of the written fringes. This is true even if their spatial frequency is well within the resolution of the OASLM. The response at the peaks of the fringes may be saturated while the response in the valleys is approximately linear. Because the diffraction pattern depends on both the shape and the visibility of the readout fringes, spatial distortions due to the nonlinear intensity transfer characteristic of the OASLM affect the resultant MTF curve. In cases where the write-light fringes are of nonunity visibility (i.e., the intensity in the fringe valleys is not absolutely zero) erroneous conclusions can be drawn. Thus the falloff in the intensity of the diffracted light with spatial frequency is a function of both extrinsic, measurement related, effects, and intrinsic resolution loss mechanisms in the OASLM which are genuinely due to limitations in the device. Examples of intrinsic processes which can reduce the effective visibility of the write-light fringes within the device are field spreading within the liquid crystal, charge spreading laterally within the photosensor, and stray light from multiple refections in the substrates.

One might be led to believe that the spatial resolution of an OASLM falls off at high write-light intensities because the first-order diffraction efficiency has fallen off with intensity. The correct interpretation might be that the falloff in measured diffraction efficiency is partially due to spatial distortions in the shape of the output fringes. The

readout intensity in the valleys has increased with the increased write-fringe intensity, but the readout intensity of the peaks has not increased accordingly because the device has saturated. It does not necessarily follow that the spatial resolution of a truly binary input pattern would decrease under similar conditions.

A procedure has been developed to account for the nonlinear intensity transfer characteristic of an OASLM in deriving MTF curves [Landreth and Moddel 1992]. The procedure is somewhat arduous, but it allows one to distinguish between resolution loss mechanisms which are intrinsic to the device from those which result from an interaction between the nonlinearity of the device and measurement conditions. In the procedure the reduction in fringe visibility by the OASLM from input to output is modeled as a two-step process consisting of a (i) linear reduction in the visibility, followed by (ii) a nonlinear intensity transfer operation based on the experimentally measured transfer characteristic (Fig. 36).

The procedure to derive MTF curves from the diffraction data is made up of the following five steps. The first three steps are carried out before the diffraction efficiency data are consulted.

Step 1. The write-fringe intensity is assumed to be of the form

$$I_i(\mathrm{x}) = \frac{I_0}{2}[1 + m_i \cos(2\pi f_x x)] \tag{10}$$

where I_0 is the peak intensity of the write fringes, m_i is the visibility of incident write fringes, and x is a spatial coordinate in the plane of the OASLM active layers. The first process which reduces the resolution is assumed to depend only upon spatial frequency. A linear reduction of the visibility is performed using a modulation reduction parameter m_r ($0 \leq m_r \leq 1$). After this reduction of the visibility the effective write-light intensity pattern becomes

$$I_e(\mathrm{x}) = \frac{I_0}{2}[1 + m_i m_r \cos(2\pi f_x x)] \tag{11}$$

Given values for I_0 and m_r the $I_e(\mathrm{x})$ is computed.

Step 2. A point-by-point nonlinear intensity transfer operation is carried out. This accounts for the electrical, optical and temporal switching characteristics of the FLC. The intensity transfer operation represents the input/output response of the OASLM to a spatially uniform write light. The normalized readout intensity $I_r(x)$ is computed numerically by the operation of the experimentally measured intensity transfer characteristic (Fig. 36) on $I_e(x)$.

Step 3. A discrete Fourier transform of $I_r(x)$ is computed, to simulate the operation performed by the output lens. The calculated diffraction efficiency in the first diffraction peak is recorded for the given values of I_0 and m_r. Then the values for I_0 and m_r are stepped. Steps 1 through 3 are repeated until a lookup table for the diffraction efficiency as a function of I_0 and m_r is compiled.

Step 4. For each experimentally determined diffraction efficiency value and measured I_0 the actual $m_r(I_0, f_x)$ is found by interpolating the data in the lookup table.

Step 5. Finally, the absolute MTF is calculated from the modulation reduction parameter and the zero spatial frequency modulation using

$$MTF = m_r(I_0, f_x)M(f_x \to 0) \tag{12}$$

The MTF is determined as a function of spatial frequency and intensity.

The validity of the results can be verified by comparing fringes of calculated readout intensity versus position to experimental data. As long as the two coincide this procedure is valid [Landreth and Moddel 1992].

Resolution of FLC OASLMs

An example of MTF curves determined by the procedure of the previous section are shown in Fig. 39. As one would expect, the MTF decreases with increasing spatial frequency for all write-fringe intensities. For intensities between 0.4 and 1.0 mW/cm^2, the 50% MTF point occurs at approximately 40 lp/mm for a frame rate of 500 Hz. The resolution increases for higher frame rates because there is less time available for charge to spread. The resolution at 50% MTF for a-Si:H/SSFLC OASLMs determined by the standard procedure vary from 28 lp/mm [Williams et al. 1988] to 135 lp/mm [Kurokawa and Fukushima 1992].

The spreading of charge in the photosensor and field spreading in the liquid crystal limit the resolution. These mechanisms are a function of the thickness of the photosensor and the modulating layers, the capacitance of each of the layers, the sheet resistivity and carrier mobility in the photosensor, the dielectric properties and response time of the liquid crystal, the write-light intensity and wavelength, and the shape and frequency of the electrical drive waveforms. Field spreading [Roach 1974, Owechko and Tanguay 1984] and lateral transport due to fringing fields [Nolte 1992] have been taken into account in deriving analytic expressions for the resolution of OASLMs. For liquid crystal OASLMs, time-dependent lateral carrier spreading must be taken into account. Simulations which do so show that the effective mobility of carriers in the photosensor must be very low, well below 1 cm^2 V^{-1} s^{-1} at the liquid crystal interface, to obtain reasonable resolution [Barbier et al. 1994].

Some insight may be gained into the factors which determine the resolution from the following simple derivation based upon charge spreading in the photosensor [Li et al. 1989]. Consider an area of the photosensor in which a dark strip of length l and of width w is surrounded by two illuminated strips. The resistance R between an illuminated

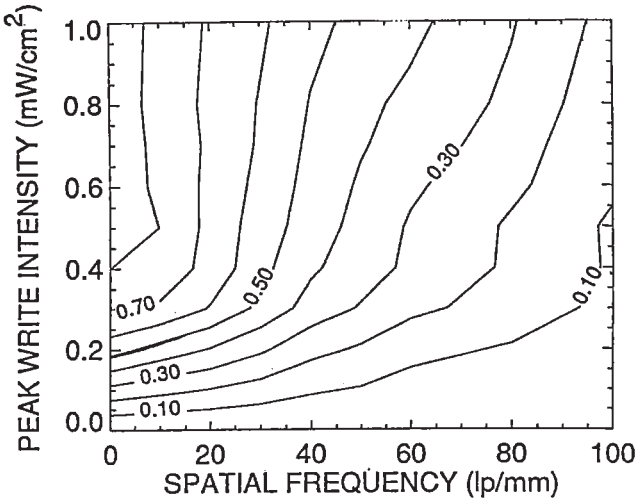

Figure 39 Contour plot showing MTF as a function of spatial frequency and peak write-fringe intensity for an a-Si:H photodiode/SSFLC OASLM. The plotted data were derived from diffraction efficiency measurements, as described in the text. (From B. Landreth and G. Moddel, *Appl. Opt.*, *31*, 3937–3944 (1992))

strip and the center of the dark strip is $R = (w/2l)\rho_{\square}$, where $\rho_{\square}$ is the sheet resistivity of the a-Si:H layer adjacent to the liquid crystal. The capacitance of the dark strip is wlC, where the capacitance per unit area $C = C_{\text{a-Si}} + C_{\text{FLC}}$. The minimum width of the dark strip is determined by that width which produces an RC time constant which is equal to the write/read period $\tau_{w/r}$, i.e., $\tau_{w/r} = \rho_{\square}Cw^2/2$. The resolution $f_x = 1/2w$ is then

$$f_x = \sqrt{\frac{\rho_{\square}C}{8\tau_{w/r}}} \tag{13}$$

For example, for $\rho_{\square} = 10^{10}\ \Omega/\square$, $C = 10\ \text{nF/cm}^2$, and $\tau_{w/r} = 100\ \mu\text{s}$, then $f_x = 35$ lp/mm. This expression is only approximate and probably underestimates the resolution because much of the charge in the a-Si:H near the interface is immobilized by the ferroelectric polarization P. At very low write-light intensities the resolution rolls off because the $\tau_{w/r}$ is insufficient for enough charge to be generated to fully switch the FLC.

4.5 Applications

A wide range of applications for FLC OASLMs has been demonstrated [Mao et al. 1992]. In high-resolution projection displays the OASLM forms the transducer to amplify an image from a CRT [Bone et al. 1991] or laser scanner [Nakajima et al. 1991]. In a joint transform correlator the Fourier transform of the input scene interferes with the reference on an OASLM [Jared et al. 1990]. Such a joint transform correlator may be combined with a position-sensitive detector to measure real time displacements by correlation of speckle patterns [Kobayashi et al. 1993]. In optical neural network computers, the OASLMs may be used to store synaptic weights which may be modified as the computer learns, and used as input and output display devices [Johnson and Moddel 1989, Killinger et al. 1992, 1991]. In optical phase conjugate mirrors, the reference and object beams form an interference pattern of the OASLM [Johnson et al. 1990, Mao et al. 1991a]. Similarly, Fresnel holograms [Fukushima et al. 1991] and computer-generated binary holograms [Fracasso et al. 1990] may be written on the OASLMs. Because of the FLC OASLMs inherent nonlinear thresholding capabilities, these devices may be used to implement Boolean logic gates and edge detection [Cambon and Bougrenet de la Tocnaye 1989] and digital optical memory [Curlander et al., 1993]. They can perform novelty and monotony filtering of moving images in scenes [Mao et al. 1991b] and edge enhancement [Mao et al. 1992]. OASLMs can also be used to perform intensity inversion [Radehaus et al. in press] and compression of images.

5 MATRIX-ADDRESSED SLMs

In considering electrically addressed optical arrays a distinction may be drawn between SLMs and displays [Collings et al. 1989, McKnight et al. 1989]. For SLMs the modulation of light is for the purpose of optical information processing, whereas for displays it is for displaying visual patterns. SLMs are usually operated with monochromatic light, often with light near normal incidence. The operating goals are high frame rate and high contrast. For coherent optical processing both precise amplitude and phase modulation are required. Displays are usually operated with polychromatic light and a wide viewing angle is important. The required video frame rate is low (although the required liquid crystal pixel response time may be short) and moderate contrast ratio is acceptable.

There are three main types of electrically addressed SLMs: direct addressed SLMs, matrix-addressed SLMs, discussed here, and active backplane SLMs, covered in Section

6. The area taken by interconnects in direct addressed SLMs increases rapidly with the number of pixels, limiting arrays to having approximately 16 × 16 pixels [Collings et al. 1989]. Because the frame rate of matrix-addressed arrays is low compared to active backplane devices, their chief applications are flat-panel displays and printers, whereas the active backplane SLMs are better suited to optical processing and computing and may become the preferred technology for high-resolution projection displays. The bulk of the FLC matrix-addressed arrays are for displays, not optical processing. Displays are of limited relevance here, and therefore the basic technology of matrix addressed FLC SLMs is described only briefly. References to papers which give more details are given. An excellent review of the subject as of 1989 is given by Lagerwall et al. [1989].

5.1 Background

Initial investigations of matrix arrays using FLCs were carried out by Clark, Lagerwall, and Wahl [Clark et al. 1985, Lagerwall et al. 1985, Wahl et al. 1987]. The first SSFLC matrix addressed display prototype was made by Seiko in 1985 [Harada et al. 1985]. It had 640 × 400 pixels and had a frame time of 320 ms. A number of other research groups and companies have investigated the devices, including the JOERS/Alvey collaboration in the U.K., which includes STC Technology [Bone et al. 1987, Ross 1988, Crossland et al. 1988], BDH, GEC-Marconi [Heeks et al. 1991, 1992], and Thorn-EMI [Surguy et al. 1991, Ross et al. 1992]; Toshiba [Hatoh et al. 1987, Shimizu et al. 1987, Matsumoto et al. 1988a,b]; Canon [Inaba et al. 1988, Kanbe et al. 1991]; LETI [Maltese et al. 1988a,b, Dijon et al. 1988b, 1991, Leroux et al. 1988]; Schindling [Wahl 1988]; Philips [Hartmann 1989b]; Bosch Laboratories [Reinhart et al. 1991]; Gent [Reynaerts et al. 1991a]; Hoechst with the University of Stuttgart [Rieger et al. 1991]; Semiconductor Energy Laboratory with Takasago Research Institute [Konuma et al. 1991]; Matsushita [Wakita et al. 1991, Gohara et al. 1991]; Fujitsu [Mochizuki et al. 1991b]; Optrex; Mitsubishi; and Hitachi. Citizen Watch has developed a FLC shutter array for printing 640 × 440 dots, with a resolution of 150 dots per inch and 32 gray levels on each dot. Canon is now producing 16-gray-level 24-inch monochrome and 21-inch 64-color FLC displays having 1280 × 1024 pixels.

5.2 Matrix Addressing

A large electrically addressed display may have on the order of 1000 × 1000 or 10^6 pixels. As it is a practical impossibility to directly access each pixel with a separate wire, another approach must be taken. A passive matrix of transparent electrodes is formed to address the pixels, with one set of electrode lines deposited on one substrate, and a perpendicular set deposited on the other substrate. The liquid crystal is sandwiched between the crossing electrodes. Each pixel is uniquely determined by a particular column and row electrode. With such an arrangement, 10^6 pixels can be accessed with 2000 wires.

The simplest matrix-addressing scheme would be to power a single pair of column and row electrodes to access each pixel, sequentially scanning through all of them. This is impractically slow. Instead the following multiplexing scheme is used. A "strobe" voltage pulse is applied to each row, selecting it for a particular period. In synchronism with the strobe voltage, "data" voltage pulses are applied to all the columns simultaneously. The liquid crystal experiences a voltage which is the difference between the row and column voltages. In this way, a row at a time may be addressed.

With such a row-at-a-time approach each pixel is updated after all the other rows have been strobed. The average electric field to which each pixel is exposed depends upon the duty cycle, and is therefore reduced in proportion to the number of rows in the display. The consequence for a large array is that each pixel is exposed to only a small change in voltage when it is addressed. The effect this has on the image depends upon the threshold voltage (V_{th}) and saturation voltage (V_{sat}), defined in Fig. 40. The state of the pixel is not affected if the switching threshold is sufficiently high and the transition is sufficiently sharp, i.e., if $(V_{sat} - V_{th})/V_{th}$ is sufficiently small. Therefore the number of rows which may be addressed is a function of $(V_{sat} - V_{th})/V_{th}$. For twisted nematic liquid crystals, in which the transition is fairly broad, the maximum number of lines which may be addressed is on the order of 100. Supertwisted nematic liquid crystals have a much sharper transition and have successfully been incorporated into large passive matrix addressed displays.

Even with a perfectly sharp transition the size of the display is limited, however, because variations in the voltage drop along indium tin oxide (ITO) lines can cause substantial variations in the effective data voltage threshold. Metalized lines are sometimes used to reduce the line resistivity, but at the cost of increased complexity and reduced optical transmission. The number of lines which may be addressed can be increased by including a nonlinear electrical element in each pixel, to increase the sharpness of the transition. The nonlinear elements may be diodes or metal-insulator-metal layers.

One way to circumvent the size limitation imposed by the previous duty-cycle argument is to incorporate a memory element into each pixel. Each pixel then remembers its assigned state independent of how many lines there are. Active matrix displays incorporate a thin-film transistor (TFT) into each pixel to perform this memory function and are used extensively with twisted nematic liquid crystals.

The bistability of SSFLCs provides them with intrinsic memory. Therefore SSFLC passive matrix displays have unlimited multiplexibility [Shimizu et al. 1987, Wahl et al. 1987]. As termed by Canon, they are "duty free" [Lagerwall et al. 1989].

Before a line in a passive matrix display may be accessed, the liquid crystal in the previous line must have switched. Therefore the rate at which the displayed frames may be updated is a function of the switching time of the liquid crystal and the number of

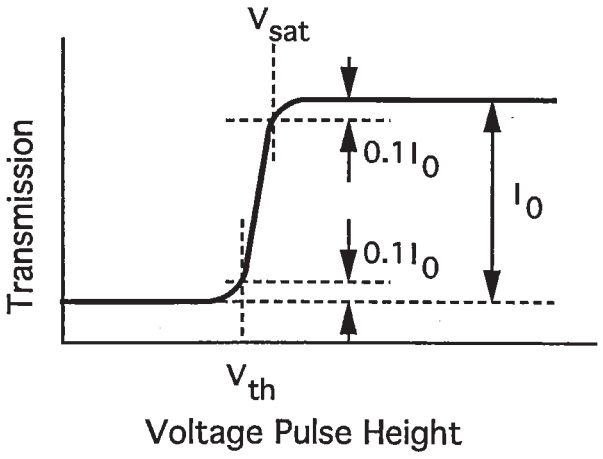

Figure 40 Definition of the threshold voltage V_{th} and the saturation voltage V_{sat}. (Adapted from K. Shimizu, Y. Tanaka, K. Sekikawa, K. Inoue, and H. Hori, *Proc. SID*, *28*, 211–215 (1987))

lines. Because SSFLCs switch faster than other liquid crystals, the frame rates of passive matrix displays which incorporate them are faster too. An image from a 128 × 128 pixel SSFLC passive matrix display is shown in Fig. 41.

5.3 Multiplexing Schemes

As discussed in the previous section, matrix addressing of a display is dependent upon the threshold of the liquid crystal. In SSFLCs the threshold is not a static threshold voltage but rather a dynamic *Vt* threshold [Clark and Lagerwall 1980], where *V* is the applied pulse voltage and *t* is its duration. If a pixel experiences a pulse below *Vt* it does not switch.

A simple multiplexing scheme used by Seiko [Harada et al. 1985] is shown in Fig. 42. Each of the pulses is followed by a pulse of the opposite polarity so that the time-averaged voltage is zero, avoiding ionic degradation. The strobe voltage pulses, applied to the row electrodes, determine when each row has been selected. The data voltage pulses determine which pixels in the selected row switch. Because the pixel experiences the difference between the row and column voltages, the first time its row is selected in the figure its column electrode voltage switches it. The second time its row is selected its column pulse voltages are of the same polarity as the row voltages, so the difference is below threshold, with the result that the pixel does not switch.

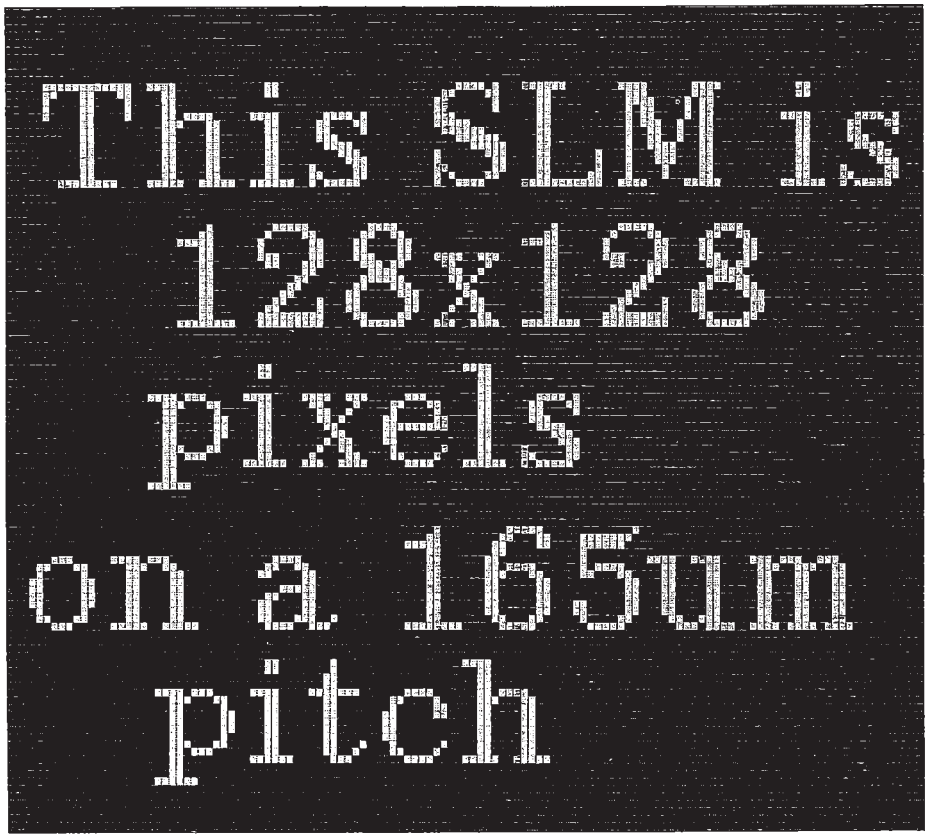

Figure 41 An image displayed on a 128 × 128 pixel SSFLC passive matrix display made by STC.

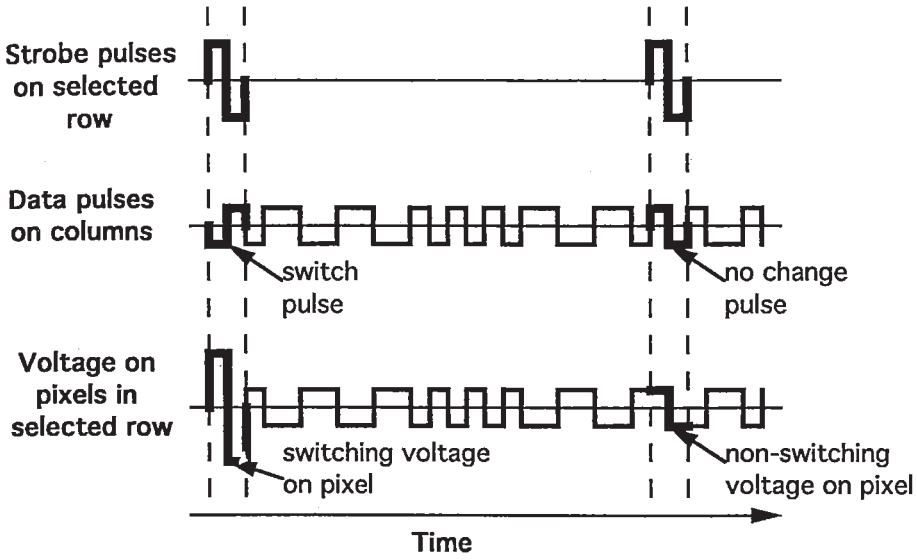

Figure 42 Multiplexing scheme used by Seiko. The voltage which results across the pixel is shown for "switch" and "no change" data pulse coincident with the row select pulses. The data pulses between the row select pulses are arbitrary.

The selection ratio is the ratio of the voltage-time product of the switching pulse to that which does not switch the pixel. It is an important property of the multiplexing scheme because it determines how sharp a liquid crystal threshold must be for switching to occur at only the correct times. It might appear that making the data pulse voltages arbitrarily large would increase the selection ratio as much as desired. This cannot be done, however, because all the pixels are interdependent, sharing row and column electrodes. Increasing the data pulse voltage could cause pixels in an unselected row to switch. Increasing the row strobe pulse voltages, similarly, would cause pixels in the unselected column to switch [Lagerwall et al. 1989]. The maximum selection ratio possible, shown in Fig. 42, is 3:1 [Wahl 1988]. A practical selection ratio for SSFLC displays is 1.5:1 [Lagerwall et al. 1989].

The frame rate is another important property of the multiplexing scheme. In the scheme shown in Fig. 42 the pixels are switched only on. To switch them off a second frame scan is used in which the polarity of the strobe pulses is reversed. This is called a four-slot multiplexing scheme because it requires four writing pulses to completely determine the state of a pixel: (i) one to dc-balance the switch-on pulse, (ii) the switch-on pulse, (iii) one to balance the switch-off pulse, and (iv) the switch-off pulse. This scheme is very inefficient.

By scanning more than a single row at a time the rows ahead of the selected row may be blanked at the same time the selected row is being switched. Such two-slot multiplexing scheme can increase the frame rate by nearly a factor of 2 over the four-slot method [Shimizu et al. 1987]. A number of different schemes which use variations of the bipolar strobe pulses shown in Fig. 42 have been developed to improve the performance of SSFLC matrix addressed displays [Wahl 1988, Dijon et al. 1991, Surguy et al. 1991]. Another approach takes advantage of the fact that the *Vt* threshold breaks down in some low spontaneous polarization (P) materials. In low-P materials which have a negative dielectric anisotropy or strong biaxiality, switching occurs at lower *Vt*

for high voltages [Ross et al. 1992]. This allows the use of a monopolar strobe to improve the performance over the bipolar strobe schemes [Surguy et al. 1991].

Because all the pixels share common row and column electrodes, they each experience, to varying extents, all of the applied pulses. It is therefore important to enhance the bistability of the SSFLC as much as possible to keep the pixels in their desired state. As mentioned in Section 3.3, the application of a high-frequency ac field to the SSFLC tends to stabilize it. For this reason the driving scheme should maximize the rms value of the data pulses [Lagerwall et al. 1989].

5.4 Gray-Level Displays

Both the intrinsic (using the natural analog properties of the SSFLC) and extrinsic (using imposed dithering) approaches to obtain gray levels from SSFLCs, described in Section 2.2, have been applied to matrix addressed displays. The first approach was to use temporal dithering [Clark et al. 1985]. The Seiko four-slot scheme was used to obtain four gray levels in a 64 × 64 display [Reinhart et al. 1991], and improved schemes were developed [Reynaerts et al. 1991a]. The problem with temporal dithering is that each additional gray-level uses one frame with the result that the frame rate is severely reduced. The Canon display can use spatial dithering to obtain gray levels by dividing each pixel into subdivided pixels [Kanbe et al. 1991], but at the cost of spatial resolution. A combination of spatial and temporal dithering greatly increases the number of available gray levels [Leroux et al. 1988].

Controlled inhomogeneities have also been used to obtain gray levels. An approach pioneered by Canon makes use of textured glass plates, yielding cells of varying thickness, to obtain a distribution of gray levels [Leroux et al. 1988]. Another approach of Canon's makes use of a thin dielectric layer on the ITO to increase the switching threshold. Each pixel is subdivided into regions having different thresholds [Reinhart et al. 1991]. A third approach has been to use applied electric fields to impose a texture in the SSFLC in order to obtain gray levels [Hartmann 1991].

Intrinsic approaches to obtaining gray levels by spatial averaging have involved the development of matrix-compatible driving schemes to control domain growth [Maltese et al. 1988a,b, Dijon et al. 1988b]. The *Vt* product is modified by varying the phase of the column pulse with respect to that of the row pulse. Another approach is to control the charge which each pixel receives. This was accomplished with TFT active matrix SSFLC displays [Hartmann 1989a,b].

One important consideration in producing reproducible gray levels is the variation of the liquid crystal properties with temperature [Reinhart et al. 1991]. The response time of FLCs decrease typically by a factor of 2 for every 6°C rise in temperature [Ross 1988].

Gray levels can be achieved directly with DHFLC and ELC materials. Because these liquid crystals are not bistable, the saturated gray-level response comes at the cost of active matrix addressing.

Color is another quality of some displays. Color could be generated directly with DHFLCs [Abdulhalim and Moddel 1991a], but the colors would not have sufficient saturation or be independent of viewing angle. For SSFLCs, red, green, and blue (RGB) microfilters can be incorporated into the pixels to allow control of the color. The filters may be situated between the glass and the ITO [Matsumoto et al. 1988a]. A practical color SSFLC display for laptop computers has been developed [Ross et al. 1992].

5.5 Future Prospects

The advantages of SSFLC matrix addressed displays over others are a wide viewing angle, unlimited multiplexibility, high speed, high resolution, and relative simplicity (as compared to active matrix addressed displays).

The wide viewing angle for SSFLCs as opposed to nematic liquid crystals is attributable to two effects. When the optic axis is in the plane of the cell the change of birefringence is quadratic with angle and proportional to thickness. With a tilted optic axis, the change of birefringence is linear with angle and again proportional to thickness [Wahlstrom 1969]. The first reason for the wider viewing angle of SSFLC cells is that their optic axis is in the plane of the cell, whereas for many nematic liquid crystal cells the optic axis is tilted. The second is that SSFLCs cells are much thinner than nematic liquid crystal cells.

This chapter is being written with a system which has an active matrix addressed twisted nematic liquid crystal display. If FLCs are so advantageous why are they not used in the display? The main disadvantages have been a susceptibility to mechanical stress and thermal shock, poor contrast, ghost images, and difficulty of alignment, but most of these problems have been resolved [Reiger et al. 1991, Ross et al. 1992, Konuma et al. 1991]. Antiferroelectric liquid crystals appear to be less fragile than SSFLCs and therefore promising for displays [Ouchi et al. 1991]. Time will tell if the most significant reason that FLCs are not used in the display is not simply that the competing technologies are more mature.

6 ACTIVE BACKPLANE SLMs

In an active backplane SLM each pixel has its own active circuit elements which drive it. Such SLMs may be electrically addressed (EASLM) or optically addressed (OASLM). There are several potential functions of the circuitry at each pixel, including storing charge, allowing the entire array to be addressed within a single FLC response time. This simple form of an active backplane EASLM circuit is depicted in Fig. 43. Active backplane OASLMs can perform thresholding operations. These "smart pixel" active backplane OASLMs can include a sensor, logic circuitry, and memory, and perform operations in which the state of a particular pixel is a function of the state of adjacent or even distant pixels. This is an area of rapidly growing interest [Johnson et al. 1993a].

The most common active backplane is a crystalline silicon wafer. Highly developed very large scale integration (VLSI) circuit technology is used to form the desired circuitry, and the liquid crystal is sandwiched between the processed wafer and a TCO-coated glass cover. In operation the read light is reflected from the VLSI chip surface through the liquid crystal. Another approach is to use TFTs formed on a transparent substrates to form transmission-mode active backplane SLMs. A third approach combines the advantage of crystalline silicon VLSI in forming high-performance circuits and the advantage of TFTs in allowing transmission mode operation. It is to fabricate VLSI circuits on silicon wafers and process the wafers to yield very thin films, which are then bonded to transmissive substrates to form active backplane SLMs.

Active backplane SLMs may be used in small, hand-held displays [Crossland et al. 1985], and can provide the performance required in optical computing and processing applications. Also SSFLCs on VLSI chips can be used to visualize surface potentials and analyze the chips [Picart et al. 1989]. Even with the limited frame rate of liquid crystal

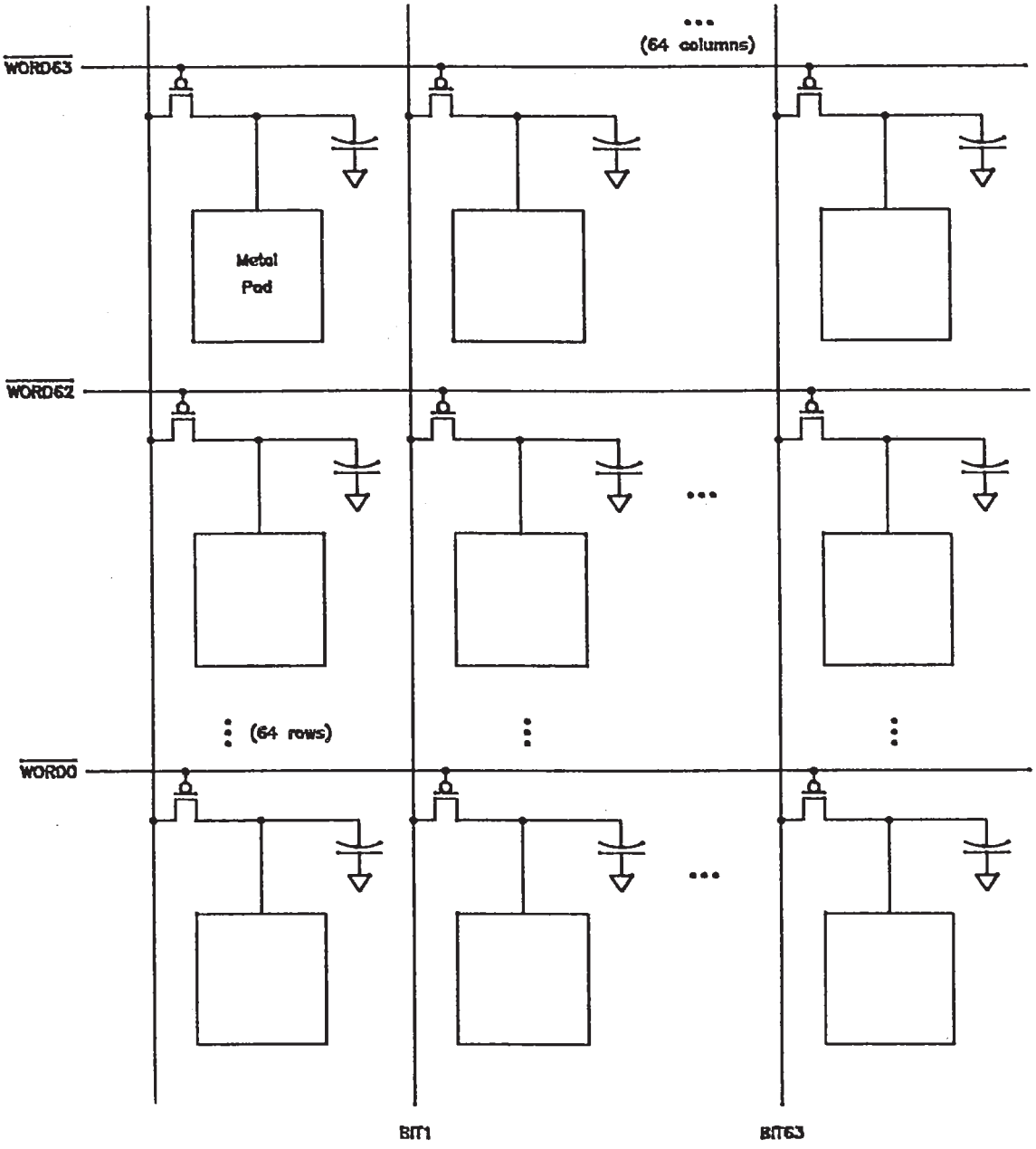

Figure 43 Simple active backplane schematic circuit diagram. In this dynamic random access memory (DRAM) approach an array of FETs is addressed via row and column electrodes. A row at a time is addressed rapidly, limited only by the *RC* time of the row. It is not necessary to wait until the FLC switches before addressing the following row. (Adapted from M. A. Handschy and M. J. O'Callaghan, Soc. Information Display Int. Symp., *Digest of Technical Papers*, Vol. 22, SID, 1991, pp. 246–249)

SLMs (<1 MHz) as compared with gallium arsenide multi-quantum-well modulators, for example, their high spatial resolution and large array sizes meet the needs of many high-performance applications [Drabik 1991]. As the array sizes increase and the cost decreases active backplane SLMs may become the preferred technology for high-resolution projection displays. With current silicon foundry lithography capabilities,

VLSI/SSFLC active backplane SLMs as large as 1024 × 1024 are feasible, running at a frame rate of 10 kHz with a contrast ratio of 100:1 [Handschy et al. 1993a].

6.1 Background

Active backplane liquid crystal SLMs were pioneered by a group at the University of Edinburgh, first with a 16 × 16 pixel array driving guest host liquid crystals [Underwood et al. 1986], and then with a 50 × 50 pixel array driving nematic liquid crystals [McKnight et al. 1989]. These electrically addressed devices used static random access memory (SRAM) circuits, in which the power is applied continuously to each of the liquid crystal pixels. This is a convenient way to supply nematic liquid crystals with an ac drive.

The application of this VLSI backplane technology to FLCs was analyzed in a collaboration between STC Technology and the University of Edinburgh [Collings et al. 1989], and the ramifications of using a simpler dynamic random access (DRAM) technology were discussed. A collaboration between Displaytech and the Georgia Institute of Technology resulted in the design, fabrication and analysis of 64 × 64 pixel SRAM [Cotter et al. 1990, Handschy 1991] and 256 × 256 pixel DRAM [Handschy et al. 1990a, 1993a] SSFLC active backplane SLMs, a thresholding active backplane OASLM [Drabik and Handschy 1990], and an edge- and motion-detecting FLC/VLSI silicon retina [Handschy and Drabik 1990b]. A 12 × 12 pixel one-transistor array incorporating both SSFLCs and DHFLCs was demonstrated by Lockheed [Armitage and Kinell 1990]. At the University of Colorado the following devices have been developed: a 64 × 64 pixel electrically addressed SLM [Jared et al. 1991b], a 32 × 32 pixel optically addressed SLM [Jared and Johnson 1991], a 256 × 256 pixel electrically addressed SLM [McKnight et al. 1993], a global maximum-sensing 32 × 32 pixel SLM [Slagle and Wagner 1992], and a zero-crossing edge detecting 32 × 32 pixel SLM [Jared and Johnson 1993]. In a collaboration between the University of Edinburgh, BNR Europe, and GEC Marconi, a 176 × 176 pixel electrically addressed SLM was built [Underwood et al. 1991, Crossland et al. 1990]. A back error propagation function for a two-layer neural network was implemented in a collaboration between the California Institute of Technology and Displaytech [Li et al. 1992]. Rockwell International and Displaytech used a VLSI active backplane optically addressed FLC SLM to perform retina-like adaptive thresholding in a nonlinear joint transform correlator [Schehrer et al. 1993]. Displaytech and Black Forest Engineering developed a multipurpose SLM that can be programmed to threshold, subtract, or invert [Handschy et al. 1993b]. All of the SLMs described above incorporate a crystalline silicon VLSI active backplane. An OASLM that incorporates an amorphous silicon TFT active backplane was fabricated at NEC [Tsujikawa et al. 1990].

6.2 Structure

Usually *n*-type metal-oxide-semiconductor (*n*MOS) or complementary MOS (CMOS) processes are used in the fabrication of EASLMs. For OASLMs bipolar junction phototransistors or other photosensing elements are incorporated. Each pixel contains circuitry and a reflective metal pad adjacent to and/or over the circuitry to form an electrode for the liquid crystal and a mirror. After fabrication and dicing, the silicon chip is ready. An alignment layer is formed on a matching TCO-coated glass chip. Spacers are used to separate the two chips, which are epoxied together, and the gap is filled with liquid crystal. The assembly is mounted in a standard integrated circuit package, and wires are connected from the silicon chip bonding pads to the pins in the package. The device is

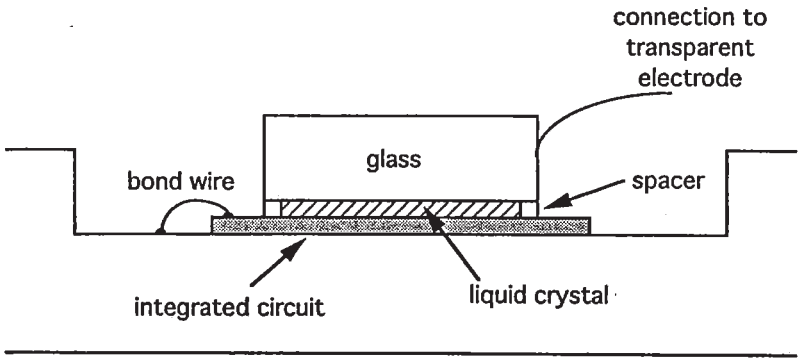

Figure 44 Cross section of an integrated circuit/liquid crystal active backplane SLM. (Adapted from D. J. McKnight, D. G. Vass, and R. M. Sillito, *Appl. Opt.*, *28*, 4757–4762 (1989))

temperature-cycled to obtain an aligned SSFLC. A cross section of an integrated circuit/liquid crystal active backplane SLM is shown in Fig. 44.

The optical quality of the SLM depends upon the smoothness of the backplane because it forms the surface from which light is reflected and because its structure determines the relative FLC thickness [Handschy et al. 1990a]. Mirrors formed over the circuitry are rough, more so for SRAMs than for DRAMs. The structure in the pixels of a SRAM-addressed device is shown in Fig. 45. The pattern of this structure causes light scattering, and the nonuniformities in FLC thickness reduce the contrast and pro-

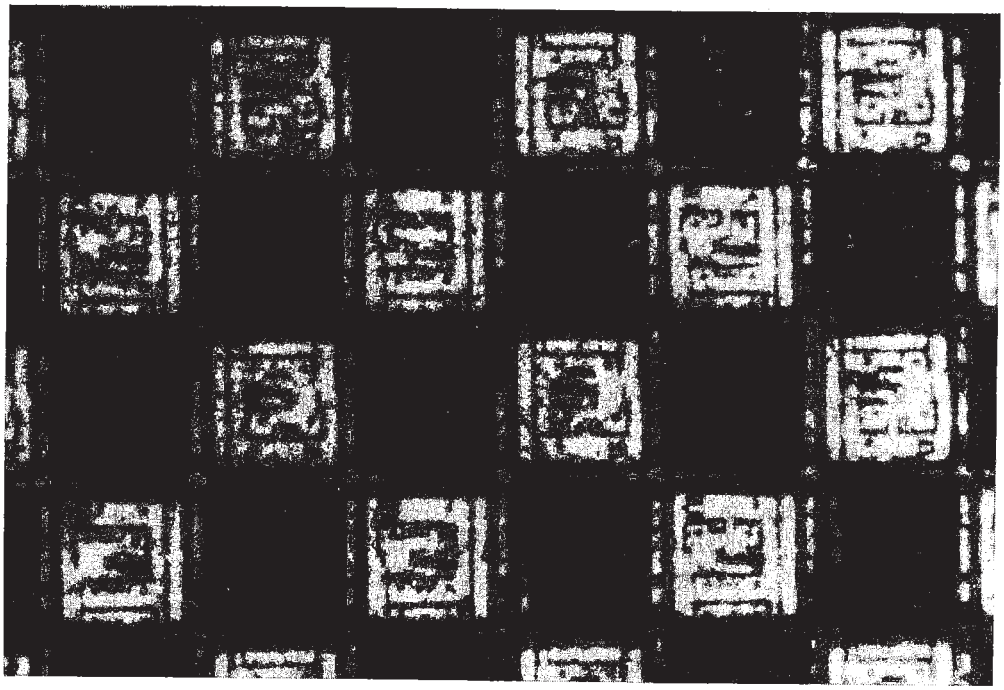

Figure 45 Reflected light microphotograph of a portion of an SRAM-addressed active backplane SLM showing structure due to underlying circuit topography. The pixels are on 60-μm centers. (Described in M. A. Handschy, T. J. Drabik, L. K. Cotter, and S. D. Gaalema, *Proc. SPIE*, *1291*, 158–164 (1990))

mote FLC defect formation. This structure should be eliminated by adopting planarization techniques used in VLSI processing [Handschy et al. 1993a].

The fill factor of the pixels is an important figure of merit. It is the ratio of the switched and optically reflective area to the area of the entire device. Mirrors which are formed off the circuitry are smooth, but without planarization the circuitry area becomes optically useless. Optically useful area is also lost to the regions between pixels which cannot be smaller than the VLSI design rules allow [Handschy et al. 1990a]. For decreasing minimum features sizes, the breakdown voltage decreases [Collings et al. 1989] which limits the driving field for the SSFLCs. For a 1.2-μm VLSI process, square elements on 30-μm centers yield a flat-area fill factor of 54% to 68%, depending upon the degree of shielding used to screen incident light from the pixel transistors [Johnson et al. 1993b].

6.3 Electrically Addressed Active Backplane SLMs

The two main types of active backplane EASLMs are based upon two types of memory used in VLSI: DRAM and SRAM.

DRAM Addressing

A basic limitation in electrically addressing SSFLCs has to do with the polarization current. Sufficient charge must be stored in the pixel capacitor during the addressing period to allow for charge loss induced by the dipole rotation during switching. This may be illustrated by the following simple approach to driving SSFLCs. Consider a DRAM circuit like the one shown in Fig. 43. (i) Charge the plates of the FLC capacitor (C_{flc}) and the associated parallel silicon backplane substrate capacitor (C_{sub}) from zero volts to the applied voltage V_{app} (e.g., by switching on a field-effect transistor (FET) whose source is connected to the applied voltage and whose drain is connected to the pad which forms one of the SSFLC electrodes). (ii) Isolate the capacitor (e.g., switch off the FET) so that no current flows. (iii) Allow the SSFLC to switch using the charge stored on C_{flc} and C_{sub}. As the SSFLC switches it reduces the voltage across the capacitors. In step (i) the capacitors receive a charge

$$Q = (C_{flc} + C_{sub})V_{app} \tag{14}$$

In step (iii) the pad voltage is reduced to V_{final} given by

$$Q = (C_{flc} + C_{sub})V_{final} + 2P \tag{15}$$

where Q is unchanged. The voltage reduction due to the SSFLC switching [Collings et al. 1989] thus reduces the voltage across the FLC to

$$V_{final} = V_{app} - \frac{2P}{C_{flc} + C_{sub}} \tag{16}$$

So that both positive and negative polarities may be applied to the FLC, the voltage on the TCO-coated glass chip is maintained at a level halfway between the maximum voltage available (usually 5 V) and zero, limiting V_{app} to 2.5 V. Because of this limitation and the fact that V_{final} cannot be less than zero, when this simple driving scheme is used for large P the switching will not be complete. If additional capacitance is not provided this voltage reduction limits the P in practical devices to tens of nC/cm^2 [Collings et al. 1989]. Most DRAM addressing employs the simple driving scheme described above, and is subject to its limitations. With a circuit that approaches SRAM addressing, multitransistor DRAMs can circumvent this limitation, but at the cost of an increase in the number of lines which must be accessed by each pixel and the cost of the pixel components

[Johnson et al. 1993a]. (Note that the limitation does not apply to matrix addressed SLMs, discussed in Section 5, because in their addressing scheme the voltage is applied to each pixel until the FLC switches.)

In the DRAM circuit shown in Fig. 43 the large square represents the SSFLC electrode and the capacitor represents $C_{flc} + C_{sub}$. When the FET is on (conducting) in each element it allows the capacitor to be charged by the bit line, and when it is off (insulating) it isolates the capacitor. The SLM is addressed a row at a time, as were the matrix addressed displays described in Section 5, but much more rapidly. This is because with an active backplane it is not necessary to wait for the SSFLC to have switched before moving to the next row. The entire addressing protocol must take into account the time required to charge the capacitor, and produce a time-averaged voltage of zero to avoid ion-induced performance degradation [Underwood et al. 1991].

The capacitor must hold the charge a sufficiently long time for the SSFLC to switch, and for a frame time if the FLC is not bistable. This is the *RC* decay time after the FET is switched off. It is not difficult to obtain sufficiently long decay times, but care must be taken to avoid a reduction of the decay time due to photoconductivity in the silicon backplane [Jared et al. 1991, Handschy et al. 1993a, Johnson et al. 1993b].

A 256 × 256 pixel array has been demonstrated which operates at ~7.5 kHz frame rates, has a pixel pitch of 21.6 μm, a flat-area fill factor of 60%, and a contrast ratio of 70:1 [McKnight et al. 1993].

SRAM Addressing

When a pixel in an SRAM-addressed SLM is switched on the electrical power remains connected to the liquid crystal for the entire frame time. Thus the FLC at a particular pixel continues to receive charge as the it switches, even if its row is no longer selected. Therefore the limitations imposed by Eq. 16 are irrelevant [Collings et al. 1989]. A diagram for an SRAM matrix is shown in Fig. 46. The first active backplane SSFLC SLM was SRAM addressed [Cotter et al. 1990]. It is a 64 × 64 pixel array which operates at 4.5-kHz frame rates, has 60-μm pixel pitch, and exhibited a single-element intensity contrast ratio of 12:1. SRAM addressed SLMs which perform special functions are discussed in Section 6.4 under "Special Function Arrays."

6.4 Optically Addressed Active Backplane SLMs

Thresholding Arrays

The active elements in an active backplane SLM are well suited to producing sharp thresholds. A 20 × 6 pixel thresholding SSFLC OASLM on a 130-μm pitch has been developed using a VLSI silicon active backplane [Drabik and Handschy 1990]. A schematic circuit diagram for the device is shown in Fig. 47. A phototransistor produces a current which is proportional to the input light intensity. Whether the SSFLC switches is determined by the difference between this current and a bias current I_0. The threshold level may be changed by changing I_0. Those pixels of the array having an input intensity above threshold switch become reflecting while those pixels below threshold remain dark. The response time of the device is approximately 2 ms. An important consideration is the uniformity of response. For the interior pixels in the array described above, there is an approximately 4% variation in the threshold.

TFTs perform more poorly than transistors in crystalline silicon, but they can be produced at lower cost and, on a transparent substrate, offer operation in transmission mode [Collings et al. 1989]. A 120 × 120 pixel thresholding SSFLC OASLM has been

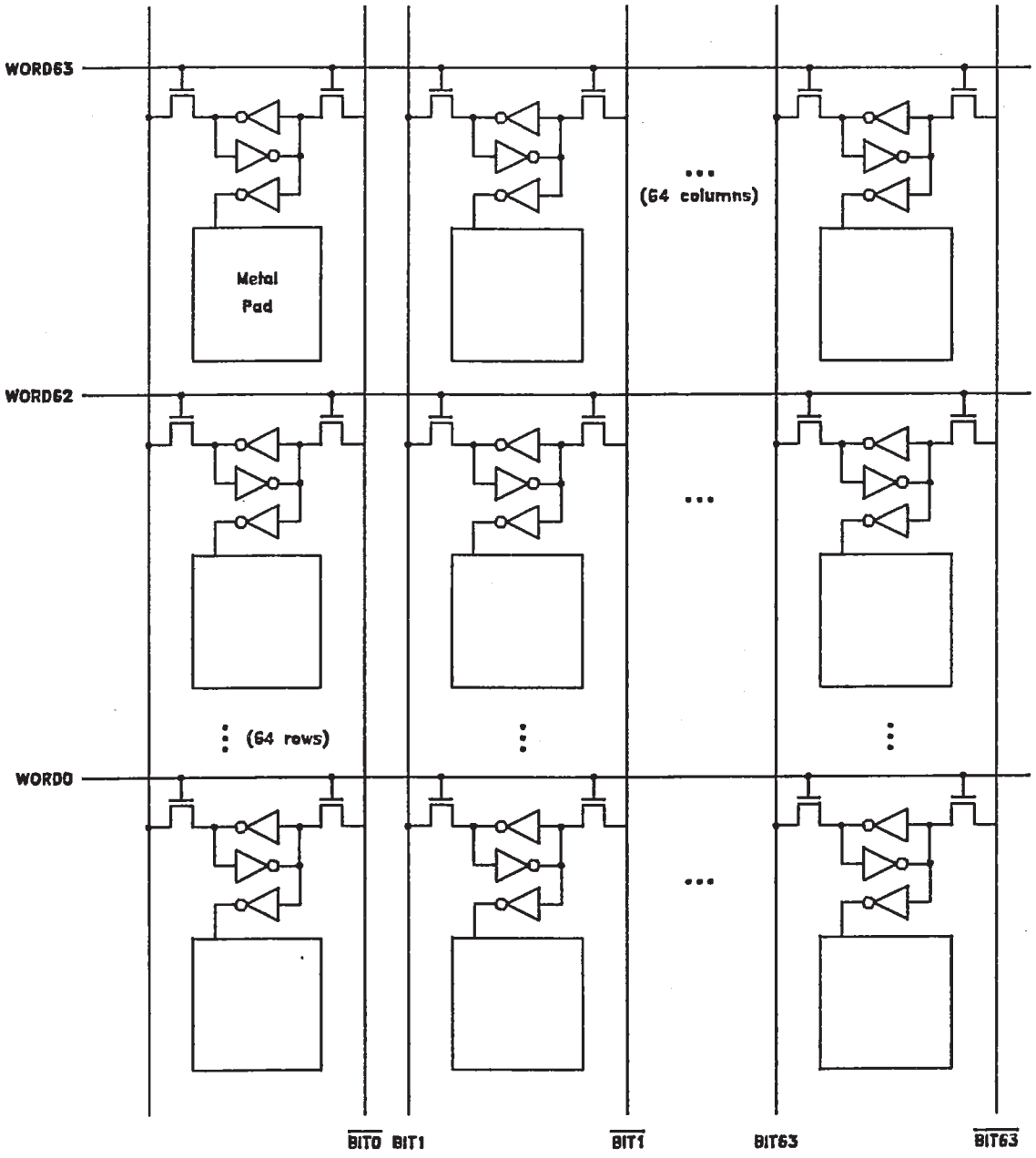

Figure 46 Simple SRAM active backplane schematic circuit diagram. In this eight-transistor matrix each cell includes a cross-coupled inverter register that drives the SSFLC electrode (a metal pad) through a third inverter buffer. (Adapted from M. A. Handschy and M. J. O'Callaghan, Soc. Information Display Int. Symp., *Digest of Technical Papers*, Vol. 22, SID, 1991, pp. 246–249)

developed using a TFT active backplane [Tsujikawa et al. 1990]. The circuit for the device is shown in Fig. 48. An amorphous silicon photoconductor senses the input light, and the difference between its resistance and that of a fixed resistor is used to switch the liquid crystal. The threshold is generated by the steep TFT switching characteristic. The elements are 330-μm squares, substantially larger than those with a silicon VLSI backplane. The device has a response time of approximately 1 ms.

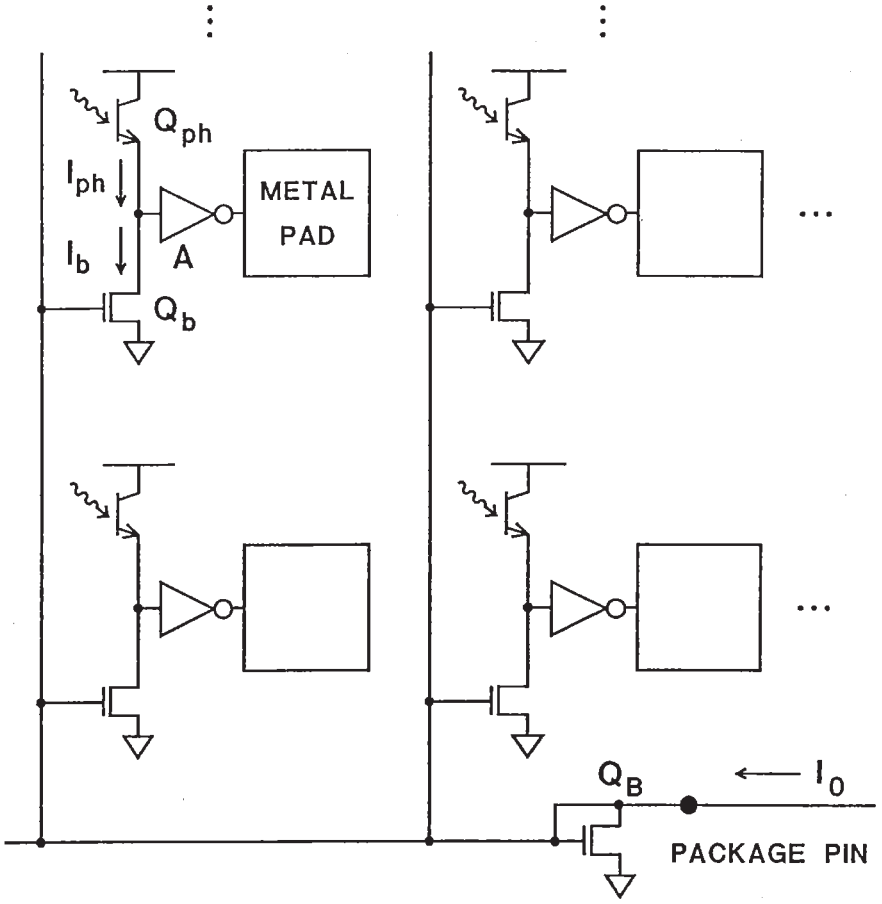

Figure 47 Thresholding optically addressed active backplane SLM schematic circuit diagram. (Adapted from T. J. Drabik and M. A. Handschy, *Appl. Opt.*, *29*, 5220–5223 (1990))

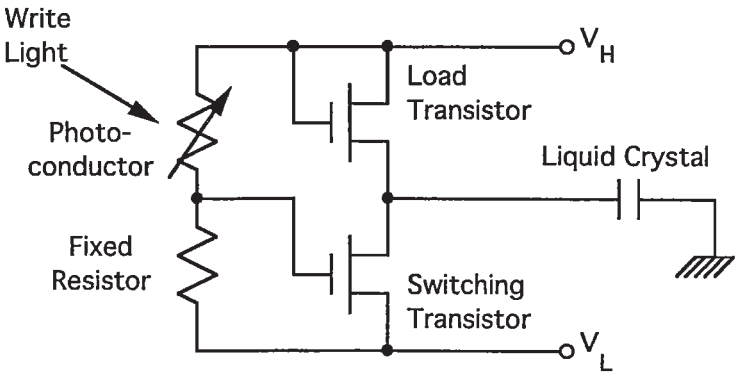

Figure 48 Thresholding SSFLC optically addressed SLM a thin-film transistor (TFT) active backplane. (Adapted from S. Tsujikawa, F. Okumura, M. Sakamoto, H. Ichinose, M. Imai, K. Sera, H. Asada, and K. Kubota, Conf. record Int. Topical Meeting Optical Computing, 1990, pp. 23–24)

Special Function Arrays

A natural extension of the basic active backplane SLMs is to smart pixel devices which perform a range of functions. One set of such functions involves early vision, in which the SLM performs detection functions which mimic the retina. An active backplane FLC/VLSI silicon retina was developed which consists of an array of 13 × 18 elements, where the size of each element is 97 μm × 112 μm [Handschy and Drabik 1990b]. The array detects edges and motion, accepting an input image and returning a binary image in which the edges and motion are enhanced. The circuit is the same as that of Mead [Mead, 1989], except for the output, which is an amplifier and rectifier to drive the FLC.

Another special function of interest is that of a maximum sensor, or winner-take-all SLM. Such devices are useful at the output of an optical correlator, to sense the location of maximum intensity that indicates a correlation in background clutter, and for other optical computing applications. A winner-take-all FLC SLM, having 32 × 32 pixels, was implemented with a VLSI active backplane [Slagle and Wagner 1992]. Each pixel is 75 μm square. By global inhibition only the pixel having the largest input intensity is selected, and becomes reflecting. All other pixels remain in their off-state. A schematic cross section of two pixels of the array is shown in Fig. 49. The device makes use of global inhibition, in which the output of each pixel depends nonlinearly on the inputs to all the pixels in the array. Input light is absorbed by photodetectors under the FLC electrode, producing a current which is input to a two-transistor competitive circuit. If the output of this circuit is above a set threshold, the FLC modulator in the selected pixel is switched.

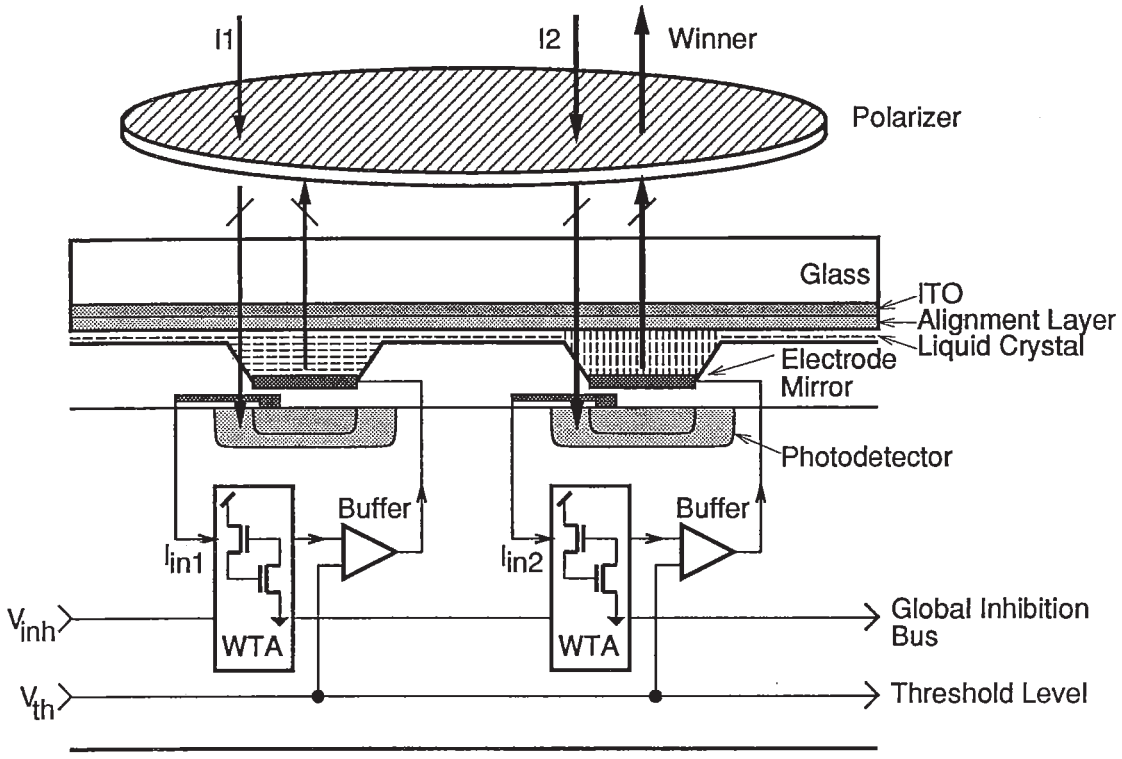

Figure 49 Schematic diagram of two pixels in a VLSI/FLC active backplane winner-take-all SLM. (From T. M. Slagle and K. Wagner, *Opt. Lett.*, *17*, 1164–1166 (1992))

A CMOS active backplane SLM which optically implements a back error propagation neural function for an optical neural network was developed [Li et al. 1992]. It consists of eight pixels (or "neurons") on an area of approximately 2 mm square. Each pixel includes a phototransistor, a SSFLC modulator, sample-and-hold circuits, and additional circuitry. A different CMOS active backplane SLM performs zero-crossing edge detection [Jared and Johnson 1993]. It consists of an array of 32 × 32 pixels, each of which incorporates a phototransistor, a transconductance amplifier with a hysteretical feedback element, a zero-crossing detection circuit, and a modulating pad.

6.5 Future Prospects

DRAM addressed SSFLC SLMs appear to be the technology of choice in making a simple SSFLC EASLM because of the small area used by the circuitry, and the simple design of a single transistor at each pixel. The frame rate is limited by the power dissipated in charging the bit lines (above which the device overheats), the bit-line current-carrying capability (above which electromigration destroys the lines), *RC* delays in propagating addressing pulses down the word lines, and ultimately by the SSFLC response time [Collings et al. 1989, Handschy et al. 1990a, Handschy and O'Callaghan 1991]. In Fig. 50 these limitations are plotted as a function of array size N for a $N \times N$ array using a 2-μm CMOS process VLSI backplane. The assumptions which went into the derivation of these limitations were that device could dissipate 1 W with heat sinking, that the array is split in two, that the word lines could carry 1.5 mA without degrading, and that the bit lines are driven from both ends to reduce propagation delay [Handschy et al. 1990a].

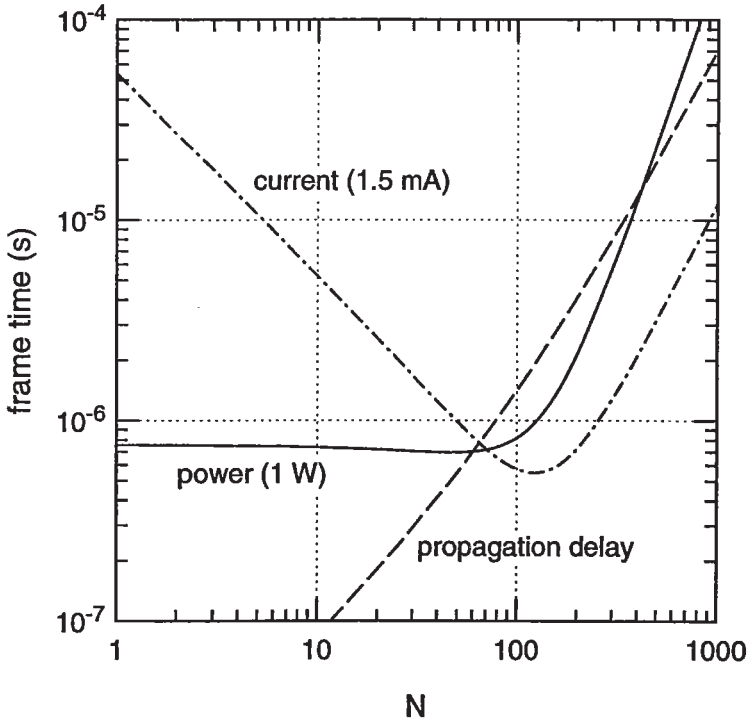

Figure 50 Limitations to the frame rate of a DRAM-addressed active matrix SLM versus array size N. Assumptions which were made to arrive at these curves are noted in the text. The limitation of the FLC response time is not included. (From M. A. Handschy, T. J. Drabik, L. K. Cotter, and S. D. Gaalema, *Proc. SPIE*, *1291*, 158–164 (1990))

Currently no room-temperature device could operate even close to the microsecond frames rates which are predicted because the FLCs respond much more slowly than that. Displays which were designed to operate at elevated temperatures, e.g., 80°C, could operate at microsecond frame rates. Improvements in the frame rates will come with faster FLC mixtures, and possibly with increased VLSI voltages to increase the FLC switching time. The shorter FLC switching time resulting from increased voltage may come at the cost of increasing some of the other limitations given in Fig. 50.

An approach which may prove useful is to operate active backplane FLC SLMs in a diffractive mode. In contrast to the standard transmissive or reflective modulators, modulation by diffraction does not require polarized light, which comes at the cost of at least 50% loss in the input polarizer. The concept of an FLC diffractive modulator was demonstrated with a grating made of stripes of FLC waveplate [Handschy and O'Callaghan 1991]. Upon switching the modulator illuminated with monochromatic light, the intensity of the undiffracted beam was reduced by a factor of 30. In theory this intensity may be reduced to zero, limited only by the nonidealities of the FLC.

A significant constraint in designing active backplane SLMs is that the area which is covered with circuitry is optically degraded because of the resultant roughness. One way to alleviate this problem is to use planarization techniques, common in the VLSI integrated circuit technology. Another, more intriguing, approach is to extend electrical vias through the silicon wafers. With that approach an entire pixel area can be covered with complex and rough circuitry which does not interfere at all with the optical quality of the modulator. The FLC modulator would be placed on the other side of the wafer, on a uniform, smooth surface.

With these and other innovations FLC active backplanes are certain to perform increasingly demanding tasks.

7 FERROELECTRIC LIQUID CRYSTAL SLMs IN PERSPECTIVE

In choosing the "best" SLM we seek high frame rate, high optical resolution, low switching energy, and, for optically addressed SLMs (OASLMs), low optical switching power. These characteristics are intertwined, so that modifications which improve one characteristic do so at the expense of another. Often the product of two characteristics is a constant, as in the gain-bandwidth product of an amplifier. In this final section interrelationships among characteristics and fundamental limits for SLMs are discussed for OASLMs and electrically addressed SLMs (EASLMs).

7.1 Optically Addressed SLMs

Generally in an OASLM the required write-light intensity to switch a pixel increases with the frame rate. In such a case the optical switching energy per bit, i.e., the write-light energy required to switch the smallest resolvable pixel, may be a constant. There are several figures of merit. The bit rate per unit area is the number of pixels which may be switched per unit time in a centimeter square area of the SLM. It is equal to $[2 \times \text{resolution (in lp/cm)}]^2 \times \text{(frame rate)}$. A second figure of merit is the optical switching energy per bit, and a third is the optical switching power, the product of the first two [Williams et al. 1988]. These quantities are plotted in Fig. 51 for several SLM technologies. (The FLC VLSI backplane OASLMs are not included because current devices are far from optimal in the plotted figures of merit.) Except for the high-cost III-V semiconductor SEED device, the bit rate of the FLC OASLM (and its near cousin the ELC OASLM) are the highest available. This is coupled with among the lowest

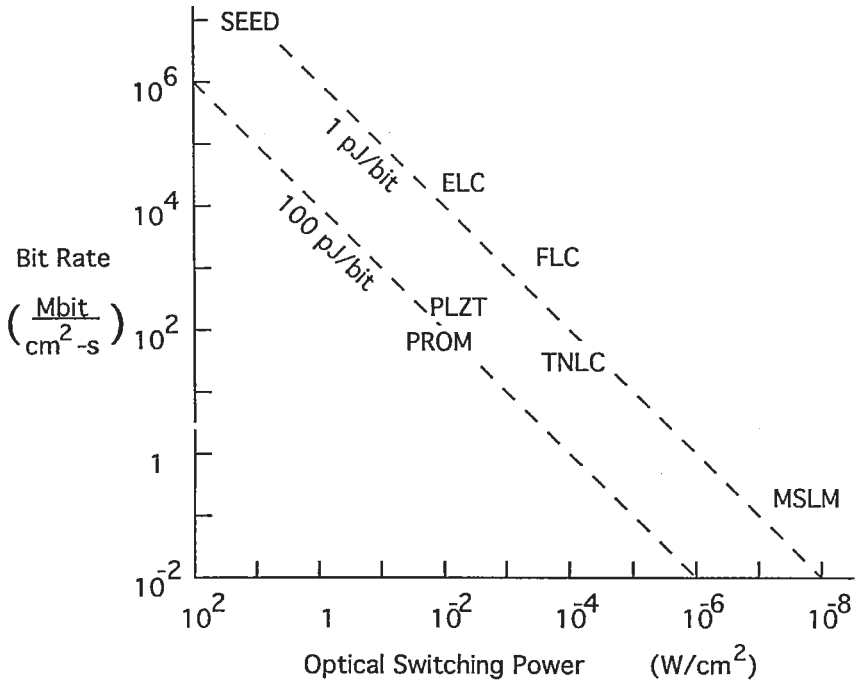

Figure 51 Bit rate per unit area vs. optical switching power for several optically addressed SLM technologies. The bit rate is [2 × resolution (in lp/cm)]² × (frame rate), where the resolution corresponds roughly to the maximum value for 50% MTF. The optical switching power is roughly the minimum write-light intensity required to switch the device at its maximum frame rate. Lines of constant switching energy per bit are plotted for 1 pJ/bit and 100 pJ/bit. Shown with the ferroelectric liquid crystal (FLC) and electroclinic liquid crystal (ELC) values are those for other devices: the twisted nematic liquid crystal modulator (TNLC), the self-electro-optic-effect device (SEED), the Pockels readout optical modulator (PROM), projected values for a silicon/PLZT modulator, and the microchannel plate/$LiNbO_3$ modulator (MSLM). (Format adapted from D. Williams, S. G. Latham, C. M. J. Powles, M. A. Powell, R. C. Chittick, A. P. Sparks, and N. Collings, *J. Phys. D, Appl. Phys.*, *21*, S156–S159 (1988). References to performances specifications are listed in A. D. Fisher, *Int. J. Optoelectron.*, *5*, 125–167 (1990))

switching energy per bit values available, 0.1 pJ/bit. It is apparent that the twisted nematic liquid crystal OASLM performs more poorly in all categories, but because it is a mature technology compared to FLCs, it enjoys much wider commercial application.

7.2 Electrically Addressed SLMs

In EASLMs as in OASLMs a desired characteristic is a high bit rate per unit area, but with some significant differences. In an EASLM the resolution is not simply a function of the physical characteristics of the materials, as is the case for many OASLMs, but is instead dependent upon the technology used to pattern the pixels and fabricate the device. Instead of the optical switching power, which is important for OASLMs, the total switching energy becomes the factor which ultimately limits the bit rate. There is a limit to the amount of power which may be dissipated by an SLM before it overheats, which is somewhere between 25 mW/cm² for a SLM without heat sinking to 10 W/cm² for an SLM which has substantial heat sinking. This limits the frame rate of SLMs no matter how short their response time might be in a single switching cycle.

The switching energy per unit area for a FLC is $W = 2PV$, where P is the spontaneous polarization and V is the applied voltage. (Charging of the geometric capacitance is neglected because the power associated with it is purely reactive.) For a switching time $t_s = 1.8\tau$, where τ is the response time given by Eq. 1, $W = 3.6\eta d/t_s$, where η is the viscosity and d is the cell thickness. Given this switching energy and a maximum allowed power dissipation U, the shortest achievable switching time is [Handschy et al. 1988]

$$t_s = \left(\frac{3.6\eta d}{U}\right)^{1/2} \tag{17}$$

For $d = 1$ μm, $\eta = 50$ mPa-s, and $U = 100$ mW/cm^2, $t_s = 13$ μs. This corresponds to the maximum speed of currently available FLC mixtures at room temperature. It is likely that higher-speed mixtures will become available in the future, and that higher power dissipation can be tolerated.

For FLCs, $LiNbO_3$, PLZT, and GaAs multi–quantum wells, the minimum intrinsic switching times are approximately 10 μs, 10 ps, <10 ns, and 100 ps, respectively [Handschy et al. 1988, Drabik 1991, Lile 1994]. It would appear that the other technologies are faster than FLCs. If one allows a generous 10 W of power dissipation, then the minimum power-dissipation-limited t_s is 2.1 μs, 1.3 ms, 42 μs, and 10 μs, respectively. Because of low power dissipation, FLC SLMs can switch more quickly than many other technologies in which the intrinsic switching times are faster.

ACKNOWLEDGMENTS

I am grateful to M. A. Handschy and B. Landreth for their significant contributions to this chapter. I would also like to thank P. Barbier, D. Doroski, A. Gabor, D. J. McKnight, S. Perlmutter, R. A. Rice, K. H. Wagner, and L. Wang for their valuable comments on the manuscript.

REFERENCES

1. Abdulhalim, I., and G. Moddel, Electrically and optically controlled light modulation and color switching using helix distortion of ferroelectric liquid crystals, *Mol. Cryst. Liq. Cryst.*, *200*, 79–101 (1991a).
2. Abdulhalim, I., and G. Moddel, Switching behavior and electro-optic response due to the soft mode ferroelectric effect in chiral smectic A liquid crystals, *Liq. Cryst.*, *9*, 493–518 (1991b).
3. Abdulhalim, I., G. Moddel, and K. M. Johnson, High-speed analog spatial light modulator using an a-Si:H photosensor and an electroclinic liquid crystal, *Appl. Phys. Lett.*, *55*, 1603–1605 (1989).
4. Akiyama, K., A. Takimoto, M. Miyauchi, Y. Kuratomi, J. Asayama, and H. Ogawa, A new optical neuron device for all-optical neural networks, *Jpn. J. Appl. Phys.*, *30*, 3887–3892 (1991).
5. Andersson, G., I. Dahl, L. Komitov, M. Matuszczyk, S. T. Lagerwall, K. Skarp, B. Stebler, D. Coates, M. Chambers, and D. M. Walba, Smectic A* materials with 11.25 degrees induced tilt angle for full gray scale generation, *Ferroelectrics*, *114*, 137–150 (1991).
6. Andersson, G., I. Dahl, W. Kuczynski, S. T. Lagerwall, K. Sharp, and B. Stebler, The soft-mode ferroelectric effect, *Ferroelectrics*, *84*, 285–315 (1988).
7. Armitage, D., Alignment of liquid crystal on a polarizing metal film, *Appl. Phys. Lett.*, *56*, 1723–1724 (1990).
8. Armitage, D., Ferroelectric liquid crystal alignment by oblique evaporation of SiO_2, *Ferroelectrics*, *122*, 239–252 (1991).

9. Armitage, D., and D. K. Kinell, Miniature spatial light modulators, *Proc. SPIE*, *1296*, 158–165 (1990).
10. Armitage, D., J. I. Thackara, N. A. Clark, and M. A. Handschy, Ferroelectric liquid crystal spatial light modulator, *Mol. Cryst. Liq. Cryst.*, *144*, 309–316 (1987).
11. Barbier, P. R., and G. Moddel, Hydrogenated amorphous silicon photodiodes for optical addressing of spatial light modulators, *Appl. Opt.*, *31*, 3898–3907 (1992).
12. Barbier, P. R., and G. Moddel, An asynchronous image subtracting optically addressed spatial light modulator, in *Amorphous Silicon Technology—1993*, Materials Research Society, Pittsburgh, 1993, pp. 993–998.
13. Barbier, P. R., L. Wang, and G. Moddel, Thin-film photosensor design for liquid crystal spatial light modulators, *Opt. Engr.*, *33*, 1322–1329 (1994).
14. Bawa, S. S., A. M. Biradar, and S. Chandra, Dynamics of helix winding, unwinding and switching of ferroelectric liquid crystals, *Jpn. J. Appl. Phys.*, *26*, 189–192 (1987).
15. Bawa, S. S., A. M. Biradar, K. Saxena, and S. Chandra, Novel alignment techniques for surface stabilized ferroelectric liquid crystal, *Appl. Phys. Lett.*, *57*, 1398–1400 (1990).
16. Bawa, S. S., K. Saxena, and S. Chandra, Removal of zig-zag defects in surface-stabilized ferroelectric liquid crystal cells, *Jpn. J. Appl. Phys.*, *28*, 662–665 (1989).
17. Beard, T. D., W. P. Bleha, and S.-Y. Wong, Ac liquid-crystal light valve, *Appl. Phys. Lett.*, *22*, 90–94 (1973).
18. Beresnev, L. A., L. M. Blinov, and D. I. Dergachev, Electro-optical response of a thin layer of a ferroelectric liquid crystal with a small pitch and high spontaneous polarization, *Ferroelectrics*, *85*, 173–186 (1988c).
19. Beresnev, L. A., L. M. Blinov, D. I. Dergachev, M. V. Loseva, and N. I. Chernova, Electrooptic response of a thin layer of ferroelectric liquid crystal with a small helicoid pitch and a high spontaneous polarization, *Sov. Tech. Phys. Lett.*, *14*, 116–117 (1988a).
20. Beresnev, L. A., L. M. Blinov, D. I. Dergachev, A. I. Zhindulis, I. S. Klimenko, S. I. Paeda, and A. A. Sergeev, Photosensitive structure consisting of a ferroelectric liquid crystal and a photoconductor, *Sov. Tech. Phys. Lett.*, *14*, 117–118 (1988b).
21. Bone, M. F., D. Coates, W. A. Crossland, P. Gunn, and P. W. Ross, Ferroelectric liquid crystal display capable of video line address times, *Displays*, *July*, 115–118 (1987).
22. Bone, M., D. Haven, and D. Slobodin, Video-rate photoaddressed ferroelectric LC light valve with grey scale, Society for Information Display International Symposium, *Digest of Technical Papers*, Vol. 22, SID, Playa del Rey, California, 1991, pp. 254–256.
23. Cambon, P., and J.-L. Bougrenet de la Tocnaye, Mathematical morphology processor using ferroelectric liquid crystal light valves: principle, *Appl. Opt.*, *15*, 3456–3460 (1989).
24. Cambon, P., M. Killinger, and J. L. de Bougrenet de la Tocnaye, Optically addressed spatial light modulator with nipin aSi:H layer and bistable ferroelectric liquid crystal, *Proc. SPIE*, *1562*, 116–125 (1991).
25. Chevrier, J. B., P. Cambon, R. C. Chittick, and B. Equer, Use of n-i-p-i-n a-Si:H structure for bistable optically addressed spatial light modulator, *J. Non-Cryst. Solids*, *137*, *138*, 1325–1328 (1991).
26. Chieu, T. C., and K. H. Yang, Transport properties of ions in ferroelectric liquid crystal cells, *Jpn. J. Appl. Phys.*, *28*, 2240–2246 (1989).
27. Chieu, T. C., and K. H. Yang, Effect of alignment layer conductivity on the bistability of surface-stabilized ferroelectric liquid-crystal devices, *Appl. Phys. Lett.*, *56*, 1326–1328 (1990).
28. Chigrinov, V. G., A. F. Denisov, A. V. Parfenov, and E. P. Pozhidaev, Ferroelectric smectic C* liquid crystal image transducers, *Ferroelectrics*, *85*, 303–312 (1988).
29. Chittick, R. C., W. A. Crossland, J. R. Brocklehurst, P. Cambon, M. Killinger, and J. L. de Bougrenet de la Tocnaye, Development and applications of a truly bistable optically addressed spatial light modulator, in *Spatial Light Modulators and Applications*, 1990 Technical Digest Series, Vol. 14, OSA, Washington, DC, 1990, pp. 136–140.
30. Clark, N. A., and S. T. Lagerwall, Submicrosecond bistable electro-optic switching in liquid crystals, *Appl. Phys. Lett.*, *36*, 899–901 (1980).

31. Clark, N. A., and S. T. Lagerwall, Introduction to ferroelectric liquid crystals, in *Ferroelectric Liquid Crystals* (J. W. Goodby et al., eds.), Gordon and Breach, Philadelphia, 1991, pp. 1–97.
32. Clark, N. A., S. T. Lagerwall, and J. Wahl, Modulators, linear arrays, and matrix arrays using ferroelectric liquid crystals, *Proc. SID*, *26*, 133–139 (1985).
33. Clark, N. A., and T. P. Rieker, Smectic-C chevron, a planar liquid-crystal defect: Implications for the surface-stabilized ferroelectric liquid-crystal geometry, *Phys. Rev. A*, *37*, 1053–1056 (1988).
34. Clerc, J. F., Alignment techniques for L.C.D's based on smectic ferroelectric, *Ferroelectrics*, *85*, 3–13 (1988).
35. Collings, N., W. A. Crossland, P. J. Ayliffe, D. G. Vass, and I. Underwood, Evolutionary development of advanced liquid crystal spatial light modulators, *Appl. Opt.*, *28*, 4740–4747 (1989).
36. Collings, N., W. A. Crossland, R. C. Chittick, and M. F. Bone, The novel application of the electroclinic electro-optic effect to light valve technology, *Proc. SPIE*, *963*, 46–50 (1988).
37. Cotter, L. K., T. J. Drabik, R. J. Dillon, and M. A. Handschy, Ferroelectric-liquid-crystal/silicon-integrated-circuit spatial light modulator, *Optics Lett.*, *15*, 291–293 (1990).
38. Crossland, W. A., M. J. Birch, D. G. Vass, I. Underwood, S. A. Reid, and S. G. Latham, Silicon active backplane spatial light modulators using ferroelectric liquid crystals, in *Spatial Light Modulators and Applications*, 1990 Technical Digest Series, Vol. 14, OSA, Washington, DC, 1990, pp. 94–97.
39. Crossland, W. A., M. Bone, and P. W. Ross, Prospects and problems of ferroelectric LCDs, *Proc. SID*, *29*, 237–244 (1988).
40. Crossland, W. A., B. Needham, and P. W. Ross, Single-crystal silicon active-matrix displays, *Proc. SID*, *26/3*, 175–181 (1985).
41. Curlander, J. C., R. A. Rice, W. T. Cathey, Ferroelectric liquid crystal based binary optical memory employing feedback, *Appl. Opt.*, *32*, 5759–5767 (1993).
42. de Gennes, P. G., *The Physics of Liquid Crystals*, Clarendon Press, Oxford, 1974.
43. Dijon, J., C. Ebel, and P. Maltese, A 6-in.-diagonal black-and-white ferroelectric panel, *Proc. SID*, *29*, 249–252 (1988b).
44. Dijon, J., E. Ebel, C. Vaucher, F. Baume, J. F. Clerc, M. Estor, T. Leroux, P. Maltese, and L. Mulatier, High speed SmC* mixtures: an evaluation of their performances, Soc. Information Display Int. Symp., Anaheim, CA, *Digest of Technical Papers*, SID, Playa del Rey, CA, 1988a, pp. 246–249.
45. Dijon, J., T. Leroux, and P. Maltese, Design of addressing schemes for FLC displays, *Ferroelectrics*, *113*, 371–386 (1991).
46. Doroski, D., S. H. Perlmutter, and G. Moddel, Alignment layers for improved surface stabilized ferroelectric liquid crystal devices, *Appl. Opt.*, *33*, 2608–2610 (1994).
47. Drabik, T. J., Devices for optoelectronic integrated systems, *Proc. SPIE*, *1562*, 194–203 (1991).
48. Drabik, T. J., and M. A. Handschy, Silicon VLSI/ferroelectric liquid crystal technology for micropower optoelectronic computing devices, *Appl. Opt.*, *29*, 5220–5223 (1990).
49. Drevillon, B., S. Kumar, P. Rocca i Cabarrocas, and J. M. Siefert, In situ investigation of the optoelectronic properties of transparent conducting oxide/amorphous silicon interfaces, *Appl. Phys. Lett.*, *54*, 2088–2090 (1989).
50. Elston, S. J., and J. R. Sambles, The observation of half splayed states in ferroelectric liquid crystal filled cells by the excitation of optic modes, *Jpn. J. Appl. Phys.*, *29*, L641–L644 (1990).
51. Elston, S. J., J. R. Sambles, and M. G. Clark, The mechanism of ac stabilization in ferroelectric liquid-crystal-filled cells, *J. Appl. Phys.*, *68*, 1242–1246 (1990).
52. Escher, C., H.-R. Dübal, T. Harada, G. Illian, M. Murakami, and D. Ohlendorf, The SSFLC switching behavior in view of chevron layer geometry and ionic charges, *Ferroelectrics*, *113*, 269–303 (1991).

53. Fracasso, B., J. L. de Bougrenet de la Tocnaye, and P. Ambs, Recording reconfigurable binary computer-generated holograms on bistable optically addressed ferroelectric liquid-crystal spatial light modulators, *Opt. Lett.*, *15*, 1473–1475 (1990).
54. Fukushima, S., T. Kurokawa, S. Matsuo, and H. Kozawaguchi, Bistable spatial light modulator using a ferroelectric liquid crystal, *Opt. Lett.*, *15*, 285–287 (1990).
55. Fukushima, S., T. Kurokawa, and M. Ohno, Real-time hologram construction and reconstruction using a high-resolution spatial light modulator, *Appl. Phys. Lett.*, *58*, 787–789 (1991).
56. Fünfschilling, J., and M. Schadt, Fast responding and highly multiplexible distorted helix ferroelectric liquid-crystal displays, *J. Appl. Phys.*, *66*, 3877–3882 (1989).
57. Fünfschilling, J., and M. Schadt, New short-pitch bistable ferroelectric (SBF) liquid crystal displays, *Jpn. J. Appl. Phys.*, *30*, 741–746 (1991).
58. Gabor, A. M., B. Landreth, and G. Moddel, Integrating mode for an optically addressed spatial light modulator, *Appl. Opt.*, *32*, 3064–3067 (1993).
59. Garoff, S., and R. B. Meyer, Electroclinic effect at the A-C phase change in a chiral smectic liquid crystal, *Phys. Rev. Lett.*, *38*, 848–851 (1977); *Phys. Rev. A*, *19*, 338–347 (1979).
60. Gohara, Y., Y. Kobayashi, S. Fujiwara, N. Wakita, T. Uemura, K. Nakao, H. Ohnishi, and K. Johten, A 1280 × 1280 matrix-addressed FLC light valve for the image projection display, Soc. Information Display Int. Symp., *Digest of Technical Papers*, Vol. 22, SID, Playa del Rey, CA., 1991, pp. 257–260.
61. Gomes, C. M., S. Tsujikawa, H. Maeda, H. Sekine, T. Yamazaki, M. Sakamoto, F. Okumura, and S. Kobayashi, Ferroelectric liquid crystal spatial light modulator with gray-scale capability, *Jpn. J. Appl. Phys.*, *30*, L386–L388 (1991).
62. Handschy, M. A., D. B. Banas, and S. D. Gaalema, Multipurpose spatial light modulator, in *Spatial Light Modulators and Applications*, 1993 Technical Digest Series, Vol. 6, OSA, Washington, DC, 1993b, pp. 62–65.
63. Handschy, M. A., and N. A. Clark, Structures and responses of ferroelectric liquid crystals in the surface-stabilized geometry, *Ferroelectrics*, *59*, 69–116 (1984).
64. Handschy, M. A., L. K. Cotter, J. D. Cunningham, T. J. Drabik, and S. D. Gaalema, One-transistor DRAM FLC/VLSI SLM, in *Spatial Light Modulators and Applications*, 1993 Technical Digest Series, Vol. 6, OSA, Washington, DC, 1993a, pp. 14–17.
65. Handschy, M. A., and T. J. Drabik, FLC/VLSI silicon retina, in *OSA Annual Meeting Technical Digest* 1990, Vol. 15 of the OSA Technical Digest Series, Optical Society of America, Washington, DC, 1990b, p. 259.
66. Handschy, M. A., T. J. Drabik, L. K. Cotter, and S. D. Gaalema, Fast ferroelectric-liquid-crystal spatial light modulator with silicon-integrated-circuit active backplane, *Proc. SPIE*, *1291*, 158–164 (1990a).
67. Handschy, M. A., K. M. Johnson, G. Moddel, and L. A. Pagano-Stauffer, Electro-optic applications of ferroelectric liquid crystals to optical computing, *Ferroelectrics*, *85*, 279–289 (1988).
68. Handschy, M. A., M. J. O'Callaghan, Ferroelectric liquid-crystal devices for high-resolution imaging, Soc. Information Display Int. Symp., *Digest of Technical Papers*, Vol. 22, SID, Playa del Rey, CA, 1991, pp. 246–249.
69. Harada, T., M. Taguchi, K. Iwasa, and M. Kai, An application of chiral smectic-C liquid crystal to a multiplexed large-area display, Soc. Information Display Int. Symp., *Digest of Technical Papers*, SID, Playa del Rey, CA, 1985, pp. 131–134.
70. Hartmann, W. J. A. M., Charge-controlled phenomena in the surface-stabilized ferroelectric liquid-crystal structure, *J. Appl. Phys.*, *66*, 1132–1136 (1989a).
71. Hartmann, W. J. A. M., Ferroelectric liquid-crystal video display, *Proc. SID*, *30*, 99–103 (1989b). Identical paper also in conference record of the IEEE 1988 Int. Display Research Conf., pp. 191–194 (1988) and in *IEEE Trans. Electron Dev.*, *36*, 1895 (1989).
72. Hartmann, W. J. A. M., Ferroelectric liquid crystal displays for television application, *Ferroelectrics*, *122*, 1–26 (1991).

73. Hartmann, W. J. A. M., and A. M. M. Luyckx-Smolders, The bistability of the surface-stabilized ferroelectric liquid-crystal effect in electrically reoriented chevron structures, *J. Appl. Phys.*, *67*, 1253–1261 (1990).
74. Hashimoto, M., Y. Fukuda, S. Ishibashi, and K.-i. Kitayama, Thresholding characteristics of an optically addressable GaAs-pin/ferroelectric liquid crystal spatial light modulator and its applications, *IEICE Trans. Electron.*, *E75-C*, 1395–1398 (1992).
75. Hatano, T., K. Yamamoto, H. Takezoe, and A. Fukuda, Alignment controls and switching characteristics in a ferroelectric liquid crystal with the phase sequence N*-S_C*, *Jpn. J. Appl. Phys.*, *25*, 1762–1767 (1986).
76. Hatoh, H., A. Murayama, S. Kamagami, and S. Matsumoto, Large-area ferroelectric multicolor LCD with high information content, *Proc. SID*, *28*, 205–209 (1987).
77. Hecht, E., *Optics*, 2nd ed., Addison-Wesley, Reading, MA, 1987, pp. 507–512.
78. Heeks, S. K., A. Mosley, B. M. Nicholas, P. C. Rundle, and P. Schlusche, Large area ferroelectric liquid crystal displays, *Ferroelectrics*, *122*, 27–35 (1991).
79. Heeks, S. K., A. Mosley, B. M. Nicholas, P. Schlusche, and P. C. Rundle, A high-resolution large-area ferroelectric LCD with a flexible electronic drive architecture, in *Digest of Technical Papers*, Vol. 23, SID, Playa del Rey, CA, 1992, pp. 221–223.
80. Horikawa, T., S. Tahata, S. Kaho, T. Masumi, N. Mikawi, K. Takahashi, M. Nunoshita, H. Nakajima, and K. Nishi, Ferroelectric liquid crystal light valve using SiO_2/a-Si:H photodiode, *Amorphous Silicon Technology—1991*, Vol. 219, Materials Research Society, Pittsburgh, 1991, pp. 203–208.
81. Hudson, T. D., R. K. Worcester, and D. A. Gregory, Performance characteristics of an optically addressed ferroelectric liquid-crystal spatial light modulator, *Appl. Opt.*, *30*, 2867–2872 (1991).
82. Inaba, Y., K. Katagiri, H. Inoue, J. Kanbe, S. Yoshihara, and S. Iijima, Essential factors in high-duty FLC matrix displays, *Ferroelectrics*, *85*, 255–264 (1988).
83. Ishikawa, K., K. Hashimoto, H. Takezoe, A. Fukuda, and E. Kuze, A practical method of preparing thin homogeneous ferroelectric smectic cells for electro-optical microsecond switches. II: Sm A liquid crystal growth under a temperature gradient, *Jpn. J. Appl. Phys.*, *23*, L211–L213 (1984).
84. Jared, D. A., and K. M. Johnson, Optically addressed thresholding very-large-scale-integration/liquid-crystal spatial light modulators, *Opt. Lett.*, *16*, 987–969 (1991).
85. Jared, D. A., and K. M. Johnson, Optically addressed zero-crossing edge detection spatial light modulator, in *Spatial Light Modulators and Applications*, 1993 Technical Digest Series, Vol. 6, OSA, Washington, DC, 1993, pp. 66–68.
86. Jared, D. A., K. M. Johnson, and G. Moddel, Joint transform correlator using an amorphous silicon ferroelectric liquid crystal spatial light modulator, *Opt. Commun.*, *76*, 97–102 (1990).
87. Jared, D. A., R. Turner, and K. M. Johnson, Electrically addressed spatial light modulator that uses a dynamic memory, *Opt. Lett.*, *16*, 1785–1787 (1991).
88. Johnson, K. M., C. C. Mao, G. Moddel, M. A. Handschy, and K. Arnett, High-speed, low-power optical phase conjugation using a hybrid amorphous silicon/ferroelectric-liquid-crystal device, *Opt. Lett.*, *15*, 1114–1116 (1990).
89. Johnson, K. M., D. J. McKnight, C. C. Mao, G. Sharp, J.-Y. Liu, and A. Sneh, Chiral smectic liquid crystals for high information content displays and spatial light modulators, in *Spatial Light Modulators and Applications*, 1993 Technical Digest Series, Vol. 6, OSA, Washington, DC, 1993b, pp. 18–21.
90. Johnson, K. M., D. J. McKnight, and I. Underwood, Smart spatial light modulators using liquid crystals on silicon, *IEEE J. Quantum Electron.*, *29*, 699–714 (1993a).
91. Johnson, K. M., and G. Moddel, Motivations for using ferroelectric liquid crystal spatial light modulators in neurocomputing, *Appl. Opt.*, *28*, 4888–4897 (1989).
92. Jones, J. C., M. J. Towler, and E. P. Raynes, The importance of dielectric biaxiality for ferroelectric liquid crystal devices, *Ferroelectrics*, *121*, 91–102 (1991).

93. Kanbe, J., H. Inoue, A. Mizutome, Y. Hanyuu, K. Katagiri, and S. Yoshihara, High resolution, large area FLC display with high graphic performance, *Ferroelectrics*, *114*, 3–26 (1991).
94. Killinger, M., J. L. de Bougrenet de la Tocnaye, and P. Cambon, Controlling the grey level capacity of a bistable FLC spatial light modulator, *Ferroelectrics*, *122*, 89–99 (1991).
95. Killinger, M., J. L. de Bougrenet de la Tocnaye, P. Cambon, R. C. Chittick, and W. A. Crossland, Bistability and nonlinearity in optically addressed ferroelectric liquid crystal spatial light modulators: applications to neurocomputing, *Appl. Opt.*, *31*, 3930–3936 (1992).
96. Kobayashi, Y., T. Takemori, N. Mukohzaka, N. Yoshida, and S. Fukushima, Real time displacement measurement with FLC-SLM by correlation of speckle patterns, in *Spatial Light Modulators and Applications*, 1993 Technical Digest Series, Vol. 6, OSA, Washington, DC, 1993, pp. 26–29.
97. Kondo, K., Y. Sato, K. Miyasato, H. Takezoe, A. Fukuda, E. Kuze, K. Faltischiler, and K. Sharp, Magnetic field effects on preparing thin homogeneous ferroelectric smectic cells for electro-optical microsecond switches, *Jpn. J. Appl. Phys.*, *1*, L12–L15 (1983).
98. Konuma, T., A. Mase, S. Yamazaki, M. Yagi, H. Kondo, and T. Hagiwara, Ferroelectric liquid-crystal display with multi-micro-domains driven by a video rate, Soc. Information Display Int. Symp., *Digest of Technical Papers*, Vol. 22, SID, Playa del Rey, CA, 1991, pp. 400–403.
99. Kuniyasu, S., H. Fukuro, S. Maeda, K. Nakaya, M. Nitta, N. Ozaki, and S. Kobayashi, The strength of rubbing worked on polyimide films for aligning nematic and chiral smectic liquid crystals: controlling pretilt angles and some electrooptic performances of LCSs, *Jpn. J. Appl. Phys.*, *27*, 827–829 (1988).
100. Kurokawa, T., and S. Fukushima, Spatial light modulators using ferroelectric liquid crystal, *Opt. Quant. Electron.*, *24*, 1151–1163 (1992).
101. Lagerwall, S. T., Comments on liquid crystal terminology, nomenclature and conventions, *Ferroelectrics*, *85*, 497–501 (1988).
102. Lagerwall, S. T., N. A. Clark, J. Dijon, and J. F. Clerc, Ferroelectric liquid crystals: the development of devices, *Ferroelectrics*, *94*, 3–62 (1989).
103. Lagerwall, S. T., J. Wahl, and N. A. Clark, Ferroelectric liquid crystals for displays, Conf. record 1985 Int. Display Res. Conf., 1985, pp. 213–221.
104. Landreth, B., C.-C. Mao, and G. Moddel, Operating characteristics of optically addressed spatial light modulators incorporating distorted helix ferroelectric liquid crystal, *Jpn. J. Appl. Phys.*, *30*, 1400–1404 (1991).
105. Landreth, B., and G. Moddel, Analog response from binary spatial light modulators, *Proc. SPIE*, *1296*, 64–72 (1990).
106. Landreth, B., and G. Moddel, Gray-scale response from optically addressed spatial light modulators incorporating surface-stabilized ferroelectric liquid crystals, *Appl. Opt.*, *31*, 3937–3944 (1992).
107. Le Pesant, J. P., J. M. Perbet, B. Mourey, M. Harenz, G. Decobert, and J. C. Dubois, Optical switching of chiral smectic C at room temperature, *Mol. Cryst. Liq. Cryst.*, *129*, 61–74 (1985).
108. Leroux, T., F. Baume, J. F. Clerc, J. Dijon, C. Ebel, M. Estor, L. Mulatier, and C. Vauchier, Black and white FLC TV panel with grey levels, Conf. record IEEE Int. Display Res. Conf., 1988, pp. 111–113.
109. Li, H.-Y., J.-J. Drolet, D. Psaltis, and M. A. Handschy, Optoelectronic chip for the implementation of back error propagation, Proc. LEOS Summer Topical Meeting Smart Pixels, 1992, pp. 79–80.
110. Li, W., R. A. Rice, G. Moddel, L. A. Pagano-Stauffer, and M. A. Handschy, Hydrogenated amorphous-silicon photosensor for optically addressed high-speed spatial light modulators, *IEEE Trans. Electron Dev.*, *36*, 2959–2964 (1989).
111. Lile, D., Optoelectronic devices, in *Modern Compound Semiconductor Technology and Devices* (P. H. Holloway and G. E. McGuire, eds.), Noyes, Park Ridge, NJ, 1994.

112. Maclennan, J. E., M. A. Handschy, and N. A. Clark, Director reorientation dynamics in chevron ferroelectric liquid crystal cells, *Liq. Cryst.*, *7*, 787–796 (1990).
113. Mada, H., and H. Suzuki, Reverse hysteresis loop of nematic liquid crystals in C-V characteristic due to electric field, *Jpn. J. Appl. Phys.*, *26*, L1092–L1094 (1987).
114. Maltese, P., J. Dijon, and T. Leroux, Fast addressing modes for ferroelectric LC display panels, Conf. record IEEE Int. Display Res. Conf., 1988b, pp. 98–101.
115. Maltese, P., J. Dijon, T. Leroux, and D. Sarrasin, Addressing cycles for fast settling grey shades in ferroelectric liquid crystal matrices, *Ferroelectrics*, *85*, 265–274 (1988a).
116. Mao, C. C., K. M. Johnson, and G. Moddel, Optical phase conjugation using optically addressed chiral smectic liquid crystal spatial light modulators, *Ferroelectrics*, *114*, 45–53 (1991a).
117. Mao, C. C., K. M. Johnson, R. Turner, D. Jared, and D. Doroski, Applications of binary and analog hydrogenated amorphous silicon/ferroelectric liquid-crystal optically addressed spatial light modulators, *Appl. Opt.*, *31*, 3908–3916 (1992).
118. Mao, C. C., B. Landreth, K. M. Johnson, and G. Moddel, Photovoltaic optically addressed spatial light modulator, *Ferroelectrics*, *122*, 455–466 (1991b).
119. Matsumoto, S., H. Hatoh, S. Kamagami, and A. Murayama, Multiplexed ferroelectric liquid crystal display, *Ferroelectrics*, *85*, 235–254 (1988b).
120. Matsumoto, S., A. Murayama, H. Hatoh, Y. Kinoshita, H. Hirai, M. Ishikawa, S. Kamagami, Large-area video-rate multicolor ferroelectric liquid-crystal display, *Digest of Technical Papers*, SID, Playa del Rey, CA, 1988a, pp. 41–44.
121. Matsunga, M., S. Masubuchi, and S. Takahashi, A full-color ferroelectric liquid-crystal shutter array, *Digest of Technical Papers*, Vol. 23, SID, Playa del Rey, CA, 1992, pp. 737–740.
122. Maximus, B., E. De Ley, A. De Meyere, and H. Pauwels, Ion transport in SSFLCD's, *Ferroelectrics*, *121*, 103–112 (1991).
123. Mead, C., *Analog VLSI and Neural Systems*, Addison-Wesley, Reading, MA, 1989, Chapter 15.
124. McKnight, D. J., K. M. Johnson and R. A. Serati, Electrically addressed 256 by 256 liquid-crystal-on-silicon spatial light modulator, *Opt. Lett.*, *18*, 2159–2161 (1993).
125. McKnight, D. J., D. G. Vass, and R. M. Sillito, Development of a spatial light modulator: a randomly addressed liquid-crystal-over-nMOS array, *Appl. Opt.*, *28*, 4757–4762 (1989).
126. Meyer, R. B., Ferroelectric liquid crystals; a review, *Mol. Cryst. Liq. Cryst.*, *40*, 33–48 (1977).
127. Meyer, R. B., L. Liebert, L. Strzelecki and P. Keller, Ferroelectric liquid crystals, *J. Phys. Lett.*, *36*, L69–L71 (1975).
128. Mochizuki, A., M. Hirose, and M. Nakatsuka, Zigzag defect free alignment and good bistability of surface stabilized S_C^* cells, *Ferroelectrics*, *113*, 353–359 (1991a).
129. Mochizuki, A., K. Motoyoshi, and M. Nakatasuka, A high contrast and high transmittance multiplexing SSFLC display utilizing naphthalene base liquid crystal materials, *Ferroelectrics*, *122*, 37–51 (1991b).
130. Moddel, G., Amorphous silicon for optically addressed spatial light modulators in *Amorphous and Microcrystalline Semiconductor Devices*: *Optoelectronic Devices* (J. Kanicki, ed.), Artech House, Norwood MA, 1991a, pp. 369–412.
131. Moddel, G., and P. B. Barbier, Response time of a-Si:H photodiodes for optically addressed spatial light modulators, in *Amorphous Silicon Technology—1991*, Vol. 219, Materials Research Society, Pittsburgh, 1991b, pp. 155–165.
132. Moddel, G., K. M. Johnson, and M. A. Handschy, Photoaddressing of high speed liquid crystal spatial light modulators, *Proc. SPIE*, *754*, 207–213 (1987).
133. Moddel, G., K. M. Johnson, W. Li, R. A. Rice, L. A. Pagano-Stauffer, and M. A. Handschy, High speed binary optically addressed spatial light modulators, *Appl. Phys. Lett.*, *55*, 537–539 (1989).

134. Moddel, G., C. T. Kuo, K. M. Johnson and W. Li, Optical addressing of high-speed spatial light modulators with a-Si:H, in *Amorphous Silicon Technology*, Vol. 118, Materials Research Society, Pittsburgh, 1988, pp. 405–410.
135. Myrvold, B. O., Epitaxial growth alignment of ferroelectric smectic C phases on rubbed polymers, *Liq. Cryst.*, *3*, 1255–1266 (1988a).
136. Myrvold, B. O., Alignment of ferroelectric liquid crystals on commercially available polyimides, *Ferroelectrics*, *85*, 25–30 (1988b).
137. Nagata, T., T. Umeda, T. Igawa, A. Mukoh, and Y. Hori, Physical properties of ferroelectric liquid crystals and ac field-stabilization effect, *Jpn. J. Appl. Phys.*, *27*, 1122–1125 (1988).
138. Nakajima, H., J. Kisaki, S. Tahata, T. Horikawa, and K. Nishi, High resolution display using a laser addressed ferroelectric liquid crystal light valve, *Proc. SPIE*, *1456*, 29–40 (1991).
139. Nakaya, K., B. Y. Zhan, M. Yoshida, I. Isa, S. Shindow, and S. Kobayashi, Electrooptic bistability of a ferroelectric liquid crystal device prepared using charge-transfer complex-doped polymide-orientation films, *Jpn. J. Appl. Phys.*, *28*, 116–118 (1989).
140. Nolte, D. D., Resolution of electo-optic spatial light modulators: the role of the lateral transport, *Opt. Commun.*, *92*, 199–204 (1992).
141. Orihara, H., and Y. Ishibashi, Switching characteristics of ferroelectric liquid crystal DOBAMBC, *Jpn. J. Appl. Phys.*, *23*, 1274 (1984).
142. Orihara, H., A. Suzuki, Y. Isyhibashi, K. Gouhara, Y. Yamada, and N. Yamaoto, Effect of a polyimide coat on the layer structure in a surface-stabilized ferroelectric liquid crystal cell, *Jpn. J. Appl. Phys.*, *28*, L676–L678 (1989).
143. Ostrovskii, B. I., and V. G. Chigrinov, Linear electrooptic effect in chiral smectic C liquid crystals, *Sov. Phys. Cryst.*, *25*, 322–325 (1980).
144. Ouchi, Y., J. Lee, H. Takezoe, A. Fukuda, K. Kondo, T. Kitamura, and A. Mukoh, Smectic layer structure of thin ferroelectric liquid crystal cells aligned by SiO oblique evaporation technique, *Jpn. J. Appl. Phys.*, *27*, L1993–L1995 (1988b).
145. Ouchi, Y., H. Takano, H. Takezoe, and A. Fukuda, Zig-zag defects and disclinations in the surface-stabilized ferroelectric liquid crystals, *Jpn. J. Appl. Phys.*, *27*, 1–7 (1988a).
146. Ouchi, Y., H. Takezoe, and A. Fukuda, Display applications of antiferroelectric liquid crystals (switching of field-induced antiferro-ferroelectric phase transition), Soc. Information Display Int. Symp., *Digest of Technical Papers*, Vol. 22, SID, Playa del Rey, CA, 1991, pp. 385–388.
147. Owechko, Y., and A. R. Tanguay, Theoretical resolution limitations of electrooptic spatial light modulators. I: Fundamental limitation, *J. Opt. Soc. Am. A*, *1*, 635–643 (1984).
148. Panarin, Yu. P., E. P. Pozhidaev, and M. I. Barnik, Bistability in ferroelectric liquid crystals, *Mol. Mat.*, *1*, 29–42 (1992).
149. Patel, J. S., Room-temperature switching behavior of ferroelectric liquid crystals in thin cells, *Appl. Phys. Lett.*, *47*, 1277–1279 (1985).
150. Patel, J. S., Ferroelectric liquid crystal modulator using twisted smectic structure, *Appl. Phys. Lett.*, *60*, 280–282 (1992).
151. Patel, J. S., and J. W. Goodby, Alignment of liquid crystals which exhibit cholesteric to smectic C* phase transitions, *J. Appl. Phys.*, *59*, 2355–2360 (1986).
152. Patel, J. S., T. M. Leslie, and J. W. Goodby, A reliable method of alignment for smectic liquid crystals, *Ferroelectrics*, *59*, 137–144 (1984).
153. Perlmutter, S. H., D. Doroski, P. R. Barbier, S. Wichart, and G. Moddel, The influence of ion migration in ferroelectric liquid crystal on the performance of optically addressed spatial light modulators, OSA Ann. Meeting Technical Digest 1992, *Technical Digest Series*, Vol. 23, OSA, Washington, DC, 1992, p. 82.
154. Picart, B., L. Dugoujon, O. Petit, C. Destrade, C. Léon, H. T. Nguyen, and J. P. Marcerou, Visualization of VLSI integrated circuits by means of ferroelectric liquid crystals, *Proc. SPIE*, *1080*, 131–139 (1989).

155. Radehaus, C. V., J. I. Pankove, S. Perlmutter, G. Moddel, M. Kuijk, P. Heremans, G. Borghs, J. Connolly, and N. Hughes, Minimum detection with a 2-D optoelectronic pnpn winner-take-all array, *Appl. Opt.*, in press.
156. Reiger, H., C. Escher, Gerd Illian, H. Jahn, A. Kalbeitzel, T. Harada, A. Weippert, and E. Lüder, FLCD showing high contrast and high luminance, Soc. Information Display Int. Symp., *Digest of Technical Papers*, Vol. 22, SID, Playa del Rey, CA, 1991, pp. 396–399.
157. Reinhart, K-F., L. Dorfmüller, K. Marx, and T. Matuszczyk, Addressing of ferroelectric liquid crystal matrices and electrooptical characterization, *Ferroelectrics*, *113*, 405–417 (1991).
158. Reynaerts, C., and A. De Vos, Hysteresis loops of ferroelectric liquid crystal displays, *Ferroelectrics*, *113*, 439–452 (1991b).
159. Reynaerts, C., J. Van Campenhout, and F. Cuypers, Time integration grey scales for ferroelectric LCD's, *Ferroelectrics*, *113*, 419–137 (1991a).
160. Rice, R. A., P. J. Close, and G. Moddel, Dynamic thresholding with the three-terminal optically addressed spatial light modulator, *Amorphous Silicon Technology—1992*, Materials Research Society, Pittsburgh, 1992a, pp. 1087–1092.
161. Rice, R. A., and G. Moddel, A circuit model for the optical and electrical response of an FLC to an arbitrary driving voltage, Soc. Information Display Int. Symp., *Digest of Technical Papers*, Vol. 23, SID, Playa del Rey, CA, 1992b, pp. 224–227.
162. Rice, R. A., G. Moddel, I. Abdulhalim, and C. M. Walker, A three-terminal spatial light modulator optically addressed by an a-Si:H photosensor, *J. Non-Cryst. Solids*, *115*, 96–98 (1989).
163. Roach, W. R., Resolution of electrooptic light valves, *IEEE Trans. Electron Dev.*, *ED-21*, 453–459 (1974).
164. Robinson, M. G., Analog nonvolatile data storage and update in an optically addressed spatial light modulator, *Opt. Lett.*, *17*, 895–897 (1992).
165. Roe, M. G., and K. L. Schehrer, High-speed and high-contrast operation of ferroelectric liquid crystal optically addressed spatial light modulators, *Opt. Eng.*, *32*, 1662–1667 (1993).
166. Rose, A., and P. K. Weimer, Physical limits to the performance of imaging systems, *Phys. Today*, *42*, 27 (1989).
167. Ross, P. W., 720 × 400 matrix ferroelectric display operating at video frame rate, Conf. record IEEE Int. Display Res. Conf., 1988, pp. 185–190.
168. Ross, P. W., K. Alexander, L. G. Banks, A. N. Carrington, L. K. M. Chan, D. J. Gibbons, R. L. Hedgley, N. Lui, M. J. Naylor, B. Needham, N. E. Riby, P. W. Surguy, A. W. Vaidya, and J. C. White, Color digital ferroelectric LCDs for laptop applications, in *Digest of Technical Papers*, Vol. 23, SID, Playa del Rey, CA, 1992, pp. 217–220.
169. Samuelson, L., H. Wieder, C. R. Guarnieri, J. Chevallier, and A. Onton, Fast photoconductor coupled liquid-crystal light valve, *Appl. Phys. Lett.*, *34*, 450–452 (1979).
170. Schehrer, K. L., L. Schirber, M. Handschy, and M. G. Roe, Retina-like adaptive thresholding in a nonlinear joint transform correlator, in *Spatial Light Modulators and Applications*, Technical Digest Series, Vol. 6, OSA, Washington, DC, 1993, pp. 89–92.
171. Shimizu, K., Y. Tanaka, K. Sekikawa, K. Inoue, and H. Hori, Matrix addressing of ferroelectric liquid-crystal displays, *Proc. SID*, *28*, 211–215 (1987).
172. Slagle, T. M., and K. Wagner, A winner-take-all spatial light modulator, *Opt. Lett.*, *17*, 1164–1166 (1992).
173. Sterling, R. D., R. D. Te Kolste, J. M. Haggerty, T. C. Borah, and W. P. Bleha, Video-rate liquid-crystal light-valve using an amorphous silicon photoconductor, Soc. Information Display Int. Symp., *Digest of Technical Papers*, Vol. 21, SID, Playa del Rey, CA, 1990, pp. 327–329.
174. Surguy, P. W. H., P. J. Ayliffe, M. J. Birch, M. F. Bone, I. Couldon, W. A. Crossland, J. R. Hughes, P. W. Ross, F. C. Saunders, and M. J. Towler, The "JOERS/Alvey" Ferroelectric multiplexing scheme, *Ferroelectrics*, *122*, 63–79 (1991).

175. Takahashi, N. S.-i., H. Asada, M. Miyahara, and S. Kurita, High-speed light valve using an amorphous silicon photosensor and ferroelectric liquid crystals, *Appl. Phys. Lett.*, *51*, 1233–1235 (1987).
176. Tsujikawa, S., F. Okumura, M. Sakamoto, H. Ichinose, M. Imai, K. Sera, H. Asada, and K. Kubota, Optically-addressed TFT liquid crystal light valve, Conf. Record Int. Topical Meeting Optical Computing, Kobe, Japan, 1990, pp. 23–24.
177. Uchida, T., M. Hirano, and H. Sakai, Director orientation of a ferroelectric liquid crystal on substrates with rubbing treatment: the effect of surface anchoring strength, *Liq. Cryst.*, *5*, 1127–1137 (1989).
178. Umeda, T., T. Nagata, A. Mukoh, and Y. Hori, Influences of alignment materials and LC layer thickness on AC field-stabilization phenomena of ferroelectric liquid crystals, *Jpn. J. Appl. Phys.*, *27*, 1115–1121 (1988).
179. Underwood, I., D. G. Vass, and R. M. Sillito, Evaluation of an nMOS VLSI array for an adaptive liquid-crystal spatial light modulator, *IEE Proc.*, *133*, 77–82 (1986).
180. Underwood, I., D. G. Vass, R. M. Sillitto, G. Bradford, N. E. Fancey, A. O. Al-Chalabi, M. J. Birch, W. A. Crossland, A. P. Sparks, and S. C. Latham, A high performance spatial light modulator, *Proc. SPIE*, *1562*, 107–115 (1991).
181. Vaxiviére, J., B. Labroo, and Ph. Martinot-Lagarde, Ion bump in the ferroelectric liquid crystal domains reversal current, *Mol. Cryst. Liq. Cryst.*, *173*, 61–73 (1989).
182. Wahl, J., Electronic addressing of FLC devices, *Ferroelectrics*, *85*, 207–233 (1988).
183. Wahl, J., T. Matuszczyk, and S. T. Lagerwall, A dynamic picture of a ferroelectric liquid crystal screen in multiplex drive, *Mol. Cryst. Liq. Cryst.*, *146*, 143–150 (1987).
184. Wahlstrom, E. E., *Optical Crystallography*, 4th ed., Wiley, New York, 1969, pp. 236–267.
185. Wakita, N., Y. Iwai, T. Uemura, S. Fujiwara, Y. Gohara, I. Ota, Y. Masumoto, Y. Miyatake, T. Tsuda, and Y. Horio, Multi-color projection display using 3 FLC LVs with 4 million pixels, *Ferroelectrics*, *114*, 27–41 (1991).
186. Williams, D., S. G. Latham, C. M. J. Powles, M. A. Powell, R. C. Chittick, A. P. Sparks, and N. Collings, An amorphous silicon/chiral smectic spatial light modulator, *J. Phys. D, Appl. Phys.*, *21*, S156–S159 (1988).
187. Williams, P. A., N. A. Clark, M. B. Ros, D. M. Walba, and M. D. Wand, Large electroclinic effect in a new chiral liquid crystal material, *Ferroelectrics*, *121*, 143–146 (1991).
188. Wu, Q. h., S. H. Perlmutter, R. A. Rice, and G. Moddel, High-reflectivity patterned metal mirror used in an optically addressed spatial light modulator, *Opt. Eng.*, *33*, 946–950 (1994).
189. Xue, J.-Z., M. A. Handschy, and N. A. Clark, Electrooptic response during switching of a ferroelectric liquid crystal cell with uniform director orientation, *Ferroelectrics*, *73*, 305–314 (1987).
190. Xue, W., N. Collings, and K. J. Weible, The performance characteristics of a ferroelectric liquid crystal light valve with pixellated metal reflector, *Opt. Comput. Process.*, *2*, 107–114 (1992).
191. Yamamoto, N., Y. Yamada, K. Mori, H. Orihara, and Y. Ishibiashi, Ferroelectric liquid crystal display with high contrast ratio, *Jpn. J. Appl. Phys.*, *28*, 524–529 (1989).
192. Yamamoto, S., Optically addressed spatial light modulators using FLCs, *Sci. Tech. Jpn.*, *9*, 20–21 (1990).
193. Yamamoto, S., T. Ebihara, N. Kato, and H. Hoshi, Ferroelectric liquid crystal spatial light modulator using a hydrogenated amorphous silicon as a photoconductor, *Ferroelectrics*, *114*, 81–92 (1991).
194. Yang, K. H., T. C. Chieu, and S. Osofsky, Depolarization field and ionic effects on the bistability of surface-stabilized ferroelectric liquid-crystal devices, *Appl. Phys. Lett.*, *55*, 125–127 (1989).
195. Yariv, A., and P. Yeh, *Optical Waves in Crystals*, Wiley, New York, 1984, pp. 143–147.

196. Yoshino, K., S. Kishio, M. Ozaki, T. Sakurai, N. Mikami, R. Higuchi, and M. Honma, Low threshold field of electro-optic effect in ferroelectric liquid crystal with extremely large spontaneous polarization, *Jpn. J. Appl. Phys.*, *25*, L416–L418 (1986).
197. Zou, Z., N. A. Clark, and M. A. Handschy, Ionic transport effects in SSFLC cells, *Ferroelectrics*, *121*, 147–158 (1991).
198. Zou, Z., N. A. Clark, and G. Moddel, A method to obtain asymmetric bistable SSFLC cells, 14th Int. Liquid Crystals Conf., Pisa, Italy, Taylor & Francis, London, 1992, p. 256.

12
Display Applications of SLMs

S. E. Shields
Hughes Aircraft Company
Carlsbad, California

1 INTRODUCTION

Displays are very commonplace in our world today. We rely on them for providing us with information about our surroundings. Since the amount of information being communicated has expanded greatly it has become more important to use images to present that information. As the old saying goes, "A picture is worth a thousand words."

The variety of displays that are in use today makes it a challenge to prepare a brief summary on the subject. Many books have been written on displays and display technology. However, my purpose here is to cover display applications of SLMs. This will narrow the field of interest a great deal. Despite this, the applications still range from large displays many meters in size down to miniature image sources smaller than 1 cm on a side. In addition, the SLM is sometimes observed directly, whereas in other systems it is part of the optical system that generates the image. I plan to cover several applications in more depth, rather than trying to survey all the myriad possible applications that have been proposed.

I intend to start with a discussion of display requirements, concentrating on quantifying those parameters that most limit our ability to communicate by way of displays. After this discussion, I will describe a number of display applications that use particular SLMs. Finally I will close with a brief summary.

2 REQUIREMENTS FOR DISPLAYS

We are all familiar with displays from our everyday experience. Common displays range from the television that we use to relax with to the status board that informs us (hopefully) that our train or plane is on time. A wide variety of technologies are used in displays. However, to be successful, all displays must meet certain minimum performance criteria.

The purpose of displays is to present information to us through our visual senses. This is the widest bandwidth channel that we have available for use. To understand how best to present that information, we need to understand a little bit about how vision works.

2.1 Human Vision

The eye is a wonderful system. Again, whole books have been written about it. However, I plan to concentrate on those factors that are most intimately related to display perception. These include brightness, contrast, spatial frequency, temporal frequency, and color. All of these factors affect how well we see an image, and thus how much information we can obtain from it. However, I will just describe some of the principal effects. Those who are interested can delve further into the literature.

Brightness (or luminosity) is a measure of how much light is reaching our eyes. The total dynamic range of our eyes is over 10^{10}:1, as shown in Fig. 1. This range includes two different sets of sensors within our eyes, the photopic ones that are appropriate for daylight and the scotopic ones for night conditions. Since scotopic vision has low acuity, or resolution, most displays are designed to operate in the photopic region (also, scotopic vision lacks color perception). Even if we limit ourselves to photopic vision the potential

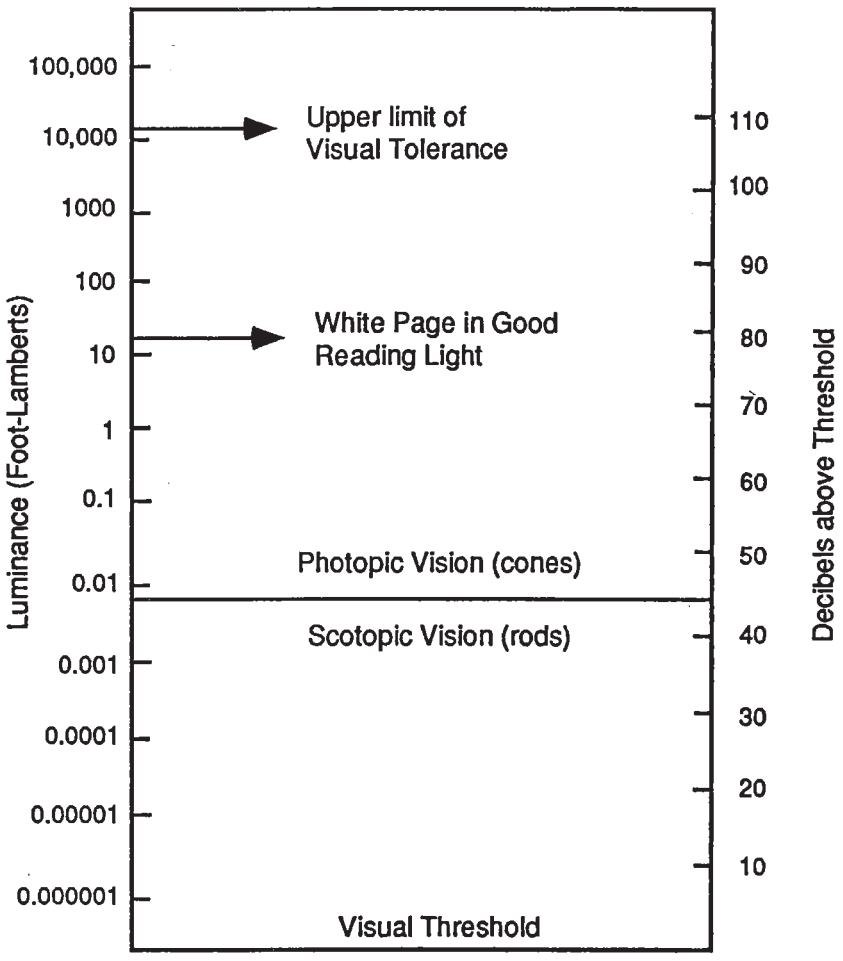

Figure 1 Range of light intensities covered by human vision. (After Bartley, Ref. 2.)

brightness range exceeds 10^6:1. However, not all of that range is available at one particular background level. The instantaneous dynamic range of the eye varies from 100:1 to 1000:1, depending on the visual adaptation level. Thus even if it were possible to make a display with 10,000:1 variations in luminosity on a single image, the eye could not perceive that entire range. For example, if the eye is adapted to 1000 fL, then any luminance below 1 fL will appear black and no luminance discriminations can be made below that level.

Contrast is an extremely important factor in display perception. It is also strongly dependent on brightness, as pointed out in the last paragraph, as well as on spatial frequency. The contrast ratio of an image can be defined simply as the ratio of the luminances of the brightest and darkest objects in the scene. Thus from the discussion above the maximum contrast ratio that can be perceived is between 100:1 and 1000:1. In some cases it may not be possible to make a display system with even 50:1 contrast. Printed ink on paper, for example, has a contrast ratio of only 15:1. However, for pictorial images with many levels of gray, a contrast ratio of 100:1 or more is required to avoid degradation of the information in the scene. Note that this ratio includes the effects of any stray light that is not intended as part of the image that is included in the light reaching the eye. Sources for such light include other lights in the room reflecting off the display screen, or scattering of light by aerosols such as fog or smoke. In any case the effect of such stray light is to raise the luminance level of the dark features and to degrade thereby the contrast ratio of the image. One example of this effect with which we are all familiar is the loss of contrast of a television picture, when sunlight falls on the screen.

Perception of gray levels is closely tied to contrast. The perceived brightness of a series of targets varies geometrically with luminance. Thus each factor-of-2 change in luminance results in an equal change in perceived brightness. Our eyes are quite sensitive at seeing small variations in luminance when those variations are adjacent. Tests have shown that we can perceive 2% variations in luminance; this is known as Weber's law. However, when two objects are separated from each other, then we have trouble telling their perceived brightness apart unless their luminances vary by more than a factor of $\sqrt{2}$. This is the basis for the standard gray scale, where each step is $\sqrt{2}$ brighter than the preceding one. Thus a system with 128:1 contrast can have at most 14 true levels of gray ($2^7 = 128$). The same system can display a much larger number of 2% luminance variations.

Spatial frequency is another key factor of image quality. The contrast sensitivity of the human visual system is shown in Fig. 2, as a function of spatial frequency. Our eyes are most sensitive for spatial frequencies near 2–4 cycles per degree. This data was measured by presenting human subjects with images consisting of alternate dark and light lines whose intensity varied like a sine wave. By varying the spatial frequency and the contrast, the experiment determined which charts were just barely discernible. Notice that the limiting acuity for human vision is near 50 cycles per degree. The data are plotted in terms of contrast sensitivity, which is the inverse of the contrast necessary to produce a defined level of detectability.

Temporal effects also affect how we see images. Indeed, our vision system requires motion to work. If an image is held in a fixed location on the retina, it fades away (this effect hides the structure of the retina from obscuring our vision). Our eyes adjust for this effect by jumping, or saccading about the image. This not only refreshes the image in our vision, but also allows the fovea, which has the highest acuity, to move from area to area in the image. The presence of these saccades is not obvious to us in reading

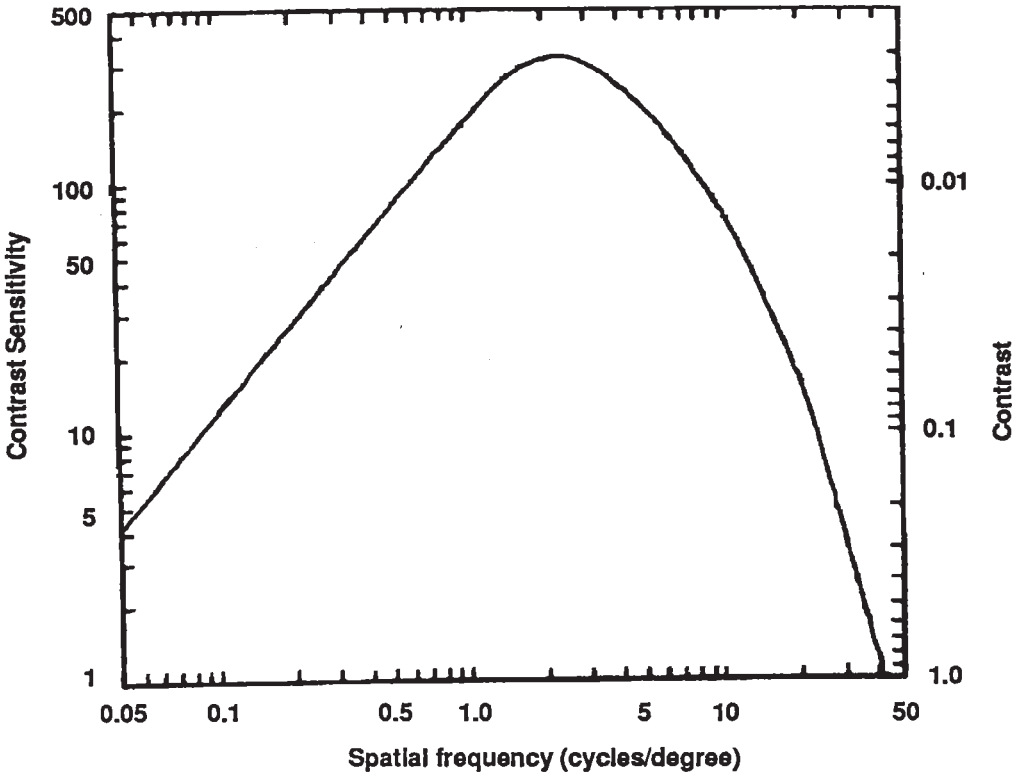

Figure 2 Contrast sensitivity of the human visual system. (After Ginsburg [6] and Schade [17].)

printed text, or looking at natural scenes; however, when the image from a display (such as a CRT) is changing quickly, there can be artifacts that appear from the interaction of the saccade and the changing information. This effect can result in multiple images.

We have all seen flicker before in bright CRT monitors. This effect is also present in active matrix liquid crystal displays (AMLCDs). Flicker results from periodic modulation of the image luminance or contrast; as shown in Fig. 3, flicker is quite pronounced at frequencies near 10 hertz, and becomes much less visible for frequencies above 50 Hz. However, the effect is also a function of brightness; flicker is easier to observe in brighter images. The figure plots data in terms of trolands, a measure of light intensity at the retina. Rogowitz estimates that 430 trolands corresponds to less than 30 fL [16]. This is a less than the luminance of many standard displays.

Color perception is important to our view of the world around us and in particular to our use of displays. Our eyes contain several different types of cells; these include cones that are sensitive to three different wavelength bands. The relative response of these sets of cells corresponds to the absorption spectra shown in Fig. 4. We put together the signals from these three different receptors to perceive color. This means that any color can be represented to our eyes by the amount of stimulus in each of these color bands. This has led to the standard CIE color coordinates, shown in Fig. 5. The curve shows the location of the pure colors of the spectrum; all possible colors lie within this curve. Less saturated colors lie near the blackbody curve shown in the center of the figure. Any color can be shown as a unique point within this figure. Any combination of two colors lies on the line connecting them on the figure. Thus for a full color system

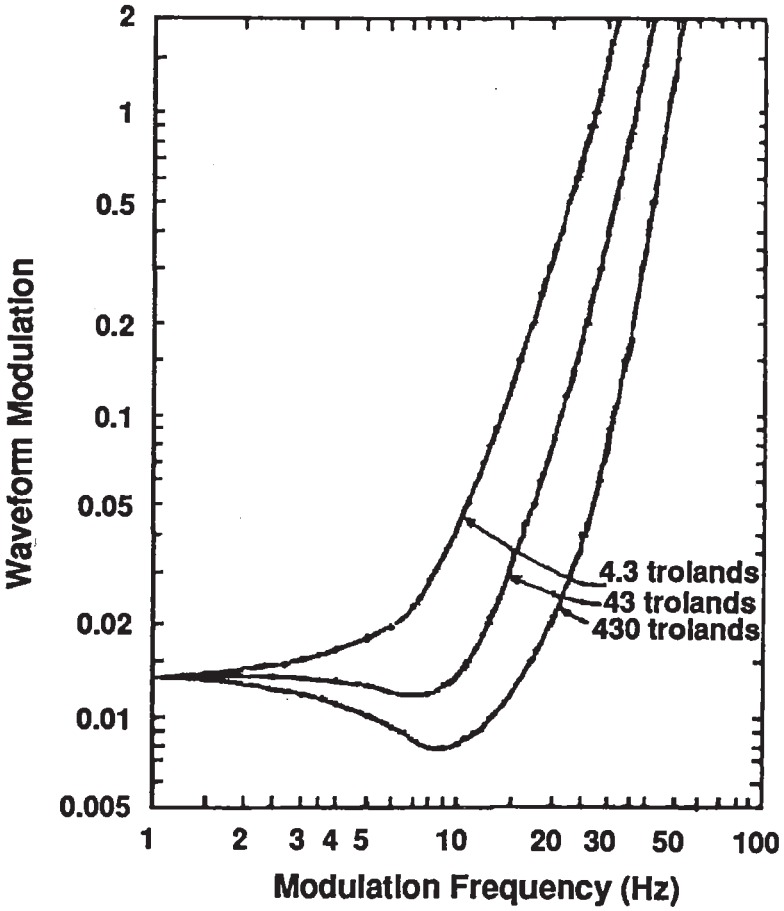

Figure 3 Standard temporal modulation sensitivity curves. (After deLange [4].)

(such as the color TV standard shown in the figure) the available colors are bounded by the triangle formed by connecting the three primary colors used in the display.

The perception of color is extremely complex. Not only does the absolute location of a color on the CIE diagram affect its perception, but also its luminance, its size, the color and luminance of the surround, and the observer all have effects as well. No wonder that display adjustment is such an individual endeavor!

In summary, the human eye is a complicated system whose performance is a complex function of image luminance, contrast, spatial and temporal frequency, and color. However, its performance sets realistic limits for display performance.

2.2 Display Performance Criteria

On the basis of the performance of our eyes, we can set some criteria for display performance. It is certainly true that there is no point in investing extra effort in our display system, if the user cannot appreciate it! On the other hand, display performance must be adequate to facilitate efficient information transfer to the observer. The following are suggestions, based on my own observations.

Display luminance should be matched to the application. Since the eye adapts to background levels, a display for use in an aircraft cockpit must be much brighter than one designed for use in a darkened theater. In general, theaters require about 10 fL of

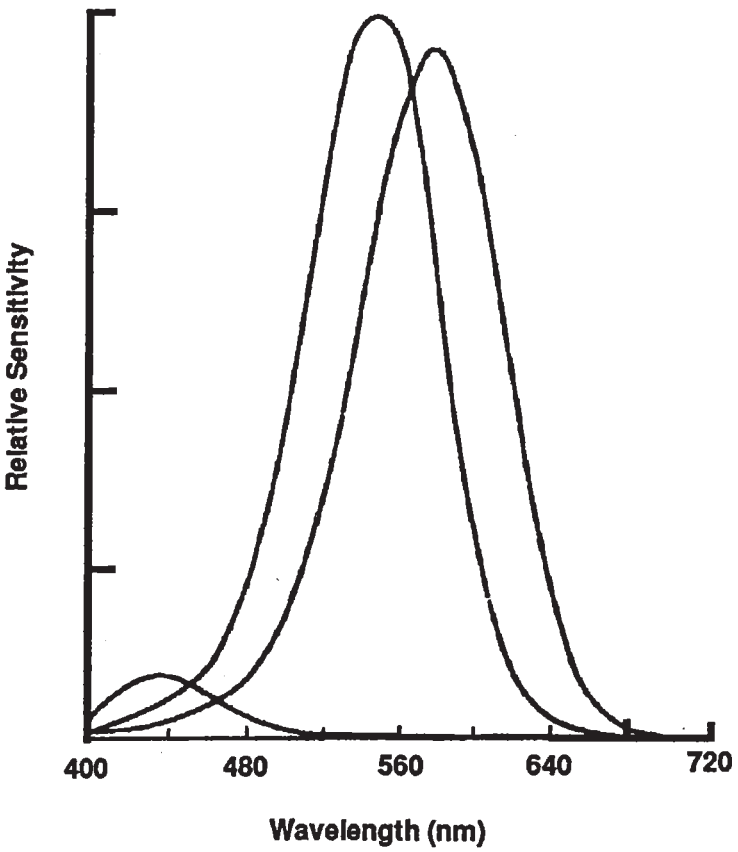

Figure 4 Absorption curves for pigments active in human vision. (After Wald [21].)

image brightness, workstations require about 50 fL of brightness, and avionics displays require 500 fL or more!

Contrast is extremely important to perceived image quality. We all tend to prefer higher contrast (just check the setting on your workstation monitor or home TV). Contrast levels of 100:1 or more are not too high, especially for displays where the system performance may be degraded further by incident light.

Spatial frequency is best described by the display's MTF, or modulation transfer function. This parameter measures the amplitude of the system response (its modulation) as a function of the frequency of the stimulus. The MTF for a typical SLM (in this case a CdS-photoconductor LCLV) is shown in Fig. 6. Notice that the MTF drops smoothly as the spatial frequency increases; there is some modulation even at quite high spatial frequencies.

The MTF for a SLM with discrete pixels is much more complicated, since the discrete structure of the SLM implies that the allowed spatial frequencies are discrete as well. However, in this era of digital display systems it is becoming more common for the image to be either computer generated, or sampled prior to the display. In these cases the display structure can be taken into account earlier in the system. In the case of a computer display it has no effect on the image quality; in the case of a video display the impact due to sampling occurs earlier in the system, and the display has no additional effect. Since the MTF for such a display can be quite high at the pixel frequency, the

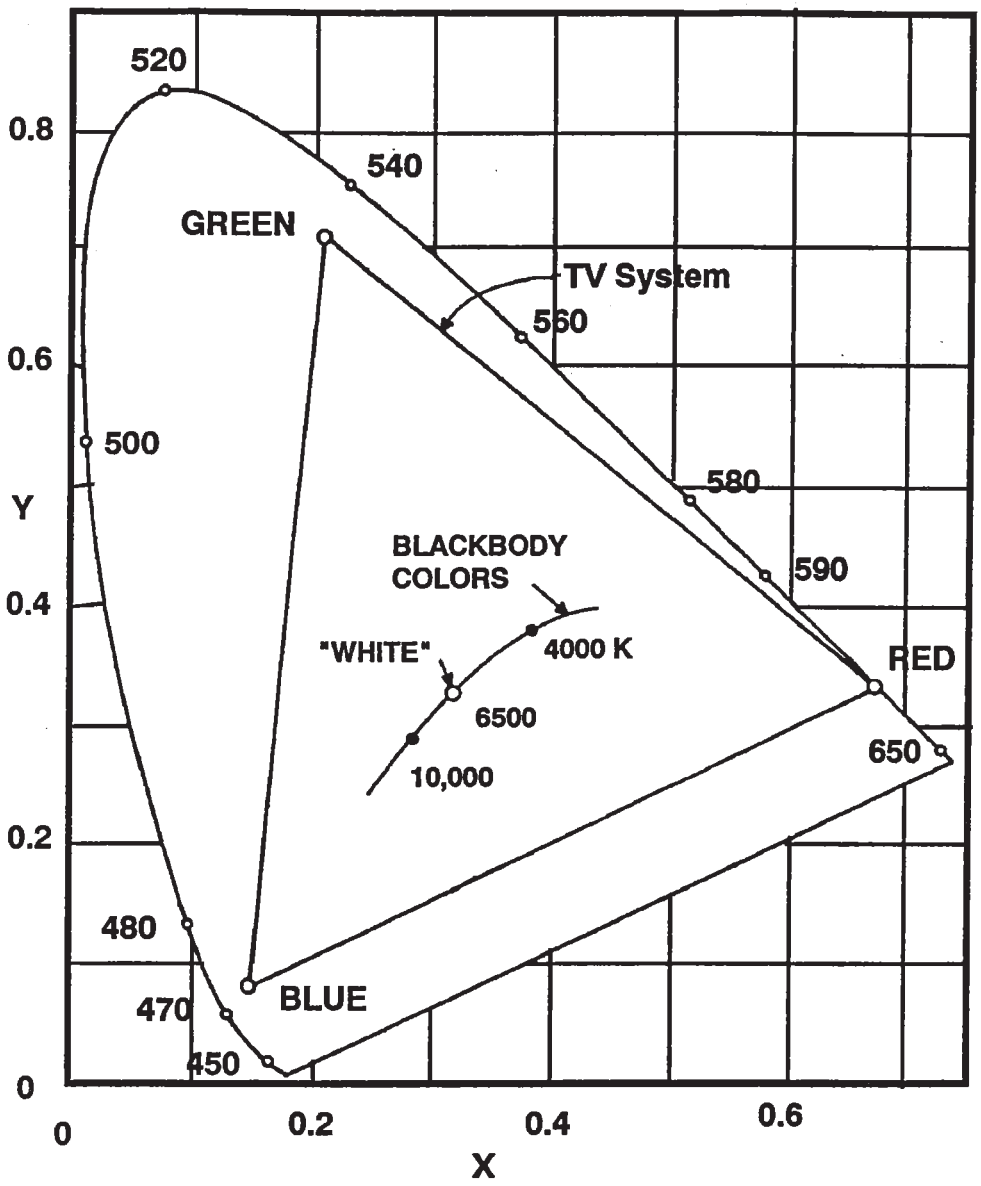

Figure 5 CIE color diagram. (After Morrell [15].)

image from such a display system is limited primarily by the discrete pixel density. However, in actual systems one usually chooses to reduce the MTF at the pixel frequency either by making the pixels small so that the observer's eye limits the system, or else by using a lens to roll off the system MTF, so that the structure of the SLM is hidden and does not cause artifacts in the image.

Temporal effects can be very important in display systems. In particular the display system designer must hide any flicker. He also must be aware of possible artifacts caused by the eye's saccading, such as color separation in field-sequential systems.

Color displays require attention to the color aspects of perception as well. In particular, the method that is chosen for generating the primary colors must cover a large-enough region in CIE space to permit all the desired colors to be rendered.

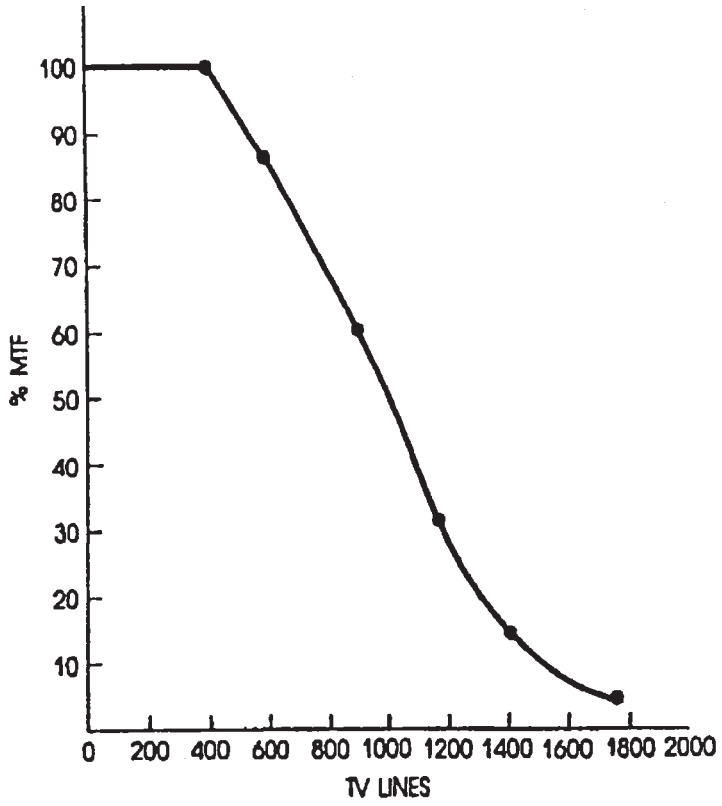

Figure 6 Measured MTF for a Cd-S photosensor LCLV.

3 POLARIZED LIGHT-BASED DISPLAY SYSTEMS

Modulation of light's polarization is used by many SLMs. In particular, it is used by many liquid crystal displays (LCDs). I intend to use two particular types of LCDs as examples of SLMs that can be used as image sources for displays that make use of polarized light. I will discuss liquid crystal light valves (LCLVs) as an example of a reflective SLM suitable for display applications, and discuss active matrix LCDs as an example of a transmissive SLM that can be similarly used.

3.1 Liquid Crystal Light Valves

As described in another chapter, liquid crystal light valves (LCLVs) are devices that take an input image and use it to control the voltage across a liquid crystal layer. The adjustment in the liquid crystal orientation that occurs in response to the varying voltage results in the imposition of this image into light from an external light source. Almost any external light source can be used. In the case of displays we typically choose to use an arc lamp to generate a bright image, that can be projected onto a large screen.

A typical LCLV is shown in Fig. 7. It consists of a photoconductor film and a nematic liquid crystal layer separated by a light-blocking layer and dielectric mirror. The device is designed such that the impedance of the photoconductor in the dark is the largest impedance in the system, followed by that of the liquid crystal layer. Thus in the dark most of the voltage applied across the device (between the two transparent conductive electrodes) is dropped across the photoconductor; most of the rest of the voltage acts to bias the liquid crystal material near its threshold. When an image is input through

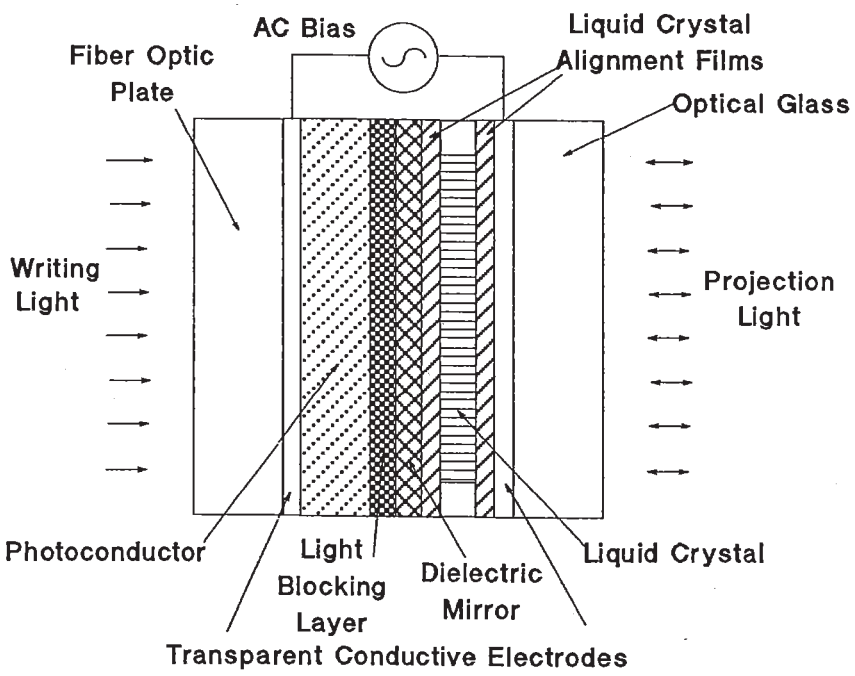

Figure 7 Cross section of a typical LCLV.

the electrode on the left of Fig. 7, the photosensor impedance is lowered in response to the input light. This decrease in impedance results in a shifting of a portion of the ac voltage present across the photosensor onto the liquid crystal. This additional voltage activates the liquid crystal locally above its threshold in a pattern that replicates the input image intensity, including gray-scale levels.

Figure 8 shows an optical schematic of a typical LCLV projection system. The light from the arc lamp is polarized by a polarizing prism. This light is then reflected from the LCLV. The reflected light is analyzed by the polarizing prism, and the resulting image is projected by the lens onto the screen.

The system shown in Fig. 8 gives a monochrome image. Most LCLV projector applications require color images. In a color system three LCLVs are used along with dichroic mirrors to generate images in the three primary colors. These images are com-

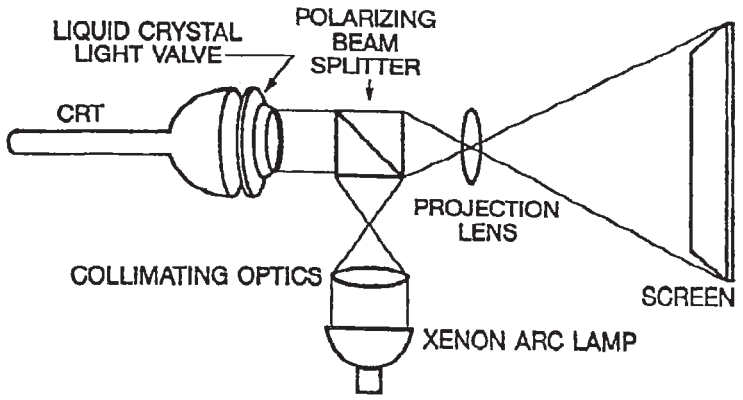

Figure 8 Optical schematic for a simple LCLV projection system.

bined, either internally or externally (at the screen) to generate a full-color image. One such system, built for the U.S. Navy, is shown schematically in Fig. 9. This system is described in more detail by Ledebuhr [11]. In this case the images from the three LCLVs are combined inside the projector, and the resulting color image is projected using a single projection lens.

The performance of this color system is described in Table 1. It is designed for application in large command-and-control centers, where a large, very bright image is needed.

Special LCLVs have been developed that have adequate speed for display of video images. These devices can be used for HDTV, because of their high inherent resolution. In addition, commercial versions of these projectors have been developed. Figure 10 shows a commercial command-and-control center located at Electronic Data Systems Corporation (EDS) that features an array of seven LCLV color projectors. These systems are used by EDs to display status information on their worldwide operations.

3.2 Active Matrix LCDs

Another device that is being developed primarily for use in displays is the active matrix LCD (AMLCD). This device consists of an array of pixels, each of which includes a nonlinear element for addressing as well as a mechanism for storing charge, that is used to address a liquid crystal layer. Such a device is shown schematically in Fig. 11. In the most common version of this device being developed today the switch is a thin film transistor, typically based on amorphous silicon.

AMLCDs are typically addressed one line at a time. The voltages on the data lines are adjusted to correspond to the information to appear on one particular row of the display. Once the voltages are in place, the control line corresponding to that row is activated, turning on all of the switches along that row. This permits the voltages on the data lines to pass through the switches, and to be stored on the storage elements associated with each pixel along that row. Then the switches are turned off, and the voltages corresponding to the information on the next row are read into the data lines.

AMLCDs are described in great detail in a number of references, such as Morozumi [14] or Luo [12]. The interested reader is urged to consult these references to learn more about AMLCDs, as they are likely to become the most common SLM available.

AMLCDs can be used to make projection displays, as are LCLVs. However, as current AMLCDs are transmissive devices, the optical system is quite different from that used with LCLVs. A typical system is shown in Fig. 12. The light from an arc lamp is split by a series of dichroic mirrors into its constituent colors. Those are modulated by three AMLCDs, recombined by a second set of dichroic mirrors and projected through a lens onto a screen. Figure 13 shows the image from such a system.

The largest application for AMLCDs in displays, however, is in direct view. Here the display is observed directly by the user, without any intervening optics. Some of the earliest applications for such displays were in portable TVs, with 2–5 inch diagonal size. Today a number of manufacturers are selling 10–14 inch computer monitors, with 480 $\times$ 640 color resolution. In addition, prototypes with much higher resolution are being demonstrated. Figure 14 shows a prototype display developed by Xerox PARC; with over 6 million pixels it has the most resolution of any AMLCD demonstrated to date. These products are the result of a huge investment that has been made by a number of manufacturers to commercialize this technology. Given this investment I expect AMLCDs to continue to be the dominant SLM technology for the foreseeable future.

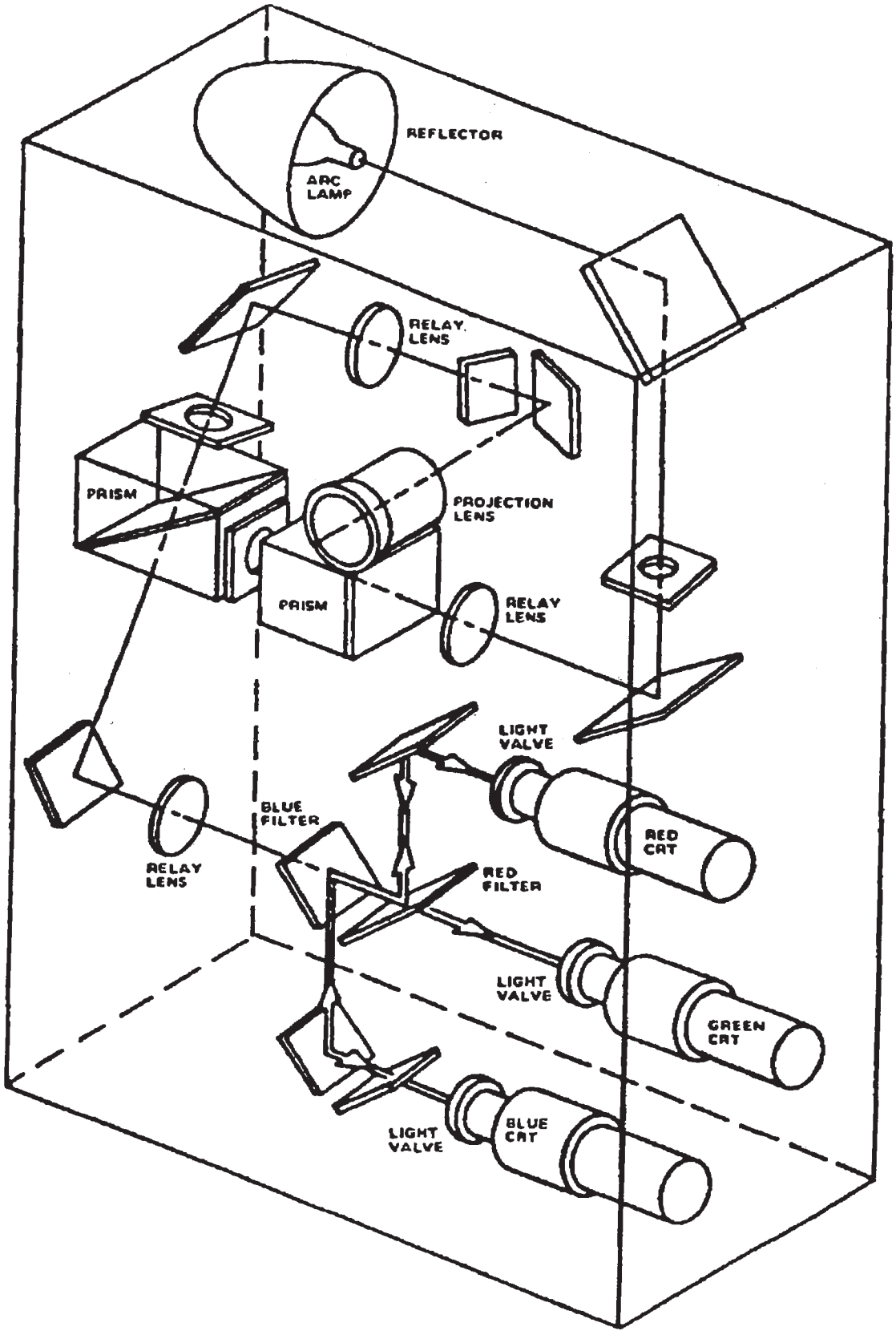

Figure 9 Perspective view of a color LCLV projection display system. (From Ledebuhr, [11] Courtesy of Society for Information Display.)

Table 1 Performance Data for a Full-Color LCLV Projector

Parameter	Measured performance
Color range	Full color
Light output (1.0-kW lamp)	>650 lumens (square aperture)
(1.6-kW lamp)	>1000 lumens (square aperture)
Contrast ratio (white)	>75:1
Screen size	1 m to 5 m^2
Throw distance	1 m to 5 m
Frame rate	30 Hz (interlaced)
Raster format	1075,625,525
Vertical resolution	>1024 scan lines
Horizontal resolution	>1800 TV lines (limiting)
Image registration	better than 0.25 pixel in white for all pixels

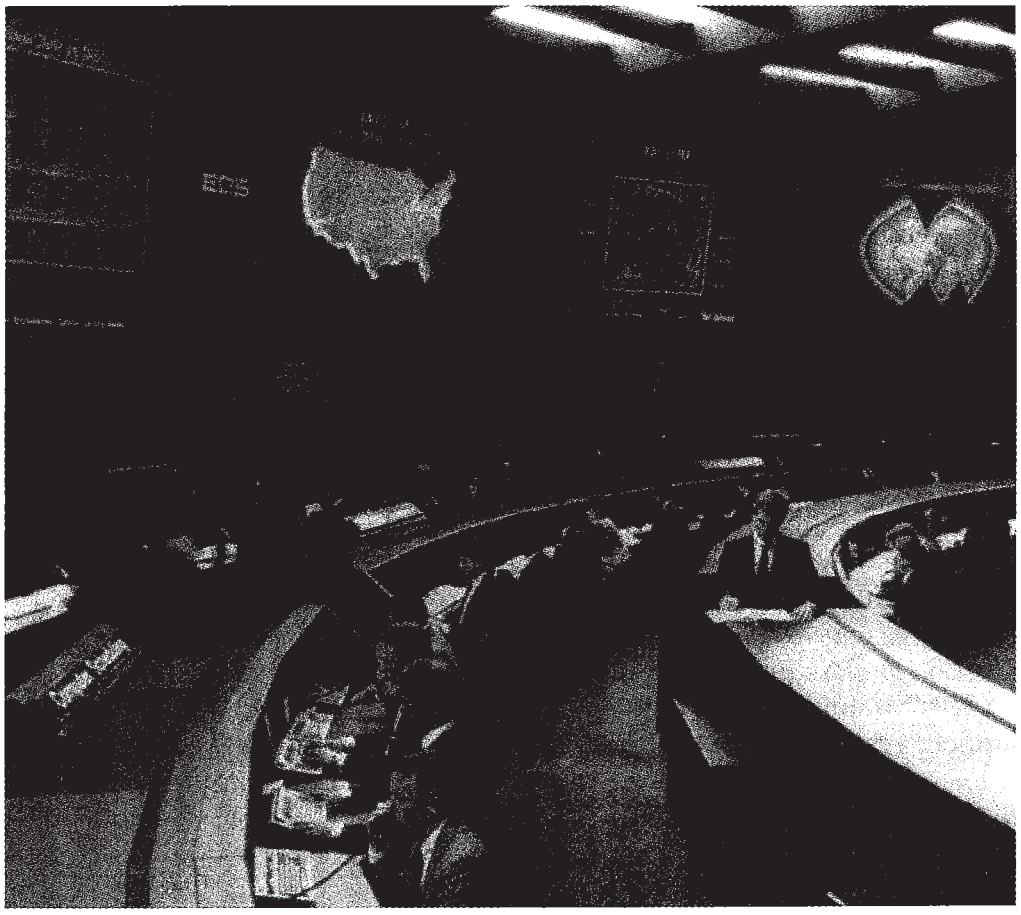

Figure 10 Large-screen projectors in use at EDS.

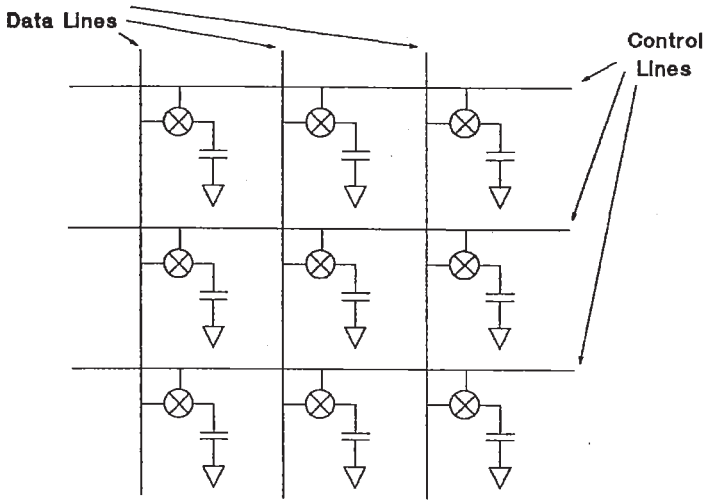

Figure 11 Schematic view of an active matrix display.

Direct-view AMLCDs generate their color differently than do most AMLCDs designed for use in projectors. Each picture element on a color AMLCD consists of a set of three or four subpixels. Each subpixel has its own switch and storage capacitor. In addition, each subpixel is covered by a color dye filter located next to the liquid crystal material. These dye filters are what give the display its color, in an analogous manner to the color dots on a shadow-mask CRT that generate the colors in a standard TV. Combinations of the three primary colors are used to generate all of the intermediate colors. AMLCDs with four subpixels per pixel typically have either two green, one red, and one blue subpixel or one each of green, red, blue, and white.

Most current AMLCDs use the standard twisted nematic, or TN, electrooptic effect. However, several companies have demonstrated AMLCDs or (more often) simpler multiplexed displays that use ferroelectric liquid crystal materials. These materials have faster response speed than do TN materials; in addition their inherent hysteresis can be used in a multiplexed display to greatly increase the number of lines that can be addressed. This hysteresis also makes gray scale more difficult with ferroelectric LCDs. One ap-

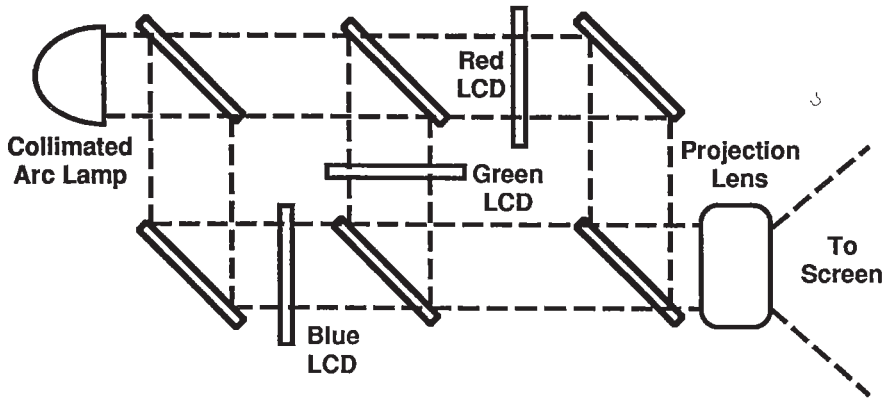

Figure 12 Dichroic color projection system using AMLCDs.

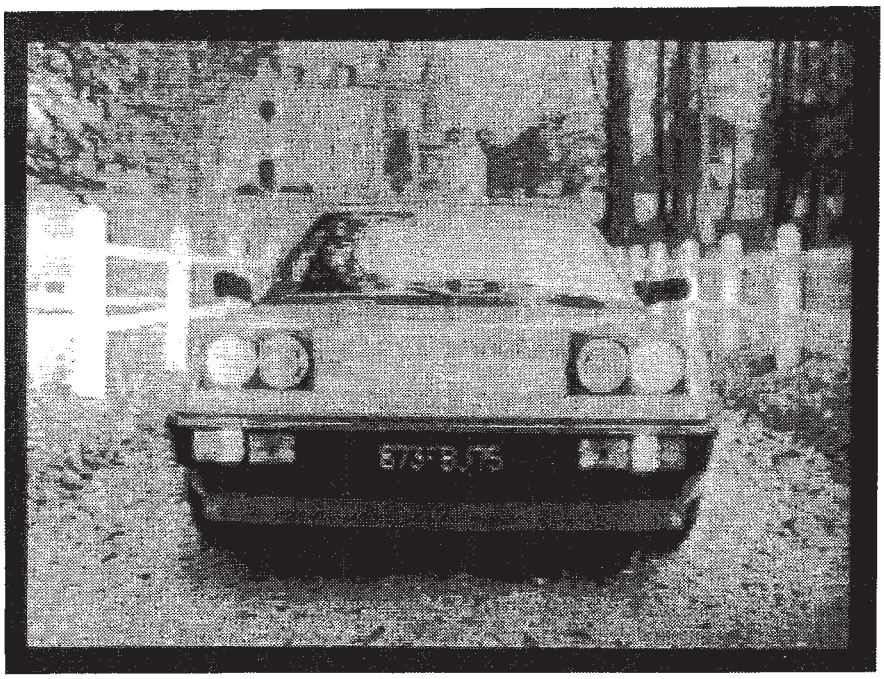

Figure 13 Displayed image from AMLCD projector. (Photograph courtesy of Seiko-Epson.)

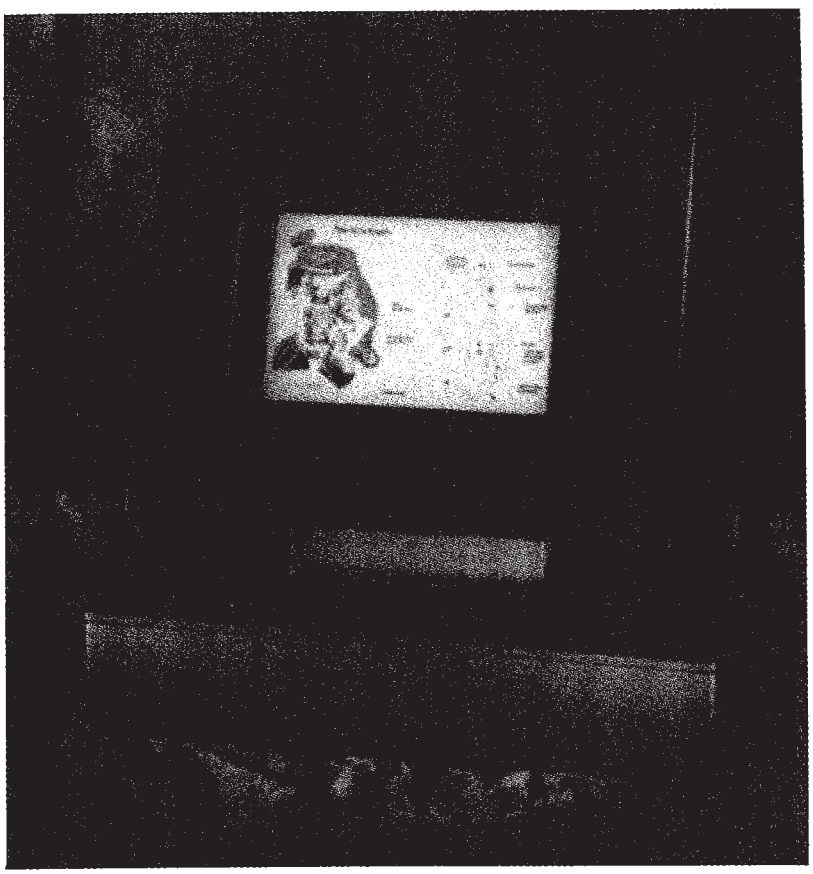

Figure 14 Xerox PARC 13-inch diagonal Monochrome AMLCD with 6.3 million (Courtesy of Xerox PARC).

proach that is used involves dividing each pixel up into smaller regions, which are independently controlled to generate different shades of gray.

A typical AMLCD direct-view display is shown in Fig. 15. Since the AMLCD does not generate light of its own, the display makes use of a separate light source. In this case a set of fluorescent bulbs is used together with a diffuser to generate uniform lighting. Other systems use electroluminescent panel backlights to generate the light. In either case the light is modulated by the AMLCD.

Unfortunately these systems are not very efficient. Over half of the light from the bulbs is absorbed in the first polarizer. Only 15% or so of the remaining light passes through the dye filters (in the case of a color display). This results in an overall efficiency of the panel below 10% (5% is more typical). Thus the majority of the light is used to heat the display, not to view it, and the majority of the power dissipated by the display system is used by the lamp, not the AMLCD. This is especially a problem in displays that must have high brightness, such as displays designed for use in advanced aircraft cockpits. However, it is less serious in displays designed for more benign applications.

4 SCATTERING-BASED DISPLAY SYSTEMS

Another optical effect that is used to generate images in displays is scattering. Again I plan to cover two examples of systems where SLMs are used as the heart of a display system. Neither of these systems is a commercial reality today; however, the deformable mirror-based system may become a reality in the future.

4.1 PLZT Ceramic-Based Display Systems

Lead lanthanum zirconate titanate (PLZT) ceramics have been studied for use as optical modulators since before 1970. These materials have a number of properties that make them potentially attractive for use as display image sources. However, a number of practical engineering problems have prevented their successful implementation into displays.

There are at least two electro-optic effects in PLZT that have been used to make displays (Maldonado [13]). Those are controllable light scattering and controllable birefringence. Displays based on birefringence are identical in their theory of operation

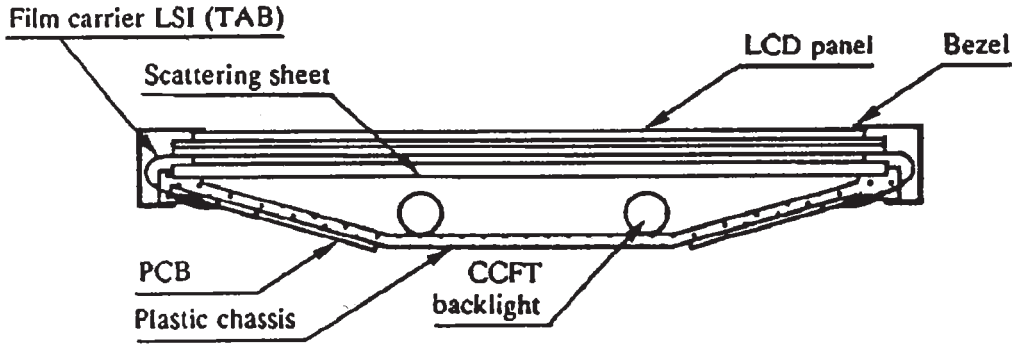

Figure 15 Typical AMLCD cross section. (From Sharp LCD Units Catalog, HT518D, 1991, p. 11, used with permission.)

to LCDs, and will not be considered in further detail here. A detailed survey of such displays, as well as of the scattering applications, is given by Maldonado [13].

A specific example of a display system using PLZT is shown in Fig. 16. The PLZT light valve used in this system consists of a symmetric structure of two photoconductor films and a thick (>125 micrometer) PLZT layer sandwiched between transparent conductive electrodes (this device is shown in an exploded view in Fig. 17). All of the domains in the PLZT are first ordered by applying a field of about 10 kV/cm between the two electrodes while the device is illuminated by the projection lamp. An image is then written into the device by using the laser to illuminate the photoconductor locally while a field opposite to the initial polarizing field is pulsed on and off. The applied pulse amplitude and duration are set to switch the remnant polarization to zero in the addressed regions. The regions that have been switched look black on the screen because they scatter the projection lamp light, rather than transmitting it. The image once written onto the slide is stored in the PLZT domain structure until a field large enough to reorient all of the grains is applied across the PLZT. Thus this slide can be removed from the display system and stored, complete with its image. Areas of the image can be selectively erased by using the laser along with field pulses similar to the original polarizing field.

The contrast ratio of one of these PLZT slides is shown in Fig. 18. This type of performance is typical for a schlieren system. Notice that the contrast ratio increases as the half angle of the aperture is decreased. In theory, the contrast ratio would be infinite at 0 half-angle. In practice, no light would be passed through the system under those circumstances. For practical systems, with a half-angle near 2.5°, the contrast ratio can be 20:1 or more.

Figure 19 illustrates how a schlieren optical system works. The light from a point source is collimated, and allowed to pass through the scattering display cell. After passing through the cell, the light is brought back to a focus, that is coincident with an aperture. The light that has not been scattered passes through the aperture, and is imaged onto the screen. Light that has been scattered is blocked by the aperture, and is not imaged. An alternative

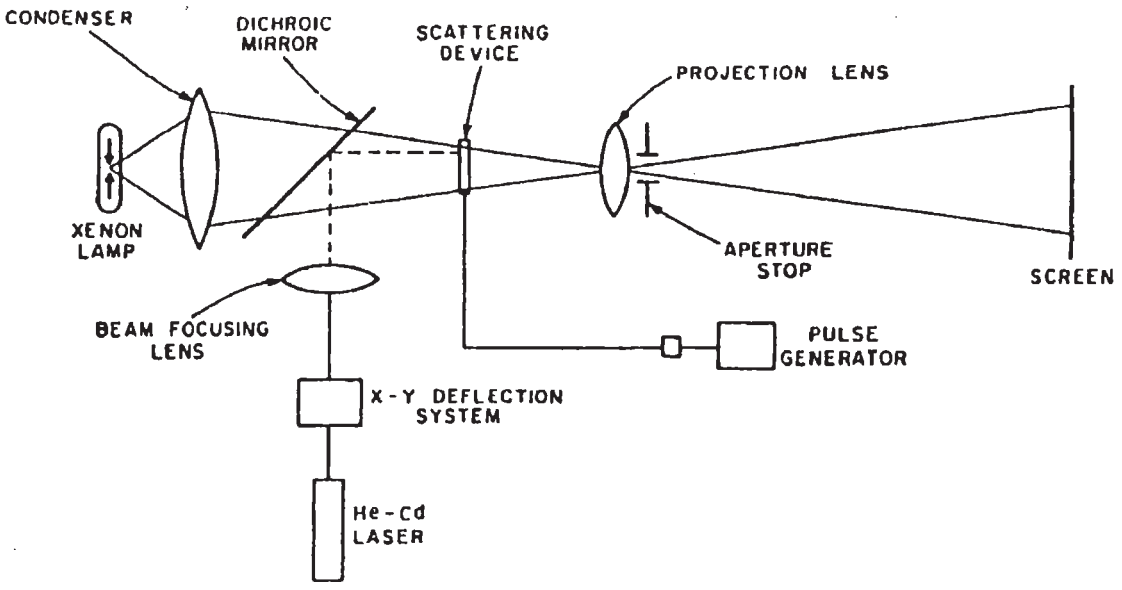

Figure 16 Slow-scan graphics system using PLZT. (From Maldonado [13], used with permission.)

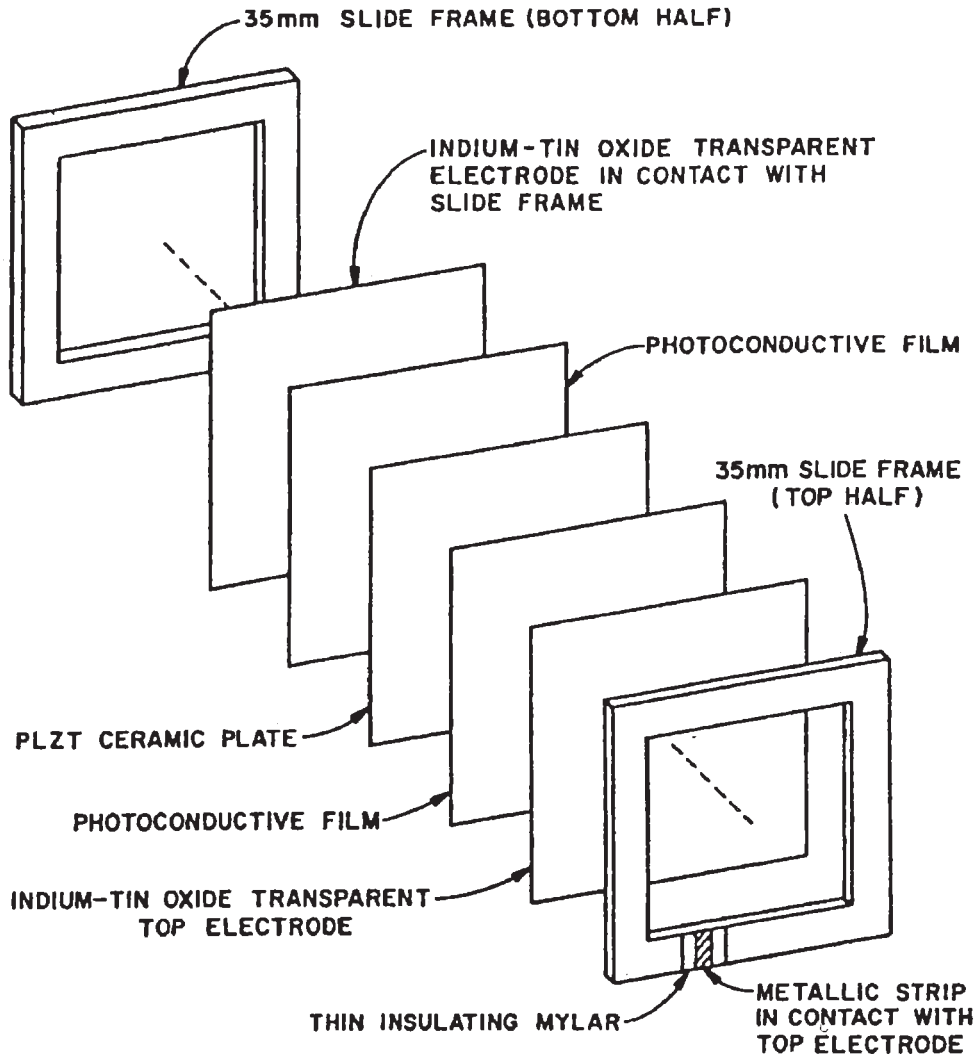

Figure 17 PLZT slide used in slow-scan graphics system. (From Maldonado [13], used with permission.)

system places an optical stop at the focus, to block the unscattered light. In this alternative system the scattered light is imaged onto the screen after passing around the stop.

This type of system can be used with any SLM that makes use of light scattering. In particular it will work with polymer-dispersed liquid crystal (PDLC) displays. It can also be modified to make a reflective system.

4.2 Deformable Mirror SLM Display Systems

My last example of a display system that uses a SLM as the image source is based on the deformable mirror-type SLM. These devices are described in another chapter of this book.

Several types of deformable mirror SLMs have been developed. In one (Tepe [20]) a single metallic mirror is deposited on top of a viscoelastic layer. The shape of this mirror is deformed by electrostatic forces exerted on it by circuitry located underneath the viscoelastic layer. In another (Hornbeck [8]) the mirror takes the form of a membrane supported at the perimeter of each pixel, while separated from the control electrodes

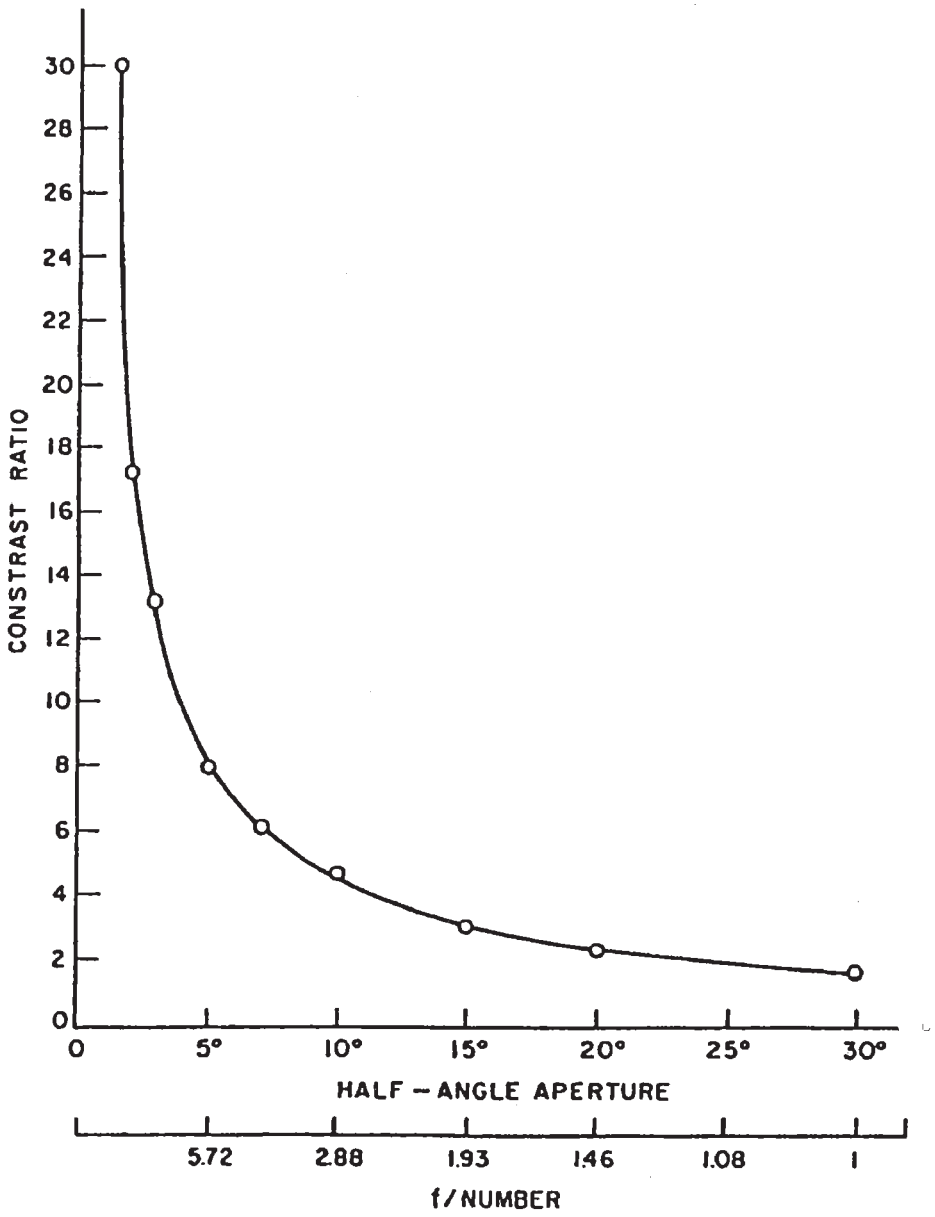

Figure 18 Contrast ratio versus aperture for PLZT slide system. (From Maldonado [13], used with permission).

by an air gap. In a third (Sampseil [22]) each pixel has its own mirror, that is held by two cantilevers in opposite corners and that can be tilted back and forth between two stable positions. All of these have the common feature that an active matrix is used to control the orientation of a mirror layer, and thus the direction into which incident light is reflected or diffracted.

A number of simple optical systems have been proposed (see, for example, Gerhard-Multhaupt [5]) that would use three SLMs to make a color projection system. One of these designs is shown in Fig. 20. The light from the light source (5) is focused onto the mirror (7), then split into its constituent colors by two dichroic mirrors (3) before being collimated onto the three SLMs (1) by three separate lenses (2). The reflected light is recombined by the dichroic mirrors. Any light that is not scattered by the SLMs (or by

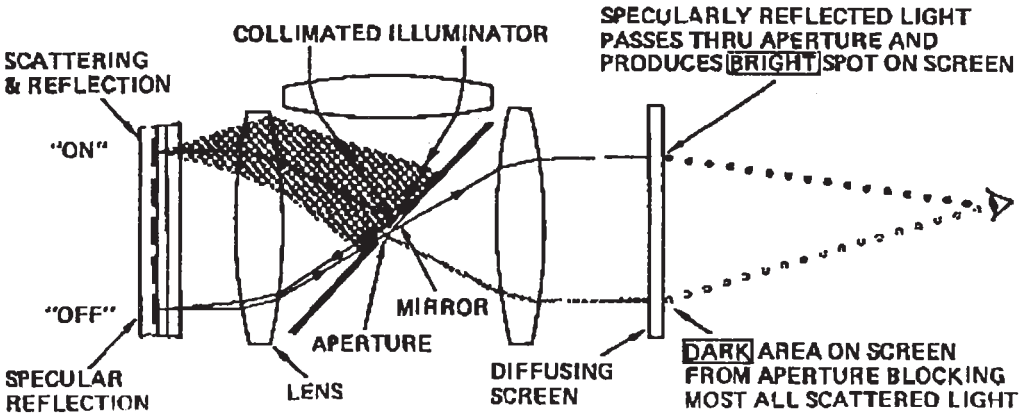

Figure 19 Simple schlieren optical system. (After Gunther [17].)

any other component in the system) is imaged back onto the reflective stop by the lenses (2), and reflected back to the light source. The scattered light goes past the stop (7) and is imaged by a projection lens (4) onto a viewing screen (not shown). This design is almost identical to one used by Gunther [17] in a system that used dynamic scattering LCDs as the image sources.

4.3 Reflective versus Transmissive Display Systems

As demonstrated by the examples above, it is possible to use either transmissive or reflective SLMs as image sources in display systems. However, there are several trade-offs between these types of systems that make one approach more attractive than the other for certain applications.

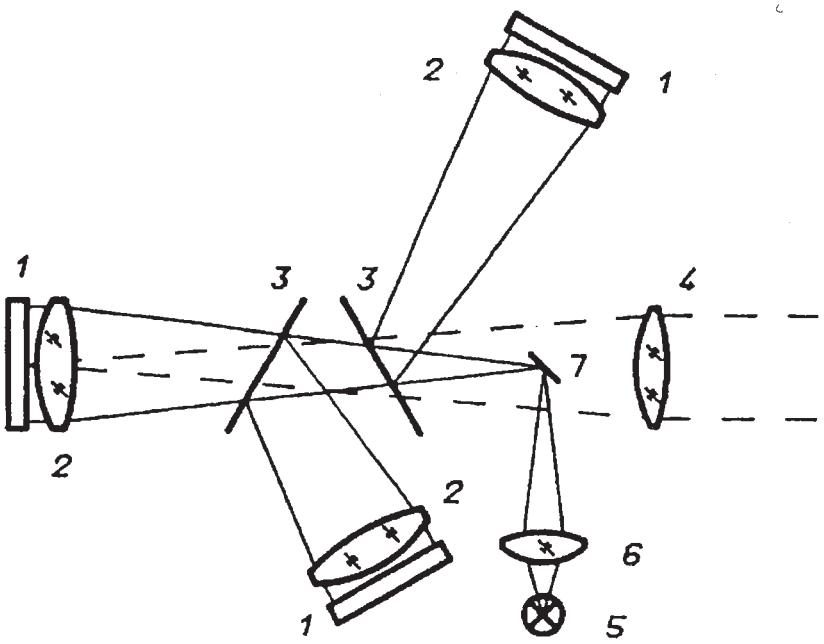

Figure 20 Schlieren optical system for color projector. (From Gerhard-Multhaupt [5], used with permission courtesy of SPIE.)

A typical SLM, such as an LCD, can be considered as a sandwich consisting of an optically active layer that is controlled by a control layer. In most SLMs having a thicker optically active layer magnifies the optical activity, but makes the work of the control layer more difficult. A thinner optically active layer does not modulate as well, but is easier to control. Thus there is a trade-off between sufficient optical thickness and adequate control capability.

For example, consider LCDs. The liquid crystal layer is the optically active one, whereas it is controlled by modulating the field across it either with a photoconductor or electrically (by means of an active matrix, say). Thicker liquid crystal layers require larger voltages to generate equivalent fields; they also have slower response speeds because the restorative forces from the alignment layers at the surfaces of the cell have less effect on the material in the middle of the cell. By making the cell reflective, rather than transmissive, one doubles the optical path length while maintaining the same cell thickness. Conversely, one can make the cell half as thick for the same optical path length. This results in a modulator that is faster and that requires less voltage for comparable performance. Thus from the standpoint of the performance of the LCD itself reflective devices can be made to outperform transmissive ones as image sources in displays.

However, reflective display systems are more complicated to design than are transmissive ones. It is more difficult to design and build a system in which the light is brought in and out of the SLM on the same side, as opposed to one in which the light comes in one side and out the other. This can be seen by comparing Figs. 8 and 12 for birefringent systems, or Figs. 16 and 20 for scattering systems. Typically in a reflective system the light passes through other components of the system twice, in addition to the optically active layer of the SLM, making it impossible to optimize them as much as if they only were to play one part in the optical system.

5 EMISSIVE DISPLAY TECHNOLOGY

All of the devices described thus far have been examples of light valves, devices that modulate the light passing through them (or reflecting off them). There is another large category of display devices that emit light on their own, without need for an external light source. Examples of such display devices include existing devices such as cathode ray tubes (CRTs), electroluminescent (EL) panels, and plasma panels, as well as new devices such as field-emission displays (FEDs). I intend to provide a brief introduction to these devices below. A more detailed description of many of these devices is included in the book *Flat-Panel Displays and CRTs* by Larry Tannas [19].

5.1 CRTs

The most ubiquitous display component today is the CRT. Dating back to the late nineteenth century, the CRT is the first electronic display. Even today, CRTs have two-thirds of the display market place. They have the advantages of generating their own light, having high resolution, adequate contrast, good color, and excellent environmental tolerance. Their biggest drawback is their large bulk and heavy weight; however, for many applications they are the technology of choice. A good review of CRTs is given by Keller [9].

A generic CRT is shown in cross section in Fig. 21. Electrons generated thermionically from a heated cathode are formed into a beam and focused by the electron gun using applied electric and magnetic fields. The beam is accelerated by a high voltage

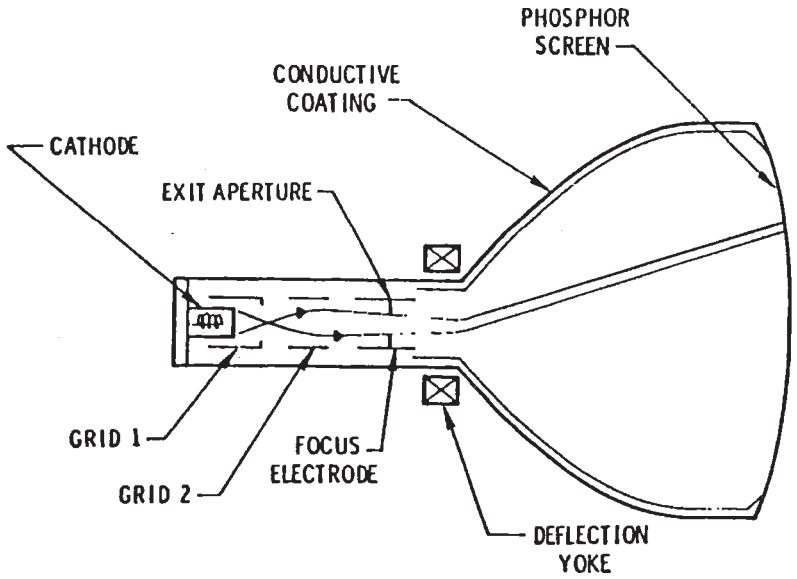

Figure 21 Cross-sectional view of a CRT. (From Tannas [19].)

and then swept across the phosphor screen by the deflection system, addressing one point on the screen at a time. The energy in the electrons is converted by the phosphor material into visible light in a highly efficient manner.

CRTs can be either monochrome or color. In a monochrome CRT a single electron gun is used to write an image onto a continuous phosphor screen. In most color CRTs, multiple electron guns are used to write separate red, green, and blue images onto a phosphor screen made up of color dots or stripes. A metal mask, called the shadow mask, is used to protect the phosphor dots of two of the colors from the electron beam that is writing the third color image. This is shown schematically in Fig. 22. Typically the shadow mask itself is used to determine the locations of the phosphor dots during manufacture, thus ensuring that the electrons from any one gun only reach phosphor dots of a particular color.

CRTs come in all sizes and shapes, from round to rectangular, from 1/2 inch diagonal to 30 inch and more, from direct view to projection, from high brightness monochrome to high resolution color. They are the standard against which all other display technologies are measured.

5.2 Electroluminescent Displays

Electroluminescent (EL) displays are rugged, thin displays. They consist of a phosphor material sandwiched between two sets of electrodes. The two sets of electrodes run at right angles to each other; their intersections define the pixels of the display. As shown in Fig. 23, the most widely used structure today uses a thin film layer of ZnS:Mn as the phosphor. This gives the display its characteristic yellow color. Other phosphors are in development, and full color prototype units have been demonstrated this year (Barrow [1]). The performance of these displays is severely limited by the poor efficiency of the blue phosphor.

EL panels are available in sizes up to 12 × 14 inches and resolutions up to 1024 × 864. For example, Planar provides a large EL panel packaged into a unit 17 inches square

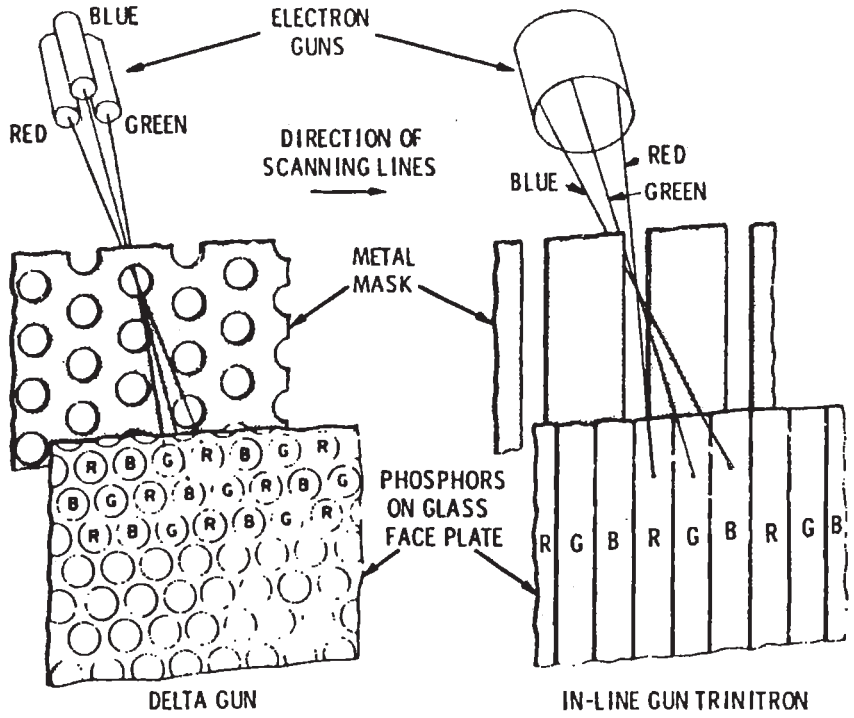

Figure 22 Schematic view of a shadow mask color CRT. (From Herold [23])

by 3 inches deep, for use as a workstation monitor. Typical luminance for (monochrome) EL panels is 20–30 fL.

5.3 Plasma Displays

Plasma displays operate by generating a discharge in a suitable gas inside a glass envelope. As in the EL displays described previously, crossed sets of electrodes are used to define the pixels. Most plasma displays are a characteristic orange, due to the emission spectrum of the neon gas used in them. Color plasma panels use a different gas (xenon) that emits ultraviolet (UV) light, and then use phosphor materials to convert the UV into visible

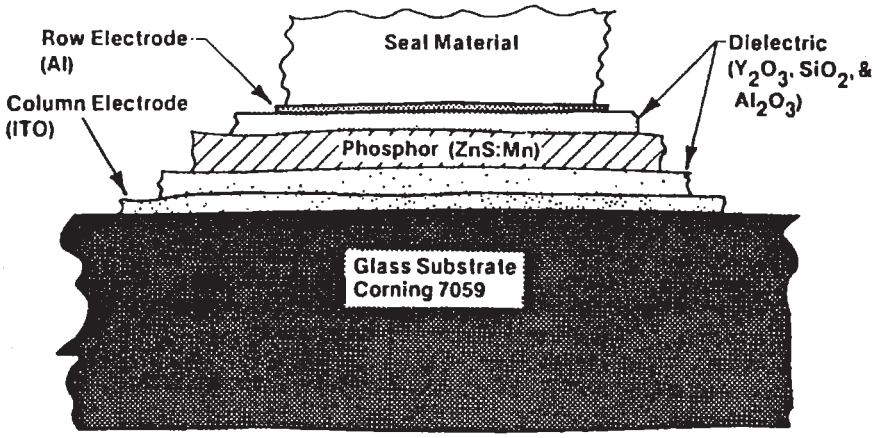

Figure 23 Cross section of a typical EL display panel. (From Tannas [19])

light (Shinoda [18]). A typical plasma panel designed as a computer monitor might be 19-inch diagonal, with 640 × 480 resolution and 25-fL area luminance.

Plasma panels are typically larger than are other flat panels, because the panel structure (shown in Fig. 24) cannot be miniaturized without reducing the emitting gas volume too severely. However, they are available in especially large sizes (up to 2-m diagonal).

5.4 Field Emission Displays

Perhaps the holy grail of display technology has been the search for a technology that could provide CRT-like performance in a truly flat package. Recently, several research groups [10,24–25] have reported progress toward realizing such a display. Their work combines a cold-cathode matrixed source of electrons with a phosphor screen similar to those used in conventional CRTs. The resulting display is flat, with many of the advantages of a traditional CRT. A cross section of this type of display is shown in Fig. 25. Currently these devices are laboratory curiosities; however, once they are reduced to practice and manufactured they have the potential to make a major impact in the display marketplace.

As shown above, a field-emission display (FED) consists of a faceplate coated with a phosphor screen that is vacuum sealed to a base plate containing an array of emitters. Each group of field emitters, which generates the electrons for one pixel of the display, is controlled by the difference in voltage between the row electrode on which the emitters are located and the column electrode. This voltage difference results in an enormous electric field at the emitter tip ($>10^7$ V/cm) which allows the electrons to tunnel through the potential barrier at the metal-vacuum interface and into the vacuum. These electrons are accelerated by the potential on the phosphor-coated faceplate, strike the screen, and cause the phosphor to generate light.

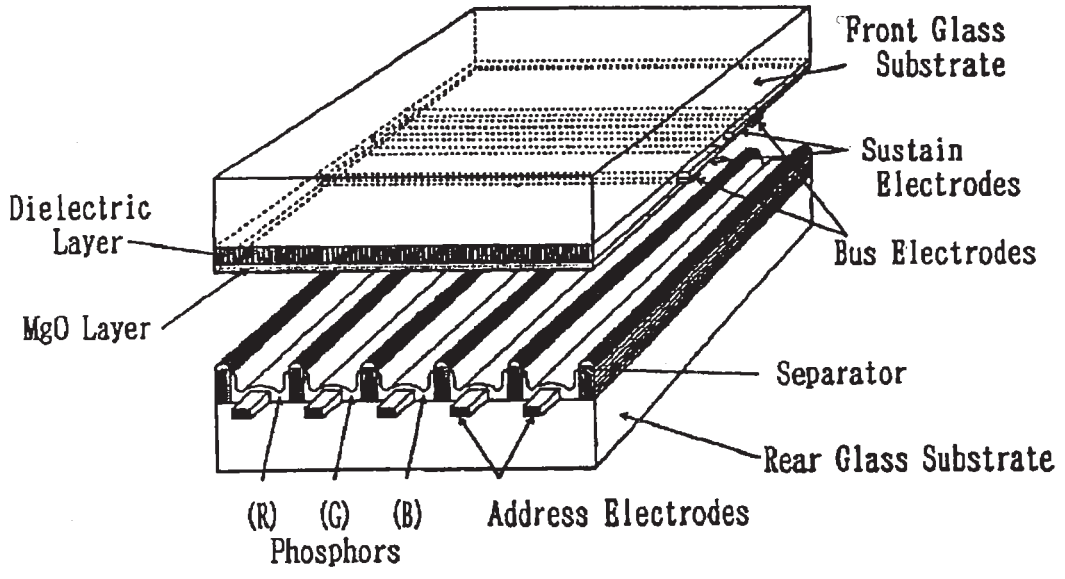

Figure 24 Plasma display cross-sectional schematic. (Courtesy of Society for Information Display [1])

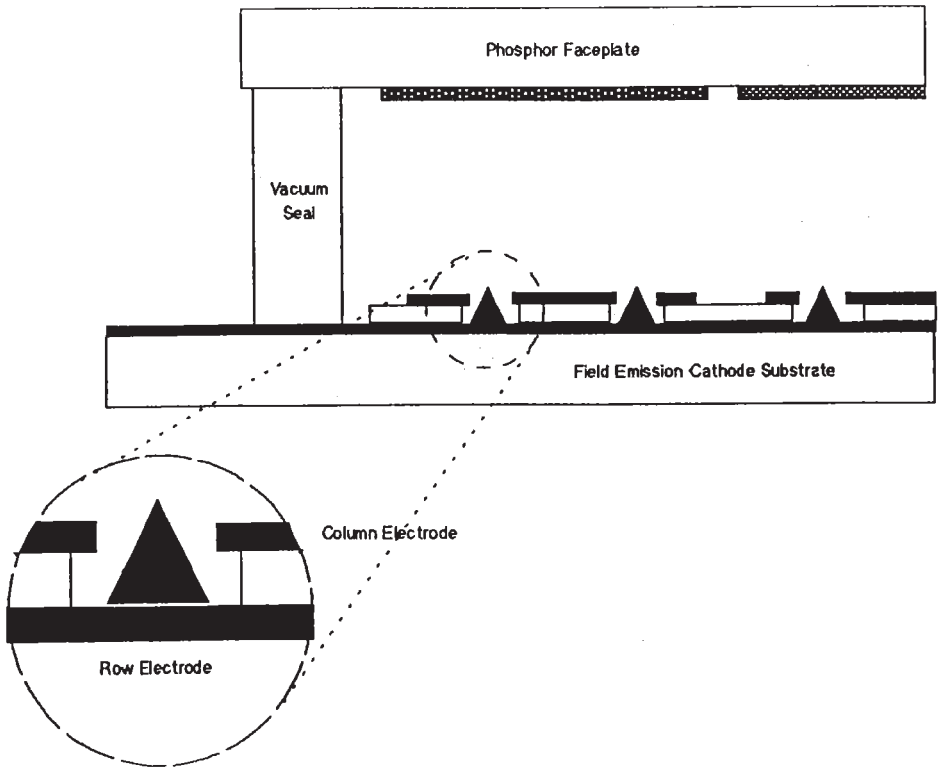

Figure 25 Field-emission display cross section.

Previous FEDs have used miniature structures, with submicron geometries, to generate the large fields required for field emission. Recent work on materials like diamond films shows promise and indicates that it may be possible to use a much less elaborate structure [10]. If this is proven out, then FEDs may become the display technology of choice for flat-panel applications.

6 CONCLUDING REMARKS

One of the most important applications of SLMs is to the generation of images for use in displays and display systems. There is a wide range of possible designs that have been proposed, as there is a wide range of possible SLMs. The applications range from large screen displays with images many meters across to small displays (less than 1 inch across) designed for such applications as viewfinders in camcorders. I hope that the discussion in this chapter can serve as a starting point from which the interested reader can gain some small understanding of the field of displays, since they are so prevalent in our lives.

REFERENCES

1. Barrow, W. A., Coovert, R. C., Dickey, E., King, C. N., Laakso, C., Sun, S. S., Tuenge, R. T., Wentross, R., and Kane, J., A new class of blue TFEL phosphors with application to a VGA full-color display, SID '93 Digest; pp. 761–764, 1993.
2. Bartley, S. H., The psychophysiology of vision, in *Handbook of Experimental Psychology* (S. S. Stevens, ed.), Wiley, New York, 1960, pp. 921–983.

3. Campbell, F. W., and Robson, J. G., Application of Fourier analysis to the modulation response of the eye, *J. Opt. Soc. Am., 54*, 581 (1964).
4. de Lange, H., Research into the dynamic nature of the human fovea. . . , *J. Opt. Soc. Am., 48*, 777–784 (1958).
5. Gerhard-Multhaupt, R., Brinker, W., Ehrke, H.-J., Molzow, W.-D., Roeder, H., Rosin, Th., and Tepe, R., Viscoelastic spatial light modulators and schlieren-optical systems, *SPIE, 1255*, 69–78 (1990).
6. Ginsburg, A. P., Visual information processing based on spatial filters constrained by biological data, *Air Force Aerospace Medical Research Laboratory, Wright-Patterson*, AFAMRL-TR-78-1129, Vols. I, II, 1978.
7. Gunther, J. E., *High Visibility Color Projection Display* (final technical report), HAC reference number F2317, 1986.
8. Hornbeck, L. J., 128 × 128 deformable mirror device, *IEEE Trans. Electron. Dev., ED-30*, 539–545 (1983).
9. Keller, P. A., *The Cathode-Ray Tube—Technology, History, and Applications*, Palisades Press, New York, 1991.
10. Kumar, N., Xie, C., Potter, N., Krishnan, A., Hilbert, C., Eichman, D., Schlam, E., Schmidt, H., and Wagal, S., Field-emission displays based on diamond thin films, SID '93 Digest, 1993, pp. 1009–1011.
11. Ledebehr, A., SID '86 Digest, 1986, pp. 379–382.
12. Luo, F. C., Active matrix LC displays, in *Liquid Crystals—Applications and Uses* (B. Bahadur, ed.), World Scientific, Singapore, 1990, pp. 397–433.
13. Maldonado, J. R., Fraser, D. B., and Meitzler, A. H., Display applications of PLZT ceramics, *Advances in Image Pickup and Display*, Vol. 2 (B. Kazan, ed.), Academic Press, New York, 1975, pp. 65–168.
14. Morozumi, S., Issues in manufacturing active-matrix displays, SID Seminar Lecture Notes, Vol. II, 1992, pp. 3-1–3-58.
15. Morrell, A. M., Law, H. B., Ramberg, E. G., and Herold, E. W., *Color Television Picture Tubes*, Academic Press, New York, 1974, p. 8.
16. Rogowitz, B. E., The human visual system: a guide for the display technologist, SID Seminar Lecture Notes, Vol. 1, 1986, pp. 4.1–4.1-56.
17. Schade, O. H., Optical and photoelectric analog of the eye, *J. Opt. Soc. Am., V. 46*, 721–739 (1956).
18. Shinoda, T., Wakitani, M., Nanto, T., Yoshikawa, K. Ohtsuka, A., and Hirose, T., Development of technologies for large-area color ac plasma displays, SID '93 Digest, 1993, pp. 161–164.
19. Tannas, L. E., *Flat-Panel Displays and CRTs*, Van Nostrand Reinhold, New York, 1985.
20. Tepe, R., Gerhard-Multhaupt, R., Brinker, W., and Molzow, W.-D., Viscoelastic spatial light modulator with active matrix addressing, *Appl. Opt. 28*, 4826–4834 (1989).
21. Wald, G., The receptors of human color vision, *Science, 145*, 1007–1017 (1964).
22. Sampsell, J. B. An overview of the digital micromirror device (DMD) and its application to projection displays, SID '93 Digest, 1993, pp. 1012–1015.
23. Herold, E. W., History and development of the color picture tube, SID, Vol. 15, No. 4, 141–149 (Fourth Quarter, 1974).
24. Brodic, Ivor, Advanced technology: flat cold-cathode CRTs, *Information Display*, I189, pp. 17–19 (1989).
25. Ghis, A., Meyer, R., Raumbaud, P., Levy, F., and Levoux, T., Sealed vacuum devices: fluorescent microtip displays, IEEE *Trans. on Elect. Devices, 38*, No. 10, (October, 1991), pp. 2320–2322.